LBL-7968

MASTER

A MEASUREMENT OF ANISOTROPY IN THE COSMIC BACKGROUND RADIATION ON A LARGE ANGULAR SCALE AT 33 GHz

Marc Victor Gorenstein
(Ph. D. thesis)

November 1978

Prepared for the U. S. Department of Energy
under Contract W-7405-ENG-48

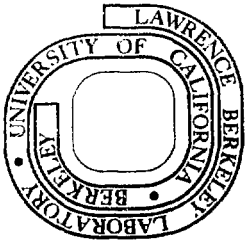

A Measurement of Anisotropy in the Cosmic Background Radiation on a Large Angular Scale at 33 GHz

Marc Victor Gorenstein

The Physics Division of the Lawrence Berkeley Laboratory,
and the Space Sciences Laboratory of the University of California
at Berkeley, Berkeley California, 94720

ABSTRACT

This thesis presents the results of a measurement of anisotropy in the 3 °K cosmic background radiation on a large-angular-scale. Observations were carried out with a dual-antenna microwave radiometer operating at 33 GHz (0.89 cm wavelength) flown on board a U-2 aircraft to 20-km altitude. In eleven flights, between December 1976 and May 1978, the radiometer measured differential intensity between pairs of directions distributed over most of the northern celestial hemisphere with an rms sensitivity of $\pm 46 \text{m °K}/\sqrt{\text{Hz}}$. The measurements show clear evidence of anisotropy that is readily interpreted as due to the motion of the earth relative to the sources of the radiation; the anisotropy is well fit by a cosine distribution of amplitude 3.61 ± 0.54 milli-degrees Kelvin (m °K), one part in 800 of 3 °K, implying a velocity of 361 ± 54 km/sec toward the direction 11.23 ± 0.46 hours right ascension, and 19.0 ± 7.5° declination. A simultaneous fit to a combined hypothesis of dipole ($\cos\theta$) and quadrupole ($\cos^2\theta$) angular distributions places a 1 m °K limit on the amplitude of most components of quadrupole anisotropy with 90% confidence. Additional analysis places a 0.5 m °K limit on uncorrelated fluctuations (sky-roughness) in the 3 °K background on an angular scale of the antenna beam width, about 7°. This thesis describes the equipment development through three engineering flights and the data acquisition in eleven additional flights. The astrophysical results are then presented from the statistical analysis of the reduced data.

Table of Contents

Chapter V - Astrophysical Analysis

List of Figures

List of Tables

Chapter I - The 3°K Background Radiation in an Expanding Universe

I.1 Introduction

The discovery of "excess antenna temperature" from the sky at a frequency of 4.08 GHz, 7.4 cm *(Penzias & Wilson, 1965)*, and its immediate interpretation as a thermal remnant of an early hot phase of the expanding Universe *(Dicke, Peebles, Roll & Wilkinson, 1965)*, heralded a new era in the study of cosmology. The existence of this radiation is strong evidence of the finite age and evolutionary character of the Universe, and it provides a unique view of an epoch that presumably predates the formation of galaxies. Considerable experimental work, stimulated by the 1965 discovery, has yielded spectral measurements that largely confirm the initial conjecture of a thermal (Planckian) radiation spectrum. Figure I.1* shows the results of measurements from wavelengths of 7 cm to 0.1 mm and the comparison with a blackbody spectrum of 2.9°Kelvin. The discovery of the radiation has also had considerable theoretical impact. It has focused the attention of most cosmologists on developing and extending the model of the hot big bang, which thus far is the only satisfactory account of this weak, apparently thermal, background radiation.

The angular properties of the radiation – its high degree of isotropy – identifies it as having cosmological origins. Isotropy, the lack of variation in intensity (temperature) between different directions in the sky, provides a critical test of the Cosmological Principle, the conjecture that, in the large, matter and energy are distributed homogeneously in space and isotropically in direction. A search for anisotropy is the most sensitive probe of deviations from what appears to be a highly symmetric Universe. Anisotropy can arise in two ways, through cosmological deviations from isotropy or from the local motion of the earth relative to the sources of 3°K background. In the first case, the distribution of the sources that last scattered the radiation or the space-time through which the radiation traversed may be anisotropic. The investigation of this "intrinsic" anisotropy tests the Cosmological Principle, and deviations from isotropy in the cosmic background can provide important information about the detailed nature of the early

*Throughout this thesis we will refer to the radiation as the 3°K background, and generally employ the value 3.0°Kelvin in calculations. Measurements in the infrared *(Woody, Mather, Nishioka & Richards, 1975)* have found a value of $2.99^{+0.07}_{-0.14}$°K. Since this spectral measurement in the infrared encompasses the greater fraction of the energy in the 3°K peak we will adopt this value. However it is the thermal nature of the radiation rather than its precise temperature that is most relevant.

Figure I.1 - Spectral Measurements of the Cosmic Background Radiation *(Woody, Mather, Nishioka & Richards, 1975)*

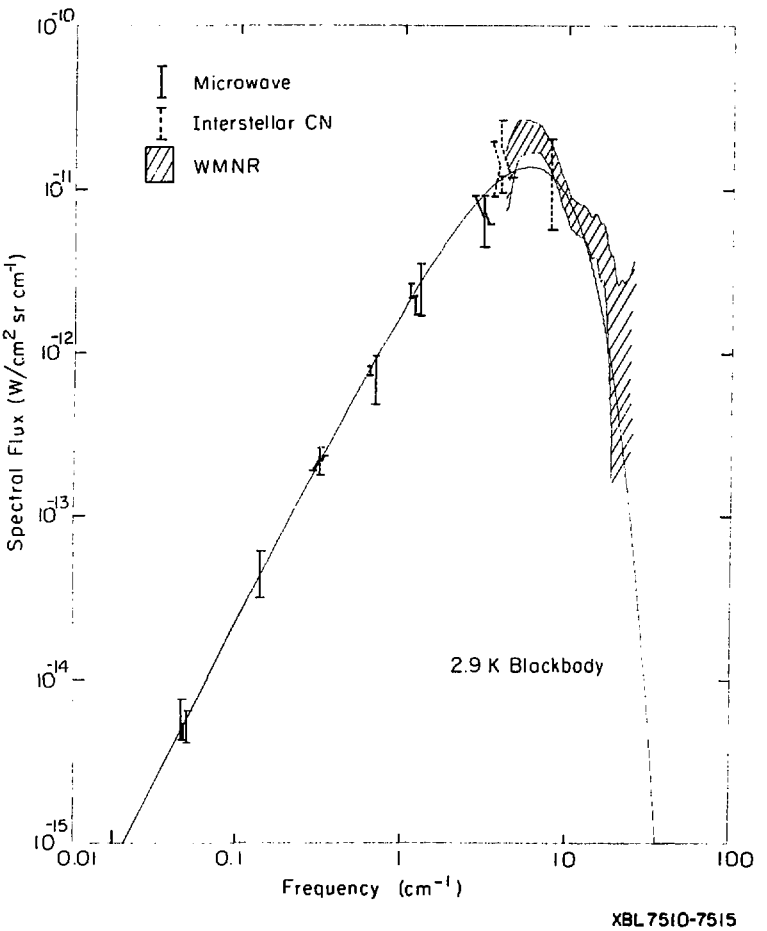

Universe. In the second case, in an otherwise isotropic Universe, an observer moving relative to the distant sources of the radiation would see a modulation of its temperature with direction. This latter effect has the form of a first order Doppler shift in the radiation temperature *(Peebles & Wilkinson, 1968)*, which is, for low velocities ($\beta << 1$),

$$T(\theta) = T_o(1+\beta\cos\theta) \qquad 1.1$$

where

β is the velocity divided by the velocity of light.

T_o is the radiation temperature, 3 °K.

θ is the angle to the observer's motion.

P.J.E. Peebles has called this cosmological motion of the earth relative to the sources of the 3 °K radiation the new Aether Drift *(Peebles, 1971)*.

The first sensitive search for anisotropy on a large-angular-scale was performed by Partridge and Wilkinson *(Partridge & Wilkinson, 1967)*. They placed limits on anisotropy at 3 millidegrees Kelvin (m °K), or one part in 1000 of 3 °K along the celestial equator. This limit on anisotropy raised a theoretical question and an experimental challenge. First, is this high degree of isotropy an inevitable consequence of an evolving expanding Universe (do the Einstein equations predict isotropy?) or, is isotropy the consequence of a special initial condition? The answer may be intimately linked with other important theoretical questions in cosmology. Processes that insure the large-scale isotropy of the radiation must at the same time allow inhomogeneities on a small scale from which galaxies can coalesce. Moreover, the damping processes that isotropise the matter in the early Universe could also generate most or all of the energy in the thermal background radiation, and thereby account for its present temperature.

Current ideas cover a spectrum of isotropising mechanisms and philosophical ideas regarding the nature and significance of isotropy. *(See for example Misner, 1968, 1969; Rees 1972; Collins & Hawking, 1973b; Barrow, 1977, 1978; and references therein.)* To pick just two examples, strong particle interactions in the first hundred microseconds after the singularity *(Barrow, 1978)* and dissipative shocks in the first million years *(Rees, 1972)* have both been proposed as fundamental mechanisms for isotropising the radiation.

Partridge and Wilkinson's limit also posed a new experimental question. Their limit is comparable to the anisotropy that is expected from the motion of the sun about the Milky Way Galaxy. It is known that the sun orbits the Milky Way Galaxy at a speed of about 250 km/sec, or $\beta \sim 10^{-3}$. Thus according to eq. 1.1, this motion alone should yield a cosine anisotropy of amplitude about 3 m °K. Their limit showed that the radiation is sufficiently isotropic that the detection of the motion of the earth relative to the sources of the radiation would be possible

with only a modest increase in sensitivity.

This thesis describes the results of measurements that continue the investigation of large-angular-scale anisotropy in the 3 °K radiation. In eleven flights, an airborne radiometer operating at 33.0 GHz (0.89 cm wavelength) collected data that gives significant evidence of anisotropy in the 3 °K background at one part in 800 of 3 °K. The detailed statistical study of the data shows (1) it is well fit by a cosine anisotropy of amplitude 3.61 ± 0.54 m °K and thus is readily interpreted as due to the motion of the sun relative to the sources of the 3 °K background radiation at 361 ± 54 km/sec toward 11.2 ± 0.5 hours right ascension (R.A.) and 19 ± 8 ° declination (dec.), and (2) that other than this 3.6 m °K anisotropy there is no other angular distribution of cosmological significance at one part in 3000 of 3 °K, or 1.0 m °K, at the 90% confidence level. Surprisingly, the motion of the Sun about the Milky Way does not account for the cosine anisotropy. The implication is that the net motion of the Milky Way relative to the 3 °K background is large, over 500 km/sec. The results from the first eight data flights have been published *(Smoot, Gorenstein & Muller, 1977)*, and the paper is reproduced as Appendix A. Preliminary results of the detection of cosine anisotropy were announced in 1977 *(Smoot, 1977a,b; Gorenstein, Smoot & Muller, 1977)*. Appendix B reproduces a previous publication describing the equipment and its design in detail *(Gorenstein, Muller, Smoot & Tyson, 1978)*.

This chapter continues with a brief account of the important experimental observations and theoretical ideas that form the basis of the modern view of the early Universe. The emphasis is on the model of the hot big bang and the manner in which it accounts for the existence and thermal nature of the 3 °K background. Speculation about the nature of anisotropy that might be observable today is discussed, and a summary of previous limits and measurements of anisotropy on a large-angular-scale is presented. The chapter concludes with the organization of the material presented in the thesis.

A history of the development of cosmology in the early 20th century is presented in *North, 1965*. Current ideas in cosmology, emphasizing the "standard" models of the evolutionary hot big bang can be found in *Peebles, 1971; Misner, Thorne & Wheeler, 1973;* and *Weinberg, 1972*. *Partridge, 1969* presents a review of the experimental status of the spectrum and isotropy measurements of the 3 °K background, and contains references describing alternate explanations of the origins of the radiation. For a non-technical discussion of the discovery of the 3 °K background radiation see *Peebles & Wilkinson, 1967*. *Muller, 1978* describes the Aether Drift in the context of big bang cosmology, and includes a description of the measurement that is the subject of this thesis. *Weinberg, 1977* contains a popular account of the modern picture of Cosmology.

1.2 Cosmology in the Early 20th Century

The gravitational properties of matter and energy determine the large-scale behavior of the Universe. In the early 1920's the Russian mathematician Alexander Friedmann was the first to find the correct cosmological solutions to Einstein's field equations of general relativity without the Cosmological term ($\Lambda = 0$). He assumed that matter in the Universe is distributed homogeneously in space and isotropically in direction. Isotropy and homogeneity, the Cosmological Principle, was assumed by Einstein, Friedmann and others in theoretical investigations before the existence of galaxies external to our own had been established. Friedmann's solutions were dynamic: he found that the Universe is either in a state of expansion or contraction.

In this same decade galaxies became the survey markers that mapped the geometry of the Universe. In the early 1920's, V.M. Slipher measured red shifts of "nebulosities" and found them to be large. In 1924 Edwin P. Hubble, measuring the brightness of Cepheid variable stars in "spiral nebulae", showed that spiral nebulae are external to the Milky Way, at distances of millions of light-years, and were in fact galaxies similar to our own. Extensive observations of galaxies, their distribution, spectra, and luminosity, culminated in Hubble's announcement in 1929 that galaxies recede at velocities proportional to their distance. Recessional velocities were determined by the observed red shifts of spectral lines in galactic spectra, and distances were measured from estimates of intrinsic galactic luminosities. Averaged over sufficiently large volumes, the distribution of galaxies in space did seem to conform to the conjectured Cosmological Principle.

The relationship between distance and velocity is known as Hubble's Law, and is linear in the limit of non-relativistic recessional velocities:

$$v = H_0 d \qquad 1.2$$

where

H_0 is Hubble's constant. A current value is 55 ± 7km/sec/Megaparsec, or $(17.7 \pm 2 \times 10^9)^{-1}$ years^{-1} *(Sandage, 1972)*. A Parsec is 3.26 light-years, and a light-year is 9.46×10^{17}cm.

v is the recessional velocity of the galaxy.

d is the distance to the galaxy.

The immediate interpretation of Hubble's law is that the Universe is expanding, in accord with the theoretical models. A linear extrapolation using this present expansion rate shows that the Universe would have started expanding from a highly compressed state about 1.8×10^{10} years ago, a time given approximately by the inverse of the Hubble Constant. In Friedmann's

relativistic cosmology the Universe does have a finite age and has in fact expanded to the present epoch from a state of infinite density. This infinity, or singularity, is unphysical and precludes knowledge about the Universe before the initial event. But Friedmann's calculation assumed a highly symmetric, idealized Universe, and perhaps in our real Universe, with its inhomogeneities, this peculiar singular state was never realized. However, Stephen Hawking and others *(Hawking & Penrose, 1969; Hawking & Ellis, 1973)* have shown that if Einstein's equations are valid then the Universe had to pass through a singularity in density at one time or another even if the Universe does not conform to perfect isotropy.

The desire to avoid the initial singularity has motivated others to search for alternate cosmologies without the unsettling infinities of the Friedmann solution. Most notable has been the Steady State theory, first advanced by Herman Bondi, Thomas Gold, and Fred Hoyle in 1948. Here the Universe has an indeterminate age: matter is created spontaneously, filling the gaps as the galaxies move apart, so an observer cannot distinguish between epochs. Although this model extends the spirit of the Cosmological Principle, by making the Universe homogeneous in time as well as in space, the observations have not borne out the conjecture. Radio source counts indicate a higher density of radio galaxies in the distant regions of space than nearby, demonstrating an evolution that goes against the basic idea of the steady state. And the existence of the thermal background has proved difficult to account for in a steady-state Universe.

Before reviewing the more recent work in cosmology, we mention two measures of time in an expanding Universe that will be useful in the discussion. The first is simply the time elapsed since the singularity as measured by a co-moving observer. By definition a co-moving observer is in a reference frame where the matter in the Universe appears to expand isotropically. The second measure is the red shift parameter z. The red shift parameter is defined by the ratio of the wavelength of radiation received by a local observer, λ_o, to the original wavelength emitted by a distant source, λ_e.

$$1 + z = \frac{\lambda_o}{\lambda_e} \qquad 1.3$$

In the expanding Universe the quantity $(1 + z)$ is the ratio of the scale size of the Universe at present to the scale size of the Universe when the radiation was emitted, and is a convenient measure of "time" relative to our present epoch. For sources whose recessional velocity is small compared to the speed of light, the relation between velocity and red shift parameter is linear:

$$\beta = z \qquad 1.4$$

where β is the recessional velocity expressed as the fractional velocity of light.

I.3 Prediction and Discovery of the 3°K Radiation

Astrophysics is concerned with the contents of the Universe. The present evidence suggests that, on a nuclear level, most of the matter comes as individual protons – hydrogen nuclei. A lesser amount, perhaps 25% by weight, is in the form of alpha particles – helium nuclei. Heavier nuclei, electrons, and radiation in various forms, make up the the remaining few percent. The significant abundance of helium seems intimately connected with the existence of a primordial background radiation, and played an important role in the prediction of the thermal background.

The idea that the early Universe would contain a radiation background was first proposed by Georges Lemaître in the early 1920's. Tolman *(Tolman, 1934)* first derived the behavior of radiation in an expanding Universe. In the early 1940's George Gamow tried accounting for the cosmic abundance of the elements by nuclear reactions occuring within minutes after the singularity *(Alpher, Bethe & Gamow, 1948)*. Gamow postulated an intense radiation background that would modulate nucleosynthesis through the mechanism of photo dissociation. For Gamow's scheme to work, the energy density of the radiation would dominate the matter energy density, and thus determine the initial expansion rate of the Universe. In this manner the singularity, or the big bang as Gamow called it, became "hot". Calculations show that within the first three minutes after the singularity neutrons and protons would combine forming deuterium, and then further synthesis would result in a mass fraction of helium of about 25%, comparable to what is observed today *(e.g. Peebles, 1966; Wagoner, Fowler & Hoyle, 1967)*. The production of helium fixes the radiation background temperature near 10^{10}°K at this epoch. Ralph Alpher and Robert Herman, working with Gamow, computed that the radiation, cooling as the Universe expanded, would now have of temperature of 5 °K *(Alpher & Herman, 1950)*.

The discovery of an isotropic, unpolarized, thermal background radiation waited 25 years. In 1964 Robert Dicke independently arrived at the idea of a hot big bang *(Peebles & Wilkinson, 1967)*. He conceived of the Universe as having oscillated through many cycles of expansion and collapse. In an oscillating Universe stellar nucleosynthesis would act to build up heavy nuclei in each cycle, resulting in an over-abundance of heavy nuclei unless there were a mechanism that would also destroy the nuclei in each cycle. A weak thermal background radiation, compressed to high temperature as the Universe contracted, would destroy nuclei as the Universe collapsed toward the singular state. While Dicke and his colleagues at Princeton were developing these ideas and preparing apparatus that would detect a weak background radiation, they were contacted by Arno Penzias of Bell Laboratories in New Jersey. Arno Penzias and Robert Wilson of Bell Laboratories had spent over a year convincing themselves that an unidentified source of radio static, detected with a receiver at Holmdel New Jersey designed for satellite communications, had an astrophysical origin. The signal's antenna temperature was

between 2.5 and 4.5 °K at 7.4 cm wavelength, and was isotropic and unpolarized within the limits of their survey. Bernard Burke of the Massachusetts Institute of Technology knew of Penzias and Wilson's result, and had also heard of the theoretical ideas being developed at Princeton from a talk by P. J. E. Peebles. Burke suggested to Penzias that he contact the group at Princeton. The result of this communication between the two groups led to back-to-back letters in the Astrophysical Journal *(Penzias & Wilson, 1965; Dicke, Peebles, Roll & Wilkinson, 1965)* announcing the result and providing its interpretation. A consensus quickly formed among most cosmologists that the background radiation was very likely the thermal remnant radiation from a primordial fireball.

1.4 The Last Scattering of the 3°K Radiation From Matter

In the early Universe the energy density of the thermal background radiation insured that matter remained in a highly ionized state. Due to the large scattering cross section off free electrons, the mean free path of the photons was short compared to the scale size of the Universe.

As the Universe expanded the energy density of the radiation fell as the inverse of the fourth power of the scale size of the Universe (the mean distance between galaxies for example), while the energy density of matter fell as the inverse third power of the scale size. Thus

$$\rho_r \propto \frac{1}{(1+z)^4} \qquad 1.5$$

$$\rho_m \propto \frac{1}{(1+z)^3} \qquad 1.6$$

where

ρ_r is the radiation energy density.

ρ_m is the matter energy density.

Three powers of $(1+z)$ account for the decreasing number density of both photons and massive particles as the Universe expands. The extra power of $(1+z)$ in eq. 1.5 is due to the additional red shift that the radiation suffers as a result of the expansion. Thus the radiation energy density ultimately drops below the energy density of the matter.

It is a peculiar coincidence that the Universe became matter-dominated ($\rho_m > \rho_r$) at about the same epoch when the radiation last had significant interactions with the matter. The "decoupling" occured when the radiation temperature had dropped enough so electrons and protons could combine forming neutral hydrogen at a radiation temperature of about 4500 °K. The photon cross section for scattering from neutral hydrogen is so low that after the decoupling the mean free path for scattering became comparable to the Hubble distance, and the the Universe became transparent to the propagation of photons.

It is interesting that the spectrum remained Planckian, even in the absence of thermalizing interactions. This is a geometric effect, in part due to the masslessness of the photons; thus *(Peebles, 1971, pg. 121)*

$$T_z = (1+z)\ T_o \qquad 1.7$$

So the epoch of decoupling occured at a red shift of

$$z = \frac{4500\,°K}{3\,°K} - 1 \approx 1500 \qquad 1.8$$

Since the era of decoupling the radiation has evolved independently of the matter and thus provides a direct view of the primordial plasma.

It should be remembered, however, that this is the generally accepted view mostly because it has withstood successful challenge. Alternate explanations usually have the radiation last interact with matter more recently than the decoupling at $z = 1500$. However, models at odds with the standard picture invariably have the radiation still arriving from distances comparable to the Hubble radius. Thus even with a more recent origin, it is unlikely that the cosmological significance of the 3 °K background or its angular properties would be much diminished. The 3 °K background radiation would still be a powerful probe of the distant matter and energy in the Universe, and the cosine anisotropy would still be a measure of velocity relative to a global reference frame.

1.5 Anisotropy in the 3°K Background Radiation

In the standard Friedmann model a co-moving observer sees an isotropic thermal background radiation. In the real Universe anisotropy in the thermal background can arise in two conceptually distinct ways. First, in an otherwise isotropic cosmology, an observer's motion at velocity β relative to the co-moving frame gives rise to anisotropy of the form *(Peebles & Wilkinson, 1968)*:

$$T(\theta) = \frac{T_o}{\gamma}\ \frac{1}{1-\beta\cos\theta} \qquad 1.9$$

where γ is the usual Lorentz factor $(1-\beta^2)^{-1/2}$. Thus *the spectrum remains thermal* but the value of the temperature varies across the sky. In the limit of low velocity, $\beta \ll 1$, this equation reduces to eq. 1.1,

$$T(\theta) = T_o(1+\beta\cos\theta) \qquad 1.10$$

or

$$T(\hat{n}) = T_o + \vec{T}\cdot\hat{n} \qquad \text{I.11}$$

where

$|\vec{T}| = T_o\beta$, $\vec{T}$ points towards the direction of motion.

$\hat{n}$ is a unit vector pointing in the direction of observation.

The motion of the solar system about the Galaxy is known to be about 250 km/sec, and should contribute an anisotropy of about 3 m°K to a potential $cos(\theta)$ anisotropy. Measuring $\vec{T}$ identifies the local frame of rest relative to the distant matter in the Universe.

Anisotropy can also be "intrinsic". Inhomogeneities in the distribution of matter or energy in the early Universe, or anisotropy in the space-time through which the radiation has passed may give rise to measurable effects. Current theoretical ideas leave much room for speculation on possible anisotropy on large-angular-scales, and, in fact, the high degree of *isotropy* is a source of speculation and debate. Do the Einstein equations predict isotropy? A simple causality argument would seem to permit large anisotropy over angular separations of more than a few degrees. At any epoch since the big bang, an observer receives photons from distances limited by light travel time since the singularity, defining an event horizon beyond which no causal interaction can take place. At the time of the decoupling the event horizon was about one million light years, and this was the largest distance over which isotropising processes could have acted. But that volume now appears as a circle of only a few degrees in angular size *(Weinberg, 1972, pg. 525)* yet the radiation is isotropic to better than one part in 1000 on all angular scales.

Misner has investigated homogeneous models* that have arbitrarily large initial anisotropies. The idea is that isotropy is a consequence of physical law if it can be shown that all initially anisotropic models evolve towards isotropy, so the present state of the Universe is insensitive to the initial conditions of its formation. Misner proposed that neutrino interactions occuring within the first second after the singularity would isotropise the matter. However, this approach has been challenged *(Barrow & Matzner, 1977, and references in Collins & Hawking, 1973b)* as being incompatible with the finite specific entropy of the Universe. The specific entropy can be expressed as the ratio of the number density of photons in the thermal background radiation to the number density of baryons. This ratio has been constant since a few minutes after the singularity, and is approximately 10^8 photons per baryon.

Rees and Barrow *(Rees, 1972; Barrow, 1977)* have pursued Misner's approach along more modest lines. Rees has postulated a 'chaotic' cosmology where shock waves isotropise large initial inhomogeneities in the matter distribution before the epoch of decoupling. This process

*Einstein's equations allow for homogeneous models that are anisotropic. The converse, however, is not allowed. Models that appear isotropic to every observer for all time must also be homogeneous.

heats the matter and thereby generates the thermal background radiation. Rees claims that his approach accounts for the approximate equality of the energy density of the radiation field with the matter field at the time of the decoupling.

Is isotropy a consequence of a special initial condition? The notion that isotropy can be explained as a consequence of physical law is challenged by Collins and Hawking *(Collins & Hawking, 1973b)* who claim to have demonstrated the extreme improbabilty of a Universe evolving to an isotropic state given the assumption that the Universe could have been created in a wide variety of initial homogeneous but anisotropic states. They account for the present, approximately isotropic, condition as the special situation that allows for the evolution of intelligent life. They claim that galaxies can form only in a Universe that is expanding close to the rate that prevents eventual re-collapse. And it is just this kinematic state that asymptotically approaches isotropy. A Universe with slow initial expansion will collapse before galaxies can coalesce from the perturbations in the matter. Thus if the Universe has oscillated through many cycles, it eventually hits one that expands sufficiently fast approaching isotropy and producing galaxies. In their view our own existence is a consequence of this observed isotropy. Barrow *(Barrow, 1978)* has questioned the assumption that all initial states of the Universe occur with equal probability. If a sufficiently stiff equation of state held when matter was at nuclear densities, within 10^{-4} seconds after the singularity, then he claims that isotropy was the stable and preferred initial condition. There is much debate on which are the important physical processes operating in the early Universe. The range of ideas presented here is intended as illustrative of the unsettled nature of present understanding of intrinsic isotropy of the 3°K background.

Global anisotropy in the large-scale space-time structure of the Universe might give rise to anisotropy with simple angular properties. Collins and Hawking and others have speculated that matter in the Universe could be rotating with respect to local inertial frames *(Collins & Hawking, 1973a; Hawking 1969a,b; K. Gödel 1949,1950; Batakis & Cohen, 1975)*. In general this gives rise to a quadrupole ($\cos^2\theta$) anisotropy. The limit on the amplitude of quadrupole radiation is the most sensitive test of the rate of universal rotation *(Hawking, 1969b)*. An observable rotation would violate Mach's principle, the conjecture that the local properties of inertia are determined from the global matter distribution. Limits on quadrupole amplitudes of about 1 m°K place a limit on the present rotation rate between 10^{-14} and 10^{-17} radians per year depending on the mass density of the Universe. Thus continued investigation of anisotropy on a large-angular-scale can detect the local co-moving frame and provide a test of the Cosmological Principle by investigating the distribution of matter and energy in the early Universe and the space-time through which the radiation has since traveled.

1.6 Previous Measurements of Anisotropy in the 3°K Radiation on a Large-Angular-Scale

In their 1965 discovery paper, Penzias and Wilson began by noting that their astrophysical signal was "isotropic, unpolarized, and free from seasonal variations". With their total power receiver they determined the temperature of the radiation to be within ± 30% of 3.5°K from the different parts of the sky they surveyed. The isotropy identified the radiation as a candidate for the thermal remnant from the primordial fireball. Partridge and Wilkinson's 1967 result was an improvement of over two orders of magnitude from Penzias and Wilson's initial limit. One motivation for further experimental work is that a modest increase in sensitivity should reveal cosine anisotropy due to the motion of the earth relative to the radiation background.

A decade has passed since the initial measurements were performed, and the results, listed in Table 1.1, show that success has not been easy. The experiments have been of similar design: a Dicke-type radiometer measures the *difference* signal between two horn antennas pointing at widely separated directions in the sky. Various switching arrangements cancel intrinsic asymmetry in the equipment. Long integration times reduce statistical uncertainty, and measurements repeated throughout the year map the sky.

Table 1.1

Measurements of Cosine (24 hour) Anisotropy in the 3°K Background

Reference	Platform	Altitude (km)	ν (GHz)	λ (cm)	Amplitude (m°K)	Directional error
Partridge & Wilkinson(1967)	ground	0	9.4	3.2	0.9±2.1	-
Conklin (1969)	mountain	3.8	8.0	3.8	1.6±0.75	-
Boughn et. al. (1971)	ground	0	35.0	0.86	7.5±11.6	-
Henry (1971)	balloon	24	10.2	2.9	3.2±0.8	±35°
Muehlner & Weiss (1976)	balloon	25	100	0.3	<3.5	-
Corey (1978)*	balloon	25	19	1.6	2.9±0.7	±22°
This work	U-2	20	33.0	0.91	3.61±0.54	±8°

*See *Corey & Wilkinson, 1976* for preliminary announcement of this result.

The measurements, however, have similar limitations. A tiny signal is being sought in the presence of large terrestrial, atmospheric, and galactic backgrounds. Atmospheric oxygen and water vapor emission limits ground based measurements and impacts the design of all

experiments performed in the atmosphere. Galactic synchrotron radiation is a spurious signal that fills the celestial sphere, and is particularly bothersome at frequencies below 30 GHz. Muehlner and Weiss used bolometric rather than microwave techniques to observe at high frequencies and encountered a new class of galactic infrared emitters.

It was the detailed choice of experimental design and implementation that allowed the significant improvement in sensitivity in the work reported here. The strength of this experiment comes from the choice of observation frequency and the use of the airborne platform provided by the U-2 aircraft. At the observation frequency of 33 GHz corrections to galactic background radiation is less than 0.2 m°K for most parts of the sky. The U-2 aircraft provided a stable and quiet platform that carried the equipment above most of the interfering atmosphere, and, through its availability, provided the best sky coverage and exposure time from the data of eleven flights.

The initial three measurements listed in Table I.1, together with the measurement by Muehlner and Weiss, yielded limits on cosine anisotropy in the 3°K background. Conklin and Henry found the first clear evidence of anisotropy in the 3°K radiation, but their measurements were limited by galactic backgrounds and they could not determine the angular properties of the anisotropy. (Conklin claimed that his measurement of a non-zero amplitude of cosine anisotropy was significant, but he underestimated the errors on a large galactic background correction to his data.) The measurement of Corey and Wilkinson is an improved version of Henry's measurement. The work reported here produced the first clear evidence for cosine anisotropy *(Smoot, Gorenstein & Muller, 1977)*.

I.7 Thesis Organization

The thesis continues with a brief introduction to the radiometer used in the measurements. Chapter II describes the components of the radiometer and their function, with attention to the design features that reduce or cancel systematic backgrounds. The emphasis in this thesis is on those aspects of the experiment which have not been previously published, for example, the detailed description of the radiometer design and equipment performance is left to Appendix B which is reproduction of a previously published paper *(Gorenstein, Muller, Smoot & Tyson, 1978)*.

The equipment development and data taking proceeded through a sequence of 14 flights. Chapter III describes the initial difficulties encountered with the equipment, their resolution, and the data taking flights. The data analysis of this experiment is, in principle, straightforward. The equipment records measurements of anisotropy once every two seconds. Since we are really interested in the average of many thousands of measurements, we resort to computerized techniques that sort, display, and average the data. Chapter IV describes the data reduction,

instrument calibration, checks for systematic effects and spurious measurements, and finally presents the list of corrected measurements and the directions in the sky they cover.

Over one hundred reduced measurements of anisotropy were obtained in eleven data flights. Chapter V presents the astrophysical results from the statistical analysis of the reduced data. In addition to the fit for cosine anisotropy, the sky coverage is sufficiently good that a preliminary limit on quadrupole anisotropy is obtained, together with a limit for "sky-roughness" on an angular scale of the antenna beam width, 7°. Most of the detailed descriptions of equipment performance, flight preparation, radiometer calibration, systematic corrections, and statistical analysis techniques are left for Appendices C through H.

Chapter II - Experimental Design and Equipment Description

A differential microwave radiometer flown on board a U-2 aircraft to 20-km (65,000 feet) altitude detected the anisotropy in the 3°K radiation reported in this thesis, Figures II.1 and II.2. The radiometer measures the difference in intensity of microwave radiation collected by two horn antennas pointed 60° apart in the sky. It operates at 33 GHz (0.89 cm wavelength) and features low-noise performance (rms sensitivity for differential intensity of ± 46 m°K/$\sqrt{\text{Hz}}$) at room temperature. The 33-GHz operating frequency and the 20-km observation altitude minimize the sum of atmospheric and galactic backgrounds. Additional subsystems include a second radiometer at 54 GHz that monitors anisotropic atmospheric emission, a rotation system that interchanges the horn antennas every 64 seconds, canceling instrumental imbalance, and a thermal monitor and control system that insures stable receiver operation.

The equipment is mounted in the U-2 aircraft just aft of the pilot's canopy and forward of the wings, Fig. II.1. The smaller 54-GHz radiometer is mounted between the two larger horn antennas of the 33-GHz radiometer. Figure II.2 shows the equipment with the windshield and RF shields removed, exposing the radiometers and support electronics packages.

The components making up the two radiometers are functionally identical. Figure II.3 is a schematic drawing of the radiometer design. A ferrite (Dicke) switch, alternating at 100 Hz between the two antennas, directs the incoming microwave radiation into the low noise receiver. A 100-Hz narrow-band amplifier first filters the detected signal from the receiver. The demodulator then analyses the signal for a component in phase with the alternation of the ferrite switch. The Datel logger records this signal after 2 seconds of averaging. In flights 8-14, the receiver was a balanced-mixer integrated with an IF amplification stage. The 180° phase-switch monitors the offset between the two input arms of the radiometer as described in Section C.3.

Appendix B reproduces a previously published article *(Gorenstein, Muller, Smoot & Tyson, 1978)* that discusses the important backgrounds that decisively influenced both the design of the radiometers and the choice of the supporting subsystems, and describes in detail the major components of the system. The introduction of this article describes the equipment and its features. The article continues by describing the astrophysical, terrestrial, and instrumental backgrounds that potentially dominate the minute signal we wish to detect. The balance of the article contains a detailed description of the equipment flown in the U-2, focusing on the techniques that reduce or cancel microwave emission from the galaxy, the atmosphere, and the

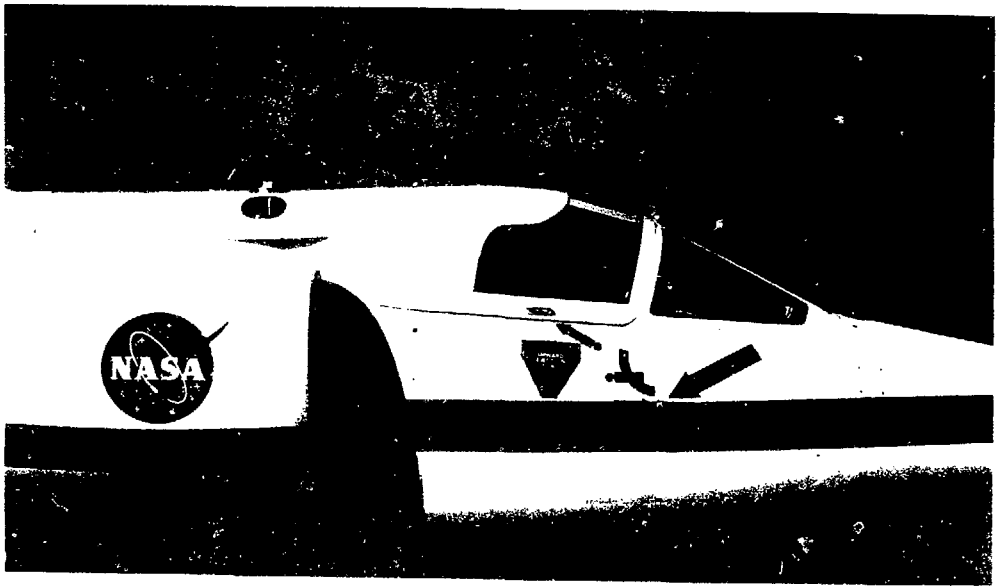

Figure 11.1 - Radiometers in Flight Configuration

CBB 770-9349

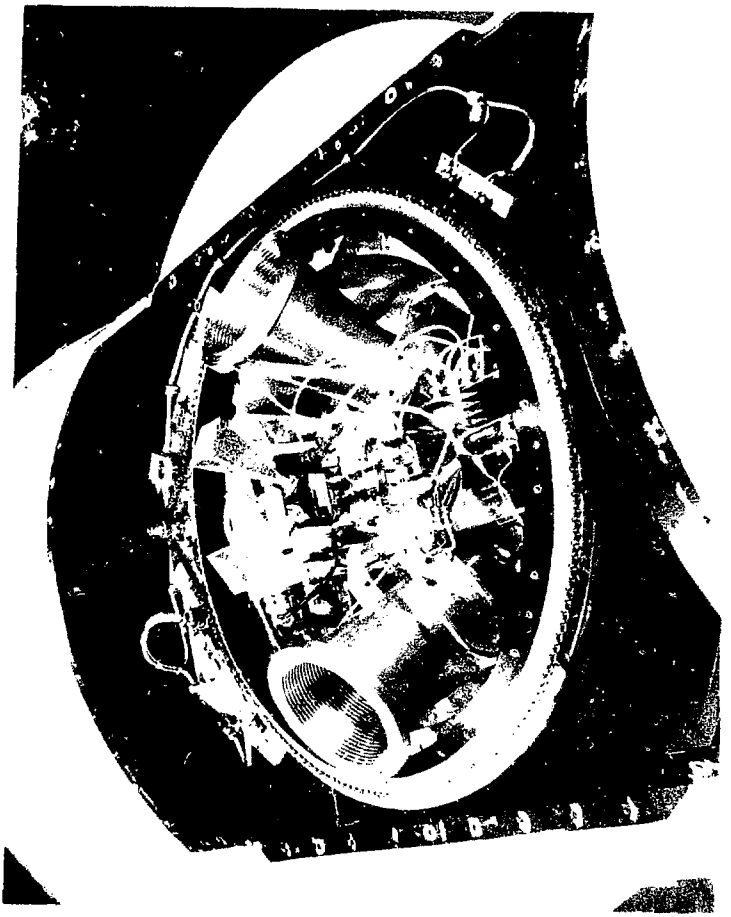

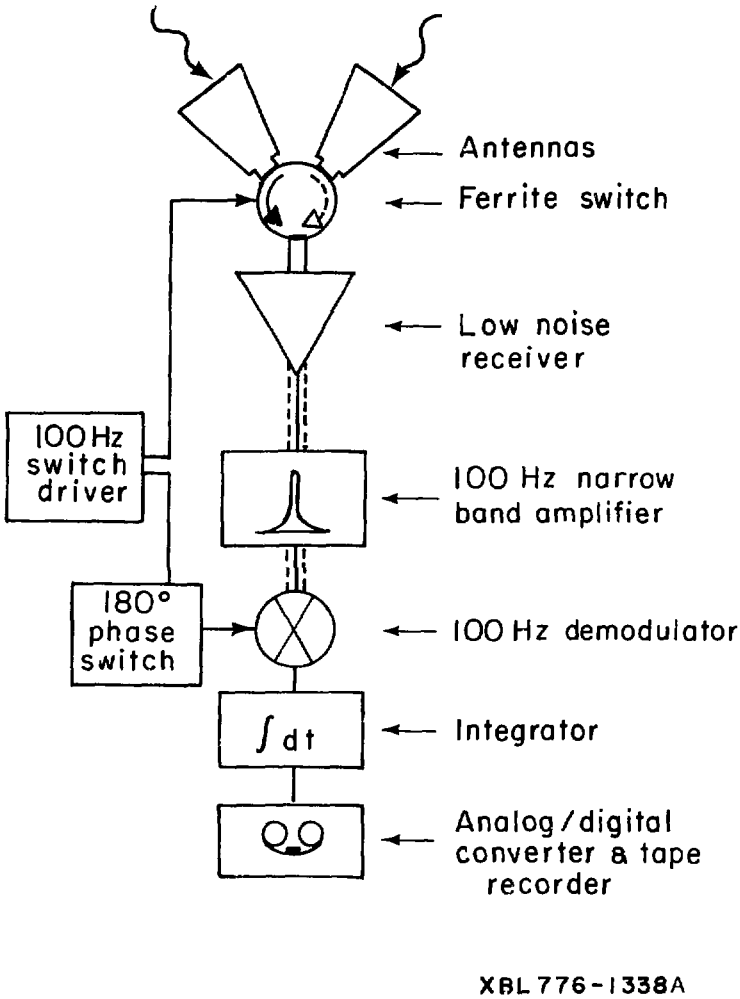

Figure II.3 - Schematic Diagram of Radiometer Components

instrument itself.

Appendix C discusses the performance of the ferrite switch, a crucial component of the radiometers. The Appendix describes the cold-load technique that we use to null unbalanced insertion loss between the input ports of the device, and the in-flight phase-switching technique that monitors the insertion loss imbalance between the radiometers arms.

Throughout this thesis we will refer to the intensity of microwave radiation in units of *antenna temperature* expressed as degrees Kelvin (°K). A blackbody radiator, radiates with a brightness B given by

$$B = kT \frac{2\nu^2}{c^2} \frac{\alpha}{e^{\alpha} - 1} ; \qquad \alpha = \frac{h\nu}{kT} \tag{II.1}$$

where

B is brightness expressed in ergs sec^{-1} cm^{-2} ster^{-1} Hz^{-1}.
k is Boltzmann's constant, 1.38×10^{-16} ergs °K^{-1}.
ν is the frequency of observation.
c is the velocity of light, 3×10^{10}cm/sec.
h is Planck's constant 6.63×10^{-27} erg sec.

The low-frequency Rayleigh-Jeans region is defined by $h\nu/kT << 1$, so for frequencies that satisfy this criterion eq. II.1 reduces to

$$B = kT \frac{2\nu^2}{c^2} . \tag{II.2}$$

We take advantage of this simple proportionality between brightness and temperature to define the *antenna temperature* of a source, filling an antenna beam, as

$$T_A \equiv B \frac{1}{k} \frac{c^2}{2\nu^2} . \tag{II.3}$$

Thus in the Rayleigh-Jeans region, $T_A = T$, from eq. II.2 and II.3. In general

$$T_A = T \frac{\alpha}{e^{\alpha} - 1} \tag{II.4}$$

from eq. II.1 and II.3. See *Kraus, 1966, pg. 76-86* for a complete discussion of antenna temperature and thermal blackbody radiation.

Chapter III - Equipment Development and Data Taking

III.1 Introduction

This chapter describes the equipment development and data taking through fourteen flights flown between July 1976 and May 1978. All flights utilized one of the two U-2 aircraft based at NASA-Ames at Moffett Field, California. Table III.1 summarizes the flight circumstances.

The flights divided into three sequences according to equipment performance. The first sequence, flights 1,2 and 3, were engineering flights, and collected data on equipment performance only. The second series, flights 4 through 7 collected useful preliminary data on anisotropy, but was a period that saw rapid changes and modifications in the original equipment configuration. In the final sequence of flights, 8 through 14, the equipment, in unchanged configuration, collected data of excellent quality. Tables III.2 through III.5 summarize the development of the 33-GHz radiometric system and its performance for each flight. Sections III.3, 4, and 5 describe each of the three series in more detail.

The flight plan for each data flight was arranged so the antennas would measure anisotropy between two pairs of directions in the sky. As an example of the data taking strategy employed in most flights, section III.5 describes the flight plan and the resulting sky coverage for the ninth flight.

After the initial engineering and development flights, the execution of a typical data flight fell into a routine. The routine of pre-flight equipment checks, flight-plan preparation, and the actual flight operations, is described in Appendix D.

III.2 Engineering Flights (Flights 1-3)

The early flights were directed towards the development and testing of the thermal control and monitoring systems, the rotation and data recording systems, and the radio-frequency shielding and mechanical vibration isolation, Table III.2. This development took place during the original fitting and testing of the equipment in the U-2, the two engineering day-flights in July and August 1976, and the first night-flight flown in September 1976.

Prior to the first flight, the complete apparatus was mated to NASA U-2 #709 for tests of mechanical and radio transmission interference. On the ground, with the equipment installed and running the pilot sequentially turned on the engine and the communication and navigation radio transmitters. The recorded data showed no interference due to engine vibration, or radio interference with the exception of a transmitter not normally used at altitude. During the first engineering flight, the pilot repeated the sequence of transmissions with similar null results.

Table III.1 - Flight Circumstances

Flight	Date Launch-Land (UT)	Pilot Aircraft	Receiver	Sensitivity[1] (m°K/√Hz)	Exposure[2] (hours)
1	7 July 76 1705-1924	J. Barnes NASA #709	33.5 GHz paramp		
2	6 Aug 76 1800-2044	R. Williams NASA #709	"		
3	23 Sept 76 0100-0620	J. Barnes NASA #709	"		
4	3 Dec 76 0132-0541	I. Webster NASA #708	"	96±9	2.78
5	10 Dec 76 0225-0623	R. Williams NASA #709	"	119±19	2.83
6	2 Feb 77 0130-0615	J. Barnes NASA #708	33.0 GHz 'old' mixer	119±1.0	3.83
7	18 Mar 77 0220-0702	J. Barnes NASA #708	"	96.4±1.0	3.85
8	1 Apr 77 0200-0608	R. Williams NASA #709	33.0 GHz 'new' mixer	44.1±0.3	3.23
9	14 Apr 77 0600-1041	R. Williams NASA #708	"	43.8±0.3	3.55
10	20 Apr 77 0112-0450	I. Webster NASA #709	"	44.1±0.3	3.87
11	26 May 77 0300-0744	I. Webster NASA #709	"	43.8±0.3	3.52
12	8 Sept 77 0230-0705	J. Barnes NASA #708	"	44.0±0.3	3.57
13	24 Feb 78 0130-0615	R. Williams NASA #708	"	44.3±0.3	3.61
14	16 May 78 0241-0745	R. Erikson NASA #709	"	44.8±0.3	3.54
	TOTAL				38.18

[1]Determined from rms fluctuations in 33-GHz data words recorded every 2 seconds.

[2]Includes time during banks and antenna rotations.

Table III.2 - Engineering Flights

Flight	Equipment Configuration and Improvements	Flight Plan and Performance
1	33.5-GHz paramp, system sensitivity on ground is ± 44 m °K/$\sqrt{Hz}$. 54-GHz roll monitor. Antennas interchange once/128 seconds. Housekeeping system records equipment temperatures.	Daylight engineering flight, paramp overheated, data channels overvoltaged at end of flight.
2	Increase thermal conduction from paramp to thermal ballast. Improve electronics to protect against overvoltage.	Daylight engineering flight. Improved paramp regulation. Data recording system works nominally.
3	Minor mechanical and electronic improvements.	Nighttime engineering flight. Rotation system fails in CCW orientation after two cycles. Digital recorder fails after 2.5 hours.

The original task of the thermal control system was the temperature regulation of the 33-GHz ferrite switch and the baseplate of the parametric amplifier. Thermal regulation of the paramp was necessary to achieve gain stability because of its large, -0.4 db/°K thermal gain coefficient. The heat generated by the regulating circuit and internal electronics in the paramp was dissipated through a mechanical support piece to the aluminum thermal ballast. This ballast was cooled in turn by conduction to the 33-GHz horn antenna whose mouths are exposed to the external airstream. The internal heater strips, mounted in the paramp's baseplate, were to regulate the critical baseplate temperature to 35 ± 0.1 °C achieving gain stability of ± 1%.

The offset of the ferrite switch also varies as a function of temperature. The thermal-drift coefficient of 17 ± 3 m°K/°K (change in offset, per change in physical temperature) was empirically determined from data taken in the laboratory and in flight. Its detailed origin is not understood. The connection of the horn antennas to the input ports of the ferrite switch provides a thermal short to the aluminum ballast, and thus, in principle reduces potential offset drifts. A 2.5 cm length of gold-plated thin-walled stainless steel waveguide, connected to the switch's output port, thermally isolates the switch from the parametric amplifier. This greatly reduces the thermal gradient across the body of the switch that would otherwise result if the heated baseplate of the parametric amplifier were thermally shorted to the ferrite switch.

Adequate thermal regulation was not achieved in flights 2 through 5. Only one of three embedded heater circuits in the paramp baseplate worked; the other two had been damaged by an improper mount. As a result, the aluminum block temperature cooled a few degrees during the flight, causing an amplifier gain drift of about +0.4 db/hour, and a ferrite switch offset drift of about 90 m°K/hour, or 3.2 m°K per 128 second rotation cycle.

After flight 5, installation of embedded resistive heaters in the aluminum thermal ballast and replacement of the parametric amplifier with mixer-based receivers improved the situation

dramatically. The thermal regulation of the aluminum thermal ballast reduced the temperature drift to less than 0.5 °K/hour, yielding an offset drift of about 0.3 m°K during a 128 second rotation cycle. The thermal gain coefficient of the mixer-based receivers was about a factor of 10 less than the parametric amplifier. A gain drift of less than 0.04 db/hour yields a drift of 0 0014 db per 128 second rotation cycle. If the ferrite switch offset were as large as 500 m°K then this would yield a signal drift of less than 0.2 m°K during the rotation cycle.

III.3 The Initial Data Flights (Flights 4-7)

In flights 4 and 5, flown in December 1976, the rms noise fluctuations were over three times the expected value based on laboratory measurements, Table III.3. Re-measurement after the flight showed that the noise temperature of the amplifier was between 500 and 700 °K, about twice the original value of 300 °K. This degradation in sensitivity partially explained the factor of three increase of the rms fluctuations observed in flight. The exact cause of the degradation is unknown. The amplifier was shipped back to the manufacturer in Boston, TRG division of Alpha, who re-optimized the pump power level to the varactor diode, and the diode bias current, with only marginal results; the noise figure improved some 100 °K. These flights were the last flown with the parametric amplifier. It became clear that a mixer-based receiver might have significant advantages over the parametric amplifier.

Table III.3 - Preliminary Data Flights with Parametric Amplifier

Flight	Equipment Configuration and Improvements	Flight Plan and Performance
4	Regrease rotation bearing, rebuild rotation electronics. Add four temperature sensors, accelerometer and voltage monitor to housekeeping system.	First data flight. Include an initial leg on this and all subsequent flights that allows the equipment temperatures to partially stabilize before data taking commences. Rotation system and Datel work properly. Paramp noise three times too high. Ferrite switch cools at 5 °K/hour. Paramp gain increases at 0.4 db/hour. Moon calibration.
5	Reduce antenna interchange period to once/64 seconds, reducing spurious signals due to gain drift.	Similar performance as in flight 4. Gather preliminary data.

A 33.0-GHz balanced mixer made by SpaceKom in Santa Barbara, California was procured in 1974 as a prototype receiver. Its measured noise temperature is 850 °K , for a system temperature of 920 °K including the insertion loss from upstream components. With a 500 MHz IF bandwidth the system sensitivity is $\pm 90\,\text{m°K}/\sqrt{\text{Hz}}$. We replaced the parametric amplifier with this mixer in flights 6 and 7 (Table III.4) for three reasons. First, the mixer's rms sensitivity is comparable to the degraded sensitivity of the paramp receiver. Secondly, its thermal

gain coefficient is about one tenth that of the paramp. Finally, its Gunn oscillator dissipates one third the heat of the parametric amplifier system.

III.4 Preliminary Data Flights with 'Old Mixer'		
Flight	Equipment Configuration and Improvements	Flight Plan and Performance
6	Replace paramp with 500 MHz IF bandwidth, 33.0-GHz mixer. Install resistive heaters in ballast, reducing temperature drift of ferrite switch. System noise temperature on ground is ± 90 m °K/$\sqrt{\text{Hz}}$.	Gain drift of reciever is less than 0.04 db/hour. Spurious interaction of block-heater current with 33-GHz radiometer likely responsible for increase of radiometer noise to ± 119 m °K/$\sqrt{\text{Hz}}$. Gather data, and perform moon calibration.
7	Increase isolation of heater current cureuit from 33-GHz radiometer. Regulate Datel recorder temperature with new heater cureuit. Include 180° phase-switch to monitor radiometer-arm-offset once every 128 seconds, a full rotation cycle	Radiometer noise improves to ± 100 m °K/$\sqrt{\text{Hz}}$. Gather data. Phase switching reveals 1.4 °K radiometer-arm-offset.

Although the radiometer system was undergoing intense development, the data from flights 4-7 did contain useful measurements of anisotropy of the 3 °K background. The hierarchy of switching techniques successfully canceled the bulk of the spurious signals due to systematic gain and offset drifts. And the receiver noise, though larger than planned, still allowed the equipment to record data with useful sensitivity. Section V.3 describes the role of the data from flights 4-7 in providing the initial evidence for cosine anisotropy. The U-2 aircraft provided an available and reliable platform that was free from mechanical and electrical interference to the equipment.

III.4 Final Data Flights (Flights 8-14)

During the period when the equipment was flown with the mixer, a new mixer-IF amplifier was ordered from SpaceKom. Mixer diode technology and FET performance had advanced to the point where a front-end mixer had comparable sensitivity to the original specifications of the parametric amplifier receiver. The new mixer has a noise temperature of 500 ± 100 °K and an IF bandwidth of 1000 MHz. Losses from the upstream isolator, ferrite switch, and antennas increase the system noise temperature by 30%, resulting in a measured system temperature of 670 ± 50 °K, for a sensitivity of 46 ± 4 m °K/$\sqrt{\text{Hz}}$.

Flight 8 initiated a series of seven flights with the equipment in an unchanging configuration, Table III.5. In flight 8 the 33-GHz receiver sensitivity was within 5% of the measurements made in the laboratory. The gain drift of the receiver, monitored by the noise power level after the detector diode, was less than 2% over the flight.

Table III.5 - Data Flights with 'New Mixer'

Flight	Equipment Configuration and Improvements	Flight Plan and Performance
8	Replace 500 MHz IF mixer with 1000 MHz IF mixer. Rms Sensitivity on ground is 47 ± 4 m°K/$\sqrt{\text{Hz}}$. Add mu-metal shielding to ferrite switch as a precaution against the earth's magnetic field. Null offset below 30 m°K in laboratory. Reduce 180° phase-switch period, monitoring radiometer-arm-offset every 24 seconds.	Sensitivity of 33-GHz receiver comparable to ground calibrations. Ferrite switch offset 30 m°K in flight. Rotation offset 2.2 ± 0.5 m°K. Moon calibration. Data quality much improved. Evidence of cosine anisotropy in data from flights 4-8.
9	Equipment 'can' unopened since previous flight	Late evening take-off at 10 PM (PST). Check for sign change of cosine anisotropy.
10	"	Sunset launch re-checks sign change of cosine anisotropy. Announcement of results at Washington APS meeting, April 1977 and at AAS meeting June 1977 *(Smoot, 1977a; Gorenstein, Smoot & Muller, 1977).*
11	"	Publish results *(Smoot, Gorenstein & Muller, 1977).*
12	"	Radiometer-arm-offset increased to 130 m°K. Rotation offset drops to 0.2 ± 0.5 m°K.
13	Open can for first time since closed for 8th flight. Null ferrite switch offset.	Orient flight plan to measure largest signal predicted from cosine anisotropy.
14	Open can again to null offset.	Collect anisotropy data, include moon calibration.

An ideal radiometer has a null output signal for balanced input signal to the antennas; a non-zero output is called the radiometer-arm-offset. The offset is mostly due to the imbalanced insertion loss between the two circulation directions of the ferrite switch that alternates at 100 Hz. Nulling the insertion loss imbalance of the ferrite switch below 20 m°K during pre-flight preparations reduces the radiometer-arm-offset below 60 m°K for most flights; periodic interchange of the antennas, once per 64 seconds, cancels the offset, and reduces spurious signals due to slow drifts in the offset below 0.2 m°K. The ferrite switch offset drift was a few millidegrees Kelvin during twenty minute periods of data taking. The radiometer-arm-offset was less than 50 m°K during flight 8. The succeeding flights yielded comparable performance, as shown in Figure III.1, with the exception of flight 12. For an unknown reason the radiometer-arm-offset increased to about 140 m°K, requiring the ferrite switch imbalance to be re-nulled after the flight.

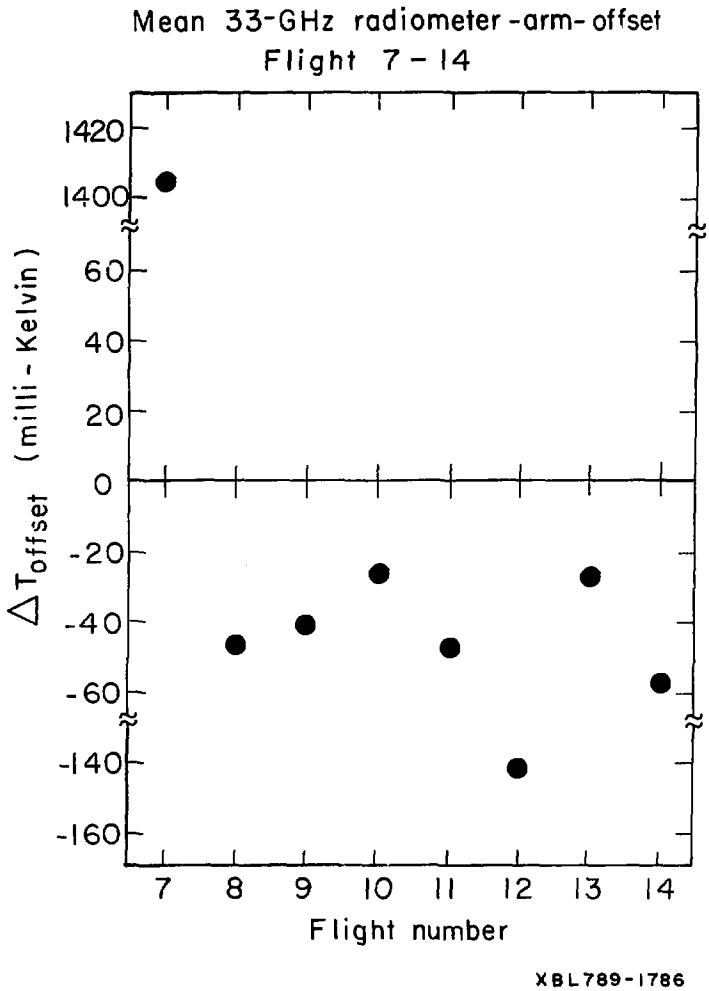

Figure III.1 - Mean 33-GHz Radiometer-arm-offset, Flight 7-14

III.5 Flight Plan and Sky Coverage

The flight plan for the ninth flight was a typical example of the data taking strategy used in flights 4-14. As in all data flights, this plan for the ninth flight was organized into segments called "legs", where a leg is a 17 to 20 minute period of straight-and-level flight terminated by a bank that re-orients the aircraft.* Legs are flown in pairs with opposing headings that cancel systematic effects intrinsic to the U-2 and 33-GHz radiometer system. Most data flights are composed of twelve legs. In the ninth flight, Fig. III.2, the U-2 first flew three pairs of legs, with alternate east-west headings, then after a 90° bank, the aircraft flew three additional pairs of legs, in alternate north-south headings.

Figure III.3 shows the sky coverage for flights 4-14 that resulted from this strategy. The latitude of the airfield, 37° north, and the 60° opening angle between the antennas restricts the expanse of the sky coverage to a region between +67° dec. and +7° dec. in the northern celestial hemisphere. The east-west oriented legs in flight nine measured anisotropy between areas in the sky separated 60° in declination; the corresponding sky coverage is illustrated as a pair of shaded capsules, one at 13.0 hours R.A., +7° dec. for the southward pointing antenna, and one at 13.0 hours R.A., +67° dec. for the northward pointing antenna. In the north-south legs the antennas point at the same declination. The eastward antenna points towards 16.8 hours R.A., +32° dec. and the westward antenna points towards 12.0 hours R.A., +32° declination. The FWHM of the antennas determines the 7° width of each capsule, and the earth's rotation in six 20 minute legs determines the 2 hour length of each capsule. We took care in the latter series of flights to avoid the galactic plane, a source of synchrotron radiation and HII emission.

*The combination of the earth's rotation and the aircraft's velocity sweeps an antenna beam 2 to 5° across the celestial sphere in 20 minutes. This swath is comparable to the 7° beam (FWHM) of the antennas, so little angular resolution is lost.

Figure III.2 - Geographical Flight Plan, Ninth Flight

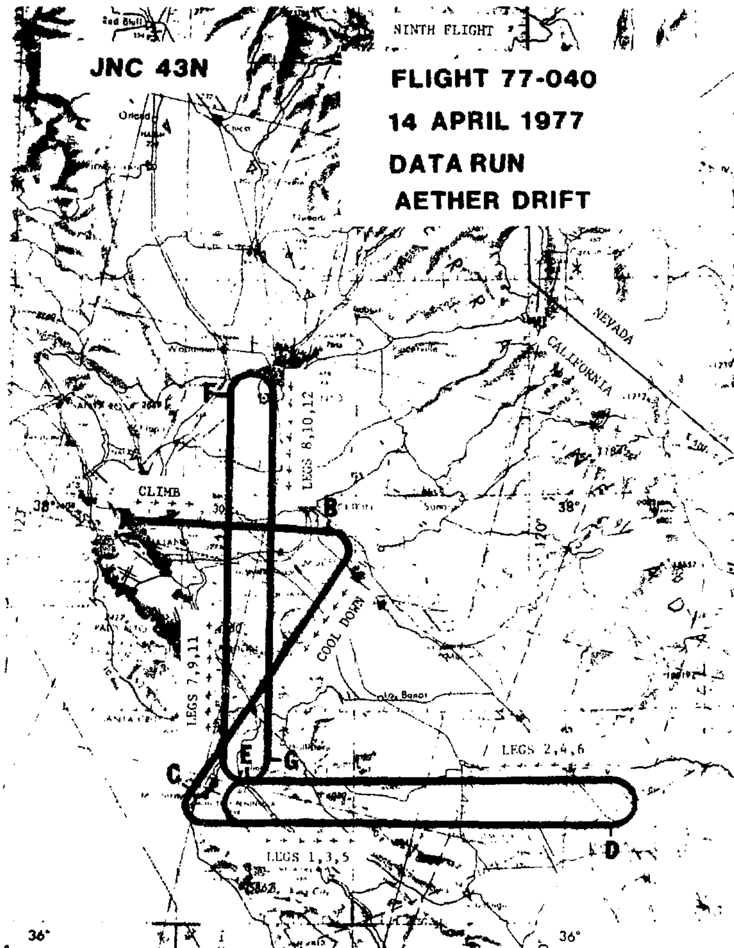

Figure III.3 - Sky Coverage, Flights 4-14

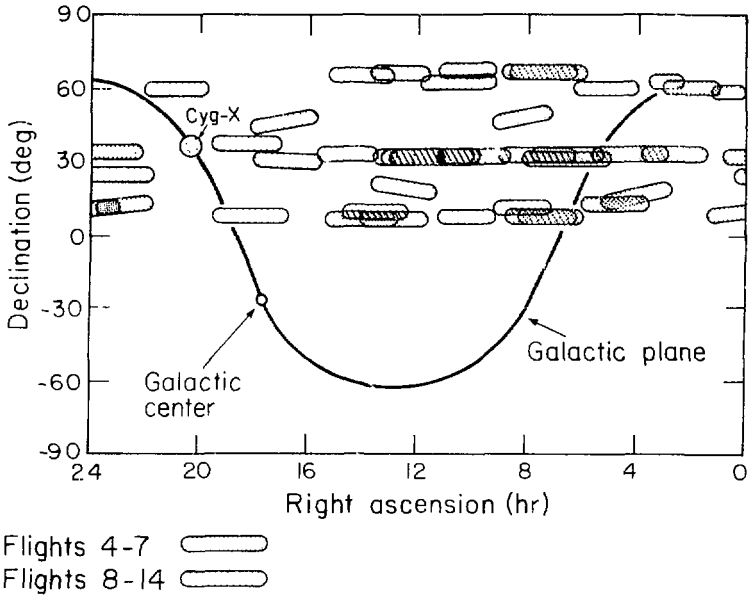

XBL 788-1594

Chapter IV - Data Reduction

IV.1 Introduction

The reduction and analysis of the flight data proceeds in three stages. In the first stage, computer programs display the 33-GHz data, the 54-GHz data, and the housekeeping data. This procedure, though crucial in the early phases of equipment development, mostly verified proper equipment operation in the later series of data flights and documented the equipment performance.

In the second stage, the inspected 33-GHz data are edited for spurious signals – mostly words recorded during antenna rotations – and then averaged. The averaging procedure groups the words according to the leg in which they were recorded. Each average – called a "leg-measurement" – is then a measurement of anisotropy between the directions that the antennas pointed at during the leg. Section IV.2 describes these stages in detail. The rms fluctuations for each leg-measurement are computed as described in section IV.4.

The final stages in the reduction process prepares the leg-measurements for the subsequent astrophysical analysis:

(1) A calibration constant converts the leg-measurements, recorded in empirical units, to units of antenna temperature in milli-degrees Kelvin. A series of pre-flight measurements determined the calibration constant for each receiver configuration.

(2) A computer program computes the directions that the antennas pointed at during each leg and assigns these directions, expressed in celestial coordinates, to the corresponding leg-measurement.

(3) Slight adjustments to the leg-measurements corrects for spurious galactic and atmospheric emission.

(4) A final correction converts the calibrated and corrected measurements from differential antenna temperature to differential physical temperature of a 3 °K radiation spectrum.

Section IV.3 and its subsections describe these steps in detail.

The procedures that monitor radiometer gain and determine radiometer calibration are described in Appendix E. Appendix F documents the slight corrections applied to the leg-measurements for galactic and atmospheric emission. A constant offset, of unknown origin, subtracted from the leg-measurements prior to astrophysical analysis is discussed in section IV.3c and is the subject of Appendix G. Section IV.5 describes the deletion of several spurious leg-measurements, and Section IV presents the reduced data from flights 4 through 14. The effect of spurious terrestrial thermal emission on the data is discussed in section IV.7.

IV.2 Editing and Averaging the 33-GHz Anisotropy Data

Figure IV.1 diagrams the data reduction process from acquisition to the final stage of astrophysical analysis. This section concentrates on the **Edit, Average,** and **Display** procedures which extract measurements of anisotropy from the flight data.

In the post-flight analysis, **Average** reduces the 33-GHz data recorded in each leg into a single measurement of anisotropy. The units are empirical, determined by the lock-in amplifier gain setting, and the 12 bit resolution of the Datel LPS-16 data logger. In the following discussion, these averages will be referred to as ΔT_{leg}, both individually and collectively, depending on the context.

Every two seconds at altitude the Datel logger digitizes the integrated 33-GHz anisotropy signal and records it on a cassette tape. This yields one 33-GHz data word. In the **Edit** stage, data words recorded during antenna rotations and aircraft banks are automatically removed. The **Edit** routine retains 56 seconds of data taken during the 64 seconds between rotations. Data words are deleted by hand if inspection of the 54-GHz roll monitor indicates a spurious roll of more than 1°, or if there appears to be fluctuation in the 33-GHz data which are inconsistent with Gaussian statistics. Only 5 minutes of spurious data were deleted from the 38 hours collected in flights 4-14 due to spurious rolls. A deletion of 40 seconds of data from flight 10 removed two spikes in the 33-GHz data inconsistent with receiver noise fluctuations. The 33-GHz, 54-GHz, and housekeeping data are **Display**-ed in time plots or scatter plots. These plots, made at various stages in the editing process facilitate inspection for spurious signals and allow a graphical check of proper equipment performance.

In averaging the data, account must be taken of the 180° phase reversal which occurs every 12 seconds. If we first consider only the data taken in one phase state, then the difference between the 33-GHz data words recorded when the antennas were oriented clockwise (CW) and those recorded when the antennas were oriented counterclockwise (CCW) is the desired measurement of anisotropy, or ΔT_{leg}.

Thus,

$$\Delta T_{leg} = [\Delta T_{CW} - \Delta T_{CCW}]/2 \qquad \text{IV.1}$$

where

ΔT_{CW} and ΔT_{CCW} are the mean of the 33-GHz data words recorded in the CW or CCW antenna orientations, respectively, during the legs.

The subtraction cancels the fixed radiometer-arm-offset, ΔT_{offset}, which is mainly due to the insertion loss imbalance between the input arms of the ferrite switch.

Figure IV.1 - Data Processing Flow Chart

Cassette Tape

Display

Display
Graphical display routines. Scatter plots and histograms of 33-GHz data words vs. time, and vs. housekeeping signals.

Edit
Remove 33-GHz data words taken during banks, antenna rotations, spurious aircraft rolls, and spurious fluctuations.

Statistics
Auto- and cross-correlation and signal-average routines. Check for Gaussian statistics.

Display

Average
Compute ΔT_{leg}, ΔT_{offset}, and rms fluctuations in data. Summarize housekeeping data.

Cover
Compute antenna directions from flight plan corresponding to ΔT_{leg}.

Correct
Subtract spurious astrophysical and roll signals from data, ΔT_{var}. Remove mean rotation offset, ΔT_{rot}, and calibrate leg-measurements to arrive at $\Delta T_{3°K}$.

Astrophysical Analysis
Fit data to dipole and quadrupole hypothesis.

Include $\Delta T_{3°K}$ from other flights.

The 180° phase switching complicates the data reduction but allows ΔT_{offset} to be determined more accurately. The switching is performed automatically every 12 seconds, resulting in an independent determination of ΔT_{leg} for the data collected in each phase state. We now give the complete algebraic expressions computed in the **Average** stage that extract ΔT_{leg} and ΔT_{offset} from the data.

The analysis first computes the four quantities ΔT_{CW+}, ΔT_{CCW+}, ΔT_{CW-}, and ΔT_{CCW-}. The quantity ΔT_{CW+} is given by

$$\Delta T_{CW+} = \frac{1}{N_{CW+}} \sum_{i=1}^{N_{CW+}} \delta T_{CW+} \qquad \text{IV.2}$$

where

N_{CW+} is the number of measurements recorded in the leg with antennas in CW orientation, and with the lock-in demodulation phase set at 0°.

δT_{CW+} is the i^{th} 2-second integration of the 33-GHz signal (33-GHz data word) recorded on cassette tape with the radiometer in the CW+ state.

ΔT_{CW+} is the mean measurement of anisotropy with the equipment in the CW+ state.

The three remaining quantities ΔT_{CCW+}, ΔT_{CW-}, and ΔT_{CCW-} are computed in a similar manner.

These quantities are equal to the following sums:

$$\Delta T_{CW+} = \Delta T_{leg} + \Delta T_{offset} + T_{DC\ level} \qquad \text{IV.3a}$$

$$\Delta T_{CCW+} = -\Delta T_{leg} + \Delta T_{offset} + T_{DC\ level} \qquad \text{IV.3b}$$

$$\Delta T_{CW-} = -\Delta T_{leg} - \Delta T_{offset} + T_{DC\ level} \qquad \text{IV.3c}$$

$$\Delta T_{CCW-} = \Delta T_{leg} - \Delta T_{offset} + T_{DC\ level} \qquad \text{IV.3d}$$

where

$T_{DC\ level}$ is the mean radiometer output in the absence of all signals.

The leg-averages are combined extracting these quantities as follows (these expressions are only illustrative; in practice their evaluation includes the weighting factors $\frac{1}{N_{CW+}}$ etc.):

$$\Delta T_{leg} = [(\Delta T_{CW+} - \Delta T_{CCW+}) - (\Delta T_{CW-} - \Delta T_{CCW-})]/4 \qquad \text{IV.4a}$$

$$\Delta T_{offset} = [(\Delta T_{CW+} + \Delta T_{CCW+}) - (\Delta T_{CW-} + \Delta T_{CCW-})]/4 \qquad \text{IV.4b}$$

$$\Delta T_{sky\ signal} = [(\Delta T_{CW+} - \Delta T_{CCW+}) + (\Delta T_{CW-} - \Delta T_{CCW-})]/4 \qquad \text{IV.4c}$$

$$T_{DC\ level} = [(\Delta T_{CW+} + \Delta T_{CCW+}) + (\Delta T_{CW-} + \Delta T_{CCW-})]/4 \qquad \text{IV.4d}$$

$\Delta T_{co-signal}$ is a check of the DC level. It has an expectation value of zero.

Figure IV.2 displays the four quantities defined in eq. IV.4 for the twelve legs in the ninth flight. The error bars are statistical only, and indicate the one-standard-deviation limits. There are three things to note: (1) Anisotropy in the cosmic background radiation is evident in the last six legs as an alternation of ΔT_{leg} by about 2m°K about the mean. These legs were flown in alternate north-south headings. (2) The mean value of ΔT_{leg} for all legs in the flight is 2.5 ± 0.5 m°K. This non-zero mean is called the rotation offset, ΔT_{rot}, and is discussed in section IV.3c and Appendix G. (3) The radiometer-arm-offset, ΔT_{offset}, drifts from -72 m°K in the first leg to about -25 m°K by the end of the twelfth leg.

IV.3 Calibrations and Corrections to the Leg-measurements

The **Correct** stage calibrates and modifies each leg-measurement ΔT_{leg}, arriving at a set of measurements of anisotropy in the 3°K radiation. Thus

$$\Delta T_i °K = (\Delta T_{i,v} \cdot C - \Delta T_{i,a} - \Delta T_{rot}) \frac{dT_P}{dT_i} \qquad \text{IV.5}$$

where

ΔT_i°K is the measured anisotropy in milli-degrees Kelvin from a leg's worth of data.

C is the calibration constant that converts the empirical units that ΔT_{leg} are digitized in to antenna temperature expressed in milli-degrees-Kelvin. The calibration procedure is described in section IV.3a.

$\Delta T_{i,a}$ are galactic and atmospheric corrections of a few tenths of a milli-degree that are discussed in section IV.3b.

ΔT_{rot} is a constant contribution to ΔT_{leg} of about 2 m°K, discussed in section IV.3c.

$\frac{dT_P}{dT_i}$ is a scale change that converts antenna temperature, measured by the radiometer, to the change in the physical temperature of the 3°K spectrum. $\frac{dT_P}{dT_i} = 1.024$ for $T_P = 3$°K and $\nu = 33$GHz, as discussed in IV.3d.

IV.3a The Calibration Constant C for the 33-GHz Radiometer

Before the Datel logger records a measurement of anisotropy the 33-GHz receiver amplifies the 3°K radiation over 120 db while processing it through three stages of mixing, detection, and demodulation. Useful measurements of anisotropy require that the system gain be stable during the data flights and constant from flight to flight. Also, the measurement technique employed in measuring the system gain, *i.e.* radiometer calibration, be accurate and reproducible.

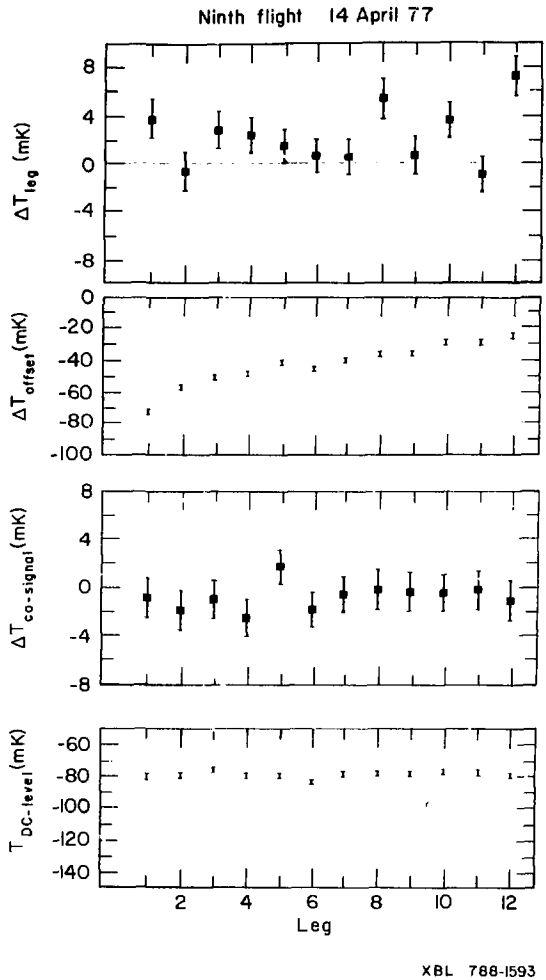

Figure IV.2 - Mean Radiometer Signals by Leg, Ninth Flight

The mixer-based receiver is a stable device: in-flight measurement of its relative gain and noise temperature are measured to be constant within ± 1% during flights, and from flight to flight. Ground based measurements, performed with blackbody targets filling the antenna beam patterns, determine the calibration constant C, eq. IV.5, with a ± 3% error

The ground based measurement involves covering the 33-GHz antenna mouths with black-body targets at room temperature (290 °K) and at liquid nitrogen temperature(77 °K). The radiometer configuration using the SpaceKom receiver was calibrated in this manner during the pre-flight preparations for flights 8, 13, and 14, and three more times after flight 14. The six measurements fluctuate ± 2% about their mean; this fluctuation, the primary uncertainty in receiver calibration, is small compared to the ± 10% statistical error on the amplitude of cosine anisotropy, presented in the next chapter.

The moon legs provide an important in-flight cross-check on the receiver calibration. Uncertainty in the emission temperature across the lunar surface limits the accuracy of the moon calibration to ± 5%. Within these errors, it confirms the ground based calibration procedures. Appendix E describes in more detail the in-flight monitoring of receiver noise temperature and relative gain, and the procedures, errors, and the techniques and results of the ground based and lunar radiometer calibrations.

IV.3b The Galactic and Atmospheric Corrections, ΔT_{cal}

Corrections to the leg-measurements for microwave emission from the galaxy and from unbalanced emission from atmospheric oxygen has small impact on the astrophysical results reported here. In the worst case these corrections, in the data from flights 8-14, are 15% of the one σ errors in the leg-measurements, and, as shown in Chapter V, change the measured cosine anisotropy by less than 30% of its one-standard deviation error.

The net correction, ΔT_{cal}, applied to the data in the **Correct** stage is the sum of the following quantities:

$$\Delta T_{cal} = \Delta T_{synchrotron} + \Delta T_{HII} + \Delta T_{O_2\ diff} + \Delta T_{earth\ orbit} \qquad IV.6$$

The corrections for galactic synchrotron and HII emission, $\Delta T_{synchrotron}$, and ΔT_{HII}, are extrapolations from maps made at lower frequency to our observation frequency of 33 GHz. The data is also slightly modified by the 0.3m °K anisotropy due the motion of the earth about the sun, $\Delta T_{earth\ orbit}$. Appendix F describes these corrections in more detail.

IV.3c The Rotation Offset Correction, ΔT_{rot}

The rotation offset is a spurious oscillation in the 33-GHz data words at the antenna rotation period. It appears as a constant signal in ΔT_{leg} in the absence of celestial anisotropy. In flights 8-14 the mean value of the rotation offset was about 2m°K and stable throughout a flight; its origin is not yet understood despite several determined investigations.

The periodic reversal of the aircraft heading throughout the flight allows us to measure ΔT_{rot} and subtract it from the data in the **Correct** stage. Although this empirical correction is the largest one applied to the leg-measurements, the subtraction of a constant does not significantly alter the best fit parameters of cosine anisotropy. Figure IV.3 plots the value of ΔT_{rot} for each flight, 4-14, and Appendix G discusses possible origins for the rotation offset.

IV.3d Conversion of Antenna Temperature to Thermodynamic Temperature, $\frac{dT_A}{dT_P}$

A final 2.4% correction accounts for the departure of the 3°K spectrum from the classical Rayleigh-Jeans spectrum at 33 GHz. For $T_P = 3$°K and $\nu = 33$ GHz, $\frac{h\nu}{kT_P} = 0.53$, and the detailed Planckian spectrum must be taken into account. Thus, from the relationship between physical temperature, T_P, and antenna temperature, T_A, given in eq. II.4,

$$T_A = T_P \frac{\alpha}{e^{\alpha}-1} \qquad \text{IV.7}$$

where

$$\alpha = \frac{h\nu}{kT_P} \ . \qquad \text{IV.8}$$

We find for $T_P = 3$°K, $\nu = 33$GHz, that

$$\frac{dT_A}{dT_P} = \frac{\alpha^2 e^{\alpha}}{(e^{\alpha}-1)^2} = \frac{1}{1.024} \ . \qquad \text{IV.9}$$

IV.4 Radiometer Sensitivity

Programs in the **Average** and **Statistics** stage compute the rms fluctuations of the recorded 33-GHz data words about the means given in eq. IV.3. Combining the measurements recorded during all legs of flights 8-14 we find the 33-GHz receiver sensitivity to be

$$\sigma_{33\text{-}GHz} = 45.58 \pm 0.09 \pm 1.8 \text{ m°K}/\sqrt{\text{Hz}} \qquad \text{IV.10}$$

where the initial error is statistical, and the final error comes from uncertainty in the radiometer

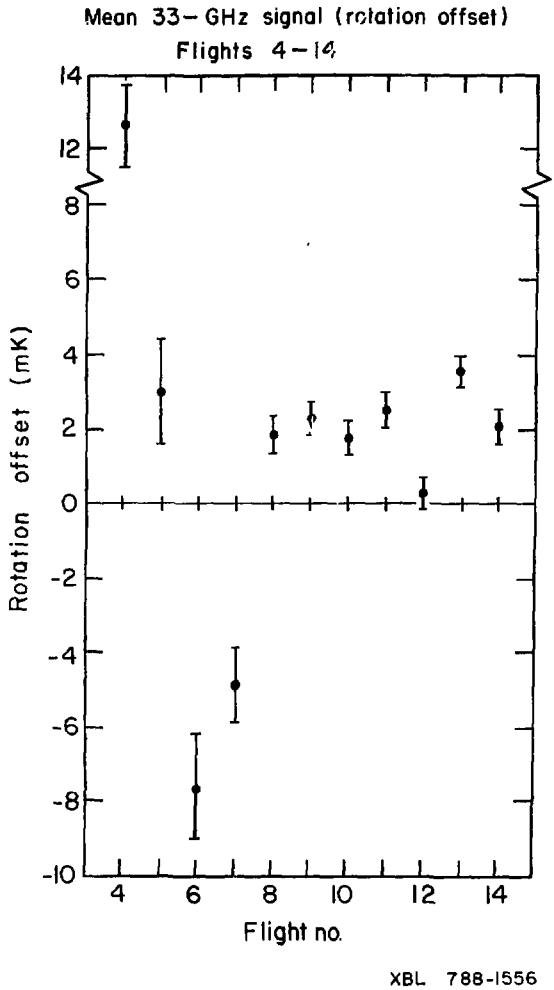

Figure IV.3 - Mean 33-GHz Signal (Rotation Offset), Flights 4-14

calibration. The initial error agrees with the expected uncertainty due to receiver noise and is evidence that the receiver gain between flights is stable to about ± 0.2%. The residual fluctuations about the mean values in eq. IV.3 are expected to be uncorrelated and distributed as Gaussian noise. The programs in **Statistics** contain auto- and cross-correlation routines that analyze the 33-GHz data words recorded in each flight.

In flights 8-14 the auto-correlation coefficients for time displacements for 2 to 128 seconds were consistent with zero, with a statistical sensitivity of ±4 m°K. The signal-averaging, performed at the rotation period, yielded a sensitivity of ±3.7 m°K for each bin that corresponded to a 33-GHz data word. The signal-average results were consistent with uncorrelated noise. The earlier flights produced anomalous results in these tests. In flights 4-7, auto-correlation of the 33-GHz data words revealed oscillations with time periods of 40 to 120 seconds, and amplitudes that varied from 10 to 45 m°K. In the latter 4 legs of flight 6, these oscillations were synchronous with the rotation period of 128 seconds. The block-heater current also showed periodic behavior in these latter legs, indicating a likely connection. (These correlations are not understood in detail.) The replacement of the parametric amplifier with the SpaceKom mixer and improvements in the isolation of the heater circuits seem to have corrected this problem. We believe that the data is still useful without a definitive identification of the source of these oscillations. Systematic signals in ΔT_{fcg} tend to cancel as the aircraft heading is periodically reversed throughout a flight. The mean values of ΔT_{fcg} for flights 4-7 are used for some astrophysical analysis with the rms errors empirically determined from the data. The final analysis in Chapter V concentrates on the data from flights 8-14 because it is the data of the best quality taken with the equipment in unchanged configuration.

IV.5 Spurious Leg-measurements

The data from the first six legs of flight 10 are excluded from the final astrophysical analysis because of slight contamination due to the sun. Take-off for the tenth flight preceded sunset on the ground, and at the 20-km altitude the sun was above the horizon for a prolonged period. The sun was far enough from the main beam of the antenna that microwave radiation into that antenna sidelobes was minimal. However the direct heating from the sun caused an oscillation of the antenna mouth temperature as the antennas rotated. The data from the temperature sensors in the mouths of the horn antennas clearly show the effect of the warming due to the sun, during the initial six legs, and the abrupt cessation of anomalous heating at sunset. A rough upper limit to the resulting spurious signal would be a few tens of milli-degrees Kelvin, as the antennas are heated about 1 °K and the net emissivity of the antenna is about 0.03. Examination of the leg-measurements shows that the effect is less than about 4 m°K.

The data from the initial two legs from flight 6 are also deleted from the data analysis. The value of the initial leg-measurement is inconsistent with the succeeding measurements, probably because of the rapid temperature changes that took place at the first exposure of the equipment to the environment.

IV.6 Anisotropy Data from Flight 4-14

Table IV.1 presents the measurements of 33-GHz anisotropy from flights 4-14. The sign convention is

$$\Delta T_3\text{°K} = T(\hat{n}_1) - T(\hat{n}_2) \qquad \text{IV.11}$$

where

$T(\hat{n}_i)$ is the temperature of the 3 °K background radiation in the $\hat{n}_i$ direction.

$\hat{n}_1$ is the direction of the antenna on the pilot's right. $\hat{n}_2$ is the direction of the antenna on the pilot's left.

Cover determines the $\hat{n}_1$ and $\hat{n}_2$ directions from the flight plan. The input data are the geographical position at the start of a leg, the heading of the U-2, its ground speed, and the start and end times of the leg. Table IV.1 also lists these mean antenna directions in celestial coordinates that **Cover** determines from these data.

Another useful set of coordinates that will be referred to in Chapter V are called the rectangular celestial coordinates. They are an orthonormal set of vectors pointing along axes defined in terms of the celestial coordinates, Table IV.2.

Table IV.2 - Rectangular Celestial Coordinates

unit vector	R.A. (hours)	dec. (degrees)
$\hat{n}_x$	0	0°
$\hat{n}_y$	6	0°
$\hat{n}_z$	-	+90°

Two cross-checks verify the sense of the sign given for ΔT_3 °K in eq. IV.11. First, right-banks of the aircraft inject a "hot" 23m °K atmospheric signal into the 33-GHz antenna direction on the pilot's right, and left-banks give a similar "hot" signal in the antenna direction on the pilot's left. The bank data are reduced in the **Average** program along with the anisotropy data, and give the sign of ΔT_{bank} as positive for a "hot" signal on the pilot's right, and negative for a "hot" signal on the pilot's left, checking the sign conventions.

Table IV.1 - Measurements of Anisotropy of 3°K Radiation, Flights 4-14

FLIGHT	LEG	TIME (UT)	SIGNAL (MK)	SIGMA (MK)	$\hat{n}_1$ R.A. (HR)	$\hat{n}_1$ DEC (DEG)	$\hat{n}_2$ R.A. (HR)	$\hat{n}_2$ DEC (DEG)
4	1	2 22	-4.45 +/- 2.70	22.22	10.9	1.39	59.3	
4	2	2.50	5.57 +/- 2.77	1.73	59.1	22.57	10.6	
4	3	3.13	-1.22 +/- 2.85	22.07	10.9	2.14	59.3	
4	4	3.36	.17 +/- 2.77	2.51	59.1	23.35	10.6	
4	6	4.21	3.24 +/- 2.39	3.07	32.4	22.63	32.4	
4	7	4.52	-4.51 +/- 2.85	23.17	32.4	4.01	32.4	
5	1	3. 3	-.97 +/- 3.12	23.26	10.9	2.44	59.3	
5	2	3.29	4.10 +/- 3.41	2.78	58.5	23.57	10.7	
5	3	3.48	-2.04 +/- 4.86	.33	9.2	2.76	63.3	
5	4	4.11	-4.58 +/- 3.57	2.96	63.4	.75	8.3	
5	6	4.57	3.19 +/- 2.66	4.54	32.6	23.69	32.6	
5	7	5.30	-1.89 +/- 2.93	.26	32.4	5.10	32.4	
6	3	2.43	5.79 +/- 3.72	4.68	11.9	1.23	57.4	
6	4	3. 5	-4.20 +/- 3.72	1.62	57.2	5.06	11.8	
6	5	3.26	-.18 +/- 3.58	5.41	12.0	1.95	57.4	
6	6	3.48	-4.97 +/- 3.97	2.33	57.2	5.78	11.8	
6	7	4.10	1.38 +/- 3.53	7.41	47.6	3.09	18.6	
6	8	4.32	2.19 +/- 3.92	3.59	16.8	7.77	51.6	
6	12	5.10	10.74 +/- 3.68	4.32	14.7	8.38	48.9	
6	13	5.33	-10.29 +/- 3.87	8.78	48.8	4.72	14.5	
7	1	2.47	-2.63 +/- 2.99	6.47	6.7	6.47	66.7	
7	2	3.13	-2.55 +/- 2.79	6.90	66.5	6.90	6.5	
7	3	3.37	-.65 +/- 2.74	7.31	6.7	7.31	66.7	
7	4	4. 0	1.33 +/- 2.89	7.70	66.5	7.70	6.5	
7	5	4.24	8.43 +/- 3.09	8.09	6.7	8.09	66.7	
7	6	4.47	-.05 +/- 2.94	8.49	66.5	8.49	6.5	
7	7	5. 8	2.89 +/- 2.79	11.15	32.9	6.34	31.1	
7	8	5.32	-3.11 +/- 2.94	6.70	33.0	11.52	31.1	
7	9	5.55	.68 +/- 2.94	11.94	32.9	7.12	31.1	
7	10	6.18	-3.07 +/- 2.65	7.47	33.0	12.28	31.1	
8	1	2.37	1.42 +/- 1.25	7.13	6.5	7.13	66.5	
8	2	2.55	-2.32 +/- 1.55	7.53	66.8	7.53	6.8	
8	3	3.14	.32 +/- 1.56	7.85	6.7	7.85	66.7	
8	4	3.31	-.64 +/- 1.49	8.13	66.8	8.13	6.8	
8	5	3.48	2.62 +/- 1.57	10.75	32.1	5.93	32.1	
8	6	4. 6	-2.80 +/- 1.56	6.25	32.1	11.07	32.1	
8	7	4.23	-.52 +/- 1.66	11.33	32.0	6.51	32.0	
8	8	4.42	-1.92 +/- 1.60	6.85	32.1	11.67	32.1	
8	9	5. 1	4.31 +/- 1.60	11.97	32.1	7.15	32.1	
8	10	5.18	-1.11 +/- 1.58	7.45	32.2	12.28	32.2	
9	1	6.39	2.57 +/- 1.61	12.10	6.5	12.10	66.5	
9	2	6.58	-2.21 +/- 1.62	12.42	66.7	12.42	6.7	
9	3	7.16	1.11 +/- 1.57	12.72	6.5	12.72	66.5	
9	4	7.34	.62 +/- 1.52	12.68	66.5	13.15	6.7	
9	5	7.52	-.43 +/- 1.40	13.32	6.5	13.32	66.5	
9	6	8. 9	-1.40 +/- 1.43	13.27	66.5	13.74	6.7	
9	7	8.26	-2.10 +/- 1.49	16.20	31.4	11.39	32.3	
9	8	8.44	3.30 +/- 1.63	11.72	32.4	16.93	31.4	
9	9	9. 2	-2.34 +/- 1.61	16.82	31.9	12.01	31.9	
9	10	9.20	1.23 +/- 1.45	12.32	31.9	17.14	31.9	
9	11	9.40	-4.30 +/- 1.56	17.45	31.9	12.44	31.9	
9	12	9.58	4.78 +/- 1.62	12.92	31.9	17.76	31.9	
10	7	3.16	1.79 +/- 1.56	11.39	32.8	6.58	31.0	
10	8	3.34	-2.81 +/- 1.48	6.91	32.8	11.71	31.0	
10	9	3.55	1.82 +/- 1.59	9.75	6.2	9.78	66.2	
10	10	4.14	-1.86 +/- 1.64	10.10	66.4	10.10	6.7	

Table IV.1 (continued)

FLIGHT	LEG	TIME (UT)	SIGNAL (MR)	SIGMA (MR)	$\hat{n}_1$ R.A. (HR)	$\hat{n}_1$ DEC (DEG)	$\hat{n}_2$ R.A. (HR)	$\hat{n}_2$ DEC (DEG)
10	11	4.37	.68 +/- 1.51		10.52	6.3	10.29	66.2
10	12	4.58	.41 +/- 1.58		10.89	66.7	10.77	6.7
11	1	3.45	.98 +/- 1.39		12.92	10.1	9.99	60.7
11	2	4. 4	1.95 +/- 1.66		10.41	61.3	13.18	9.6
11	3	4.27	1.66 +/- 1.62		13.54	10.1	10.61	60.6
11	4	4.40	-2.44 +/- 1.57		11.01	61.3	13.78	9.6
11	5	4.58	-.57 +/- 1.64		14.06	9.6	11.23	61.4
11	6	5.17	1.33 +/- 1.70		11.53	60.4	14.44	9.8
11	7	5.32	-4.24 +/- 1.54		16.23	46.9	11.84	18.7
11	8	5.50	2.83 +/- 1.57		12.13	19.2	16.55	46.5
11	9	6. 7	-2.66 +/- 1.69		16.82	45.4	12.36	19.8
11	10	6.25	1.71 +/- 1.50		12.79	18.1	17.13	48.0
11	11	6.43	-4.28 +/- 1.62		17.42	45.9	12.98	19.5
11	12	7. 0	4.13 +/- 1.52		13.15	21.4	17.71	43.5
12	1	3. 8	-1.62 +/- 1.42		17.29	8.9	20.14	59.6
12	2	3.28	.98 +/- 1.57		20.48	59.6	17.62	8.9
12	3	3.46	.55 +/- 1.57		17.92	8.9	20.78	59.6
12	4	4. 4	.55 +/- 1.46		21.08	59.6	18.22	8.9
12	5	4.22	2.83 +/- 1.58		18.53	8.9	21.38	59.6
12	6	4.40	-2.68 +/- 1.60		21.68	59.6	18.82	8.9
12	7	4.57	-2.00 +/- 1.56		22.17	25.1	17.46	39.9
12	8	5.15	2.34 +/- 1.55		17.75	39.0	22.46	25.1
12	9	5.34	-.07 +/- 1.52		22.79	25.1	18.08	39.0
12	10	5.52	2.11 +/- 1.56		18.37	39.0	23.08	25.0
12	11	6.10	-5.09 +/- 1.49		23.39	25.1	18.68	39.0
12	12	6.28	2.64 +/- 1.52		18.97	39.0	23.68	25.0
13	1	2.18	2.65 +/- 1.50		6.83	31.5	2.04	31.5
13	2	2.37	-3.61 +/- 1.62		2.38	31.4	7.16	31.4
13	3	2.56	1.79 +/- 1.62		7.46	31.5	2.68	31.5
13	4	3.14	-3.63 +/- 1.57		2.99	31.4	7.78	31.4
13	5	3.33	5.67 +/- 1.52		8.08	31.4	3.29	31.4
13	6	3.51	-2.26 +/- 1.61		3.61	31.4	8.39	31.4
13	7	4. 8	-1.90 +/- 1.50		7.34	9.7	4.38	59.7
13	8	4.26	-2.31 +/- 1.52		4.70	59.5	7.69	9.9
13	9	4.45	2.05 +/- 1.61		7.96	9.7	5.00	59.7
13	10	5. 3	-1.67 +/- 1.51		5.32	59.5	8.26	9.9
13	11	5.22	2.18 +/- 1.52		8.58	9.7	5.62	59.7
13	12	5.40	.18 +/- 1.57		5.93	59.5	8.88	9.9
14	1	3.48	-.78 +/- 1.63		13.80	30.7	9.06	30.7
14	2	4. 6	-1.20 +/- 1.56		9.39	30.7	14.09	30.7
14	3	4.27	-.73 +/- 1.64		14.46	30.7	9.71	30.7
14	4	4.44	1.54 +/- 1.58		9.90	30.7	14.72	30.7
14	5	5. 2	.01 +/- 1.66		15.01	29.6	10.28	31.5
14	6	5.21	-.23 +/- 1.60		10.60	30.7	15.34	30.7
14	7	5.39	-.03 +/- 1.74		13.34	9.4	13.34	66.4
14	8	5.56	1.73 +/- 1.56		13.36	66.6	13.36	9.6
14	9	6.15	-.19 +/- 1.66		13.99	9.4	13.99	66.4
14	10	6.32	1.41 +/- 1.57		13.96	66.6	13.96	9.6
14	11	6.49	-2.37 +/- 1.72		14.51	9.4	14.51	66.4
14	12	7. 9	-1.76 +/- 1.49		14.53	66.6	14.53	9.6

The moon legs provide an additional check of the sign convention. **Cover** computes $\hat{n}_1$ and $\hat{n}_2$ for the moon legs, and **Average** determines the value of ΔT_{moon}. Again, the moon on the pilot's right gave a positive signal as expected. The astrophysical analysis in the next chapter uses ΔT_{moon} as a check of the sign convention for the fit to cosine anisotropy.

IV.7 Systematic Errors due to Earth-Shine

Anisotropic terrestrial emission (earth-shine) into the antenna's sidelobes is a potential source of spurious signals. The earth's surface emits thermal radiation near 300 °K into the sidelobes of the 33-GHz horn antennas. Variations in the emissivity between features of the earth's surface that illuminate the sidelobes prevents the complete cancellation of the terrestrial signal between the antennas. Because anisotropic earth-shine is correlated with geography, reversing the heading of the U-2 between data legs does not cancel this signal. Rather the low sidelobes of the 33-GHz corrugated horn antennas reduce this signal to a low level. Integration of the measured antenna power patterns show that the sidelobes should reduce anisotropic emission below 0.2m °K.

Two tests performed with the data confirm this result to about the 0.5m °K level. First, the leg-measurements were fit to a model of cosine anisotropy and terrestrial emission. For example, a fit to the data for a signal with fixed east-west geographical orientation gave a measurement of 0.3 ± 0.5 m °K, westward direction cold. The second test investigated the data taken during the banks of the U-2. During a bank, one antenna is lowered about 20° in elevation, thereby receiving additional radiation in its earth-directed sidelobes. But the errors on terrestrial emission extracted from the data collected during banks is comparable to the expected magnitude of the terrestrial signal. The resulting measurement, although consistent with our expectations, does not critically test the measurement of the antenna sidelobes. Thus we consider what effect a 0.2m °K signal would have on the data, in particular on the fit for cosine anisotropy.

A 0.2 m °K spurious signal added in an uncorrelated fashion to the leg-measurements would result in a negligible 1% increase in the ± 1.6 m °K statistical noise. However the 0.2m °K sidelobe signal is correlated with geographical features so during the course of a flight it would not tend to cancel as would a fluctuating signal. Fits were performed for a cosine anisotropy hypothesis that included the effects of terrestrial emission. The results were that a 0.2 m °K sidelobe signal correlated with the geographical features contributes a vector of magnitude 0.1 m °K. Rather than try building a detailed model of the terrestrial emission, we increase the statistical errors on the parameters of cosine anisotropy presented in the next chapter by 25%, from 0.4 to 0.5 m °K. We feel this adequately takes into account the present uncertainty on the magnitude of contamination due to anisotropic terrestrial emission.

Chapter V - Astrophysical Analysis

V.1 *Introduction*

The results of a fit for cosine (dipole) anisotropy to the data listed in Table IV.1, flights 8-14, are presented in Section V.2. A significant dipole amplitude of 3.6 ± 0.5 m°K gives clear evidence of anisotropy in the cosmic background radiation. This result is consistent with other selections of data from Table IV.1, as shown in section V.3. Tests that cross-check the analysis and verify the sign of the anisotropy are also presented. The cosine anisotropy found in this data is compared with other radiometric measurements of anisotropy on a large-angular-scale, Section V.4. Statistical tests performed on the data, described in Sections V.5 and V.6, place a 1 m°K limit on most components of quadrupole anisotropy and a 0.5 m°K limit on uncorrelated fluctuations in sky temperature (sky-roughness) on a 7° angular scale set by the antenna beam width.

A cosine anisotropy of about 3 m°K was anticipated from the sun's motion about the Milky Way Galaxy. Surprisingly, the anisotropy presented here points away from this motion. The inferred motion of the Milky Way Galaxy is over 500 km/sec relative to the sources of the 3°K background radiation. Section V.7 compares this result to other measurements of solar motion with respect to various selections of nearby groupings of galaxies. The conclusion to this thesis, Section V.8, summarizes the results of this work and describes future investigations of the angular properties of the 3°K background radiation.

V.2 The Cosine (Dipole) Anisotropy Measured in Flights 8-14

We now wish to measure the amplitude of cosine anisotropy present in the reduced data of Table IV.1. The following expression describes cosine (dipole) anisotropy in the 3°K background radiation:

$$T(\hat{n}) = T_o + \vec{T}\cdot\hat{n} \qquad \text{V.1}$$

where

$T(\hat{n})$ is the radiation temperature in the direction $\hat{n}$.

$\vec{T}$ is the amplitude and direction of a $\cos\theta$ anisotropy.

T_o is the mean temperature, not measured in this experiment.

Since the 33-GHz radiometer measures the *difference* temperature between the directions $\hat{n}_1$ and $\hat{n}_2$, the following equation models cosine anisotropy for the data in Table IV.1:

$$\Delta T(\hat{n}_1,\hat{n}_2) \equiv T(\hat{n}_1) - T(\hat{n}_2) = \vec{T}\cdot(\hat{n}_1 - \hat{n}_2) \qquad \text{V.2}$$

The sum of the squared deviations of the data from this model, S, is given by

$$S = \sum_{i=1}^{M} \frac{[\Delta T_{3\,\mathrm{K}}^{i} - \vec{T} \cdot (\hat{n}_1^i - \hat{n}_2^i)]^2}{\sigma_i^2} \qquad \text{V.3}$$

where

M is the number of leg-measurements included in the fit.

$\Delta T_{3\,\mathrm{K}}^{i}$ is the i^{th} leg-measurement in the fit.

$\hat{n}_1^i$ $\hat{n}_2^i$ are the antenna directions of the i^{th} measurement.

σ_i is the one-standard-deviation uncertainty in the i^{th} measurement, scaled from the rms fluctuations of the 33-GHz data words.

The vector $\vec{T}$ that minimizes S gives the best estimate of cosine anisotropy. Section H.1 describes the fitting procedure that computes $\vec{T}$ and its errors.

Minimizing S in eq. V.3 for the data from flights 8-14 determines $\vec{T}$ to be

$$|\vec{T}| = 3.61 \pm 0.43\,\mathrm{m\,^{\circ}K} \qquad \text{V.4}$$

$$\hat{T} = 11.23 \pm 0.37\,\text{hours R.A.},\ 19 \pm 6\ ^{\circ}\text{dec.}$$

The unit vector $\hat{T}$ points towards the "hotter" hemisphere. The errors in eq. V.4 are statistical only. Table V.1 summarizes the parameters that describe cosine anisotropy in the data from flights 8-14 together with their errors and correlation coefficients. These parameters are expressed in celestial coordinates, galactic coordinates, rectangular celestial coordinates, and finally for the rectangular diagonal coordinates that have uncorrelated errors. Errors expressed in rectangular coordinates have Gaussian distribution. Their computation is described in Appendix H, Section H.1. The errors on all parameters listed in this table are 25% larger than the statistical errors. As described in Section IV.7 this accounts for uncertainty in terrestrial emission into the antenna sidelobes.

Table V.2 compares each leg-measurement with the value of anisotropy calculated from the cosine fit. The value of S computed for the fit is 71.0 for the 76 measurements. The probability that S equals or exceeds 71.0 is given by the integral of a χ^2 distribution for $76 - 3 = 73$ degrees-of-freedom (DOF). We call this probability the confidence level. The confidence level for S of 71.0 for 73 DOF is about 55%. Figure V.1 plots $\Delta T_{3\,\mathrm{K}}^{i}$ versus the angle between $\vec{T}$ and the difference vector $(\hat{n}_1^i - \hat{n}_2^i)$. The curved line is the cosine anisotropy drawn in for comparison. In contrast to the cosine anisotropy, the horizontal line, $\Delta T = 0$, gives a poor fit to the data. The value of S for this null hypothesis is 171, and gives a confidence level, for 76 DOF, of less than 10^{-9}.

Figure V.2 is a sky map of the fitted cosine anisotropy summed with galactic backgrounds.

Table V.1 - Parameters of Cosine Anisotropy - Flights 8-14 Corrected Data

χ^2/ degrees of freedom = 71.0/73, confidence level = 55%

	Best fit Parameters[1]			Correlation Coefficients[2]		
Celestial Coordinates	amplitude (m°K) 3.61±0.54	R.A. (hours) 11.23±0.46	dec. (deg.) 19.0±7.5	$C_{(amp,\,dec)}$ +0.57	$C_{(amp,R.A.)}$ −0.07	$C_{(dec,R.A.)}$ +0.06
Galactic Coordinates	amplitude (m°K) 3.61±0.54	l^{II} (deg.) 229±19	b^{II} (deg.) +66.6±6.9	$C_{(amp,b)}$ +0.24	$C_{(amp,l)}$ −0.56	$C_{(b,l)}$ −0.17
Rectangular[3] *Coordinates*	T_x (m°K) −3.34±0.44	T_y (m°K) 0.68±0.40	T_z (m°K) 1.18±0.49	$C_{(x,y)}$ −0.04	$C_{(x,z)}$ −0.56	$C_{(y,z)}$ −0.01
Diagonalized[4] *Coordinates*	T_i (m°K) 3.07±0.59	T_j (m°K) 1.72±0.30	T_k (m°K) 0.80±0.39	$C_{(i,j)}$ 0.0	$C_{(i,k)}$ 0.0	$C_{(j,k)}$ 0.0

[1]Statistical errors have been uniformly increased by 25% to take into account systematic errors as described in text.

[2]See Appendix H, eq. H.16 for definition and normilization of correlation coefficients.

[3]Unit vectors point along rectangular celestial coordinate axes. Expressed in celestial coordinates, (hrs. R.A., °dec), these unit vectors point along $\hat{x} = (0, 0°)$, $\hat{y} = (6, 0°)$ and, $\hat{z} = (+90, -)$.

[4]Unit vectors point along axes where errors are uncorrelated. Expressed in celestial coordinates, (hrs. R.A., °dec), these unit vectors point along $\hat{i} = (11.94, 49.5°)$, $\hat{j} = (12.5, -39.8°)$ and, $\hat{k} = (6.23, -4.0)$.

Table V.2 - Comparison of Data to Cosine Anisotropy, *Flights 8-14*[1]

NUM	FLT	LEG	SIGNAL	SIGMA	$\hat{n}_1$ R.A.	$\hat{n}_1$ DEC	$\hat{n}_2$ R.A	$\hat{n}_2$ DEC	DIPOLE[2]	THETA[3]	DIFF[4]	DCHI[5]	CHI-SQ[5]
1	8	1	1.92	+/- 1.25	7.13	6.5	7.13	66.5	.02	89.7	1.90	1.3	1.3
2	8	2	-2.32	+/- 1.55	7.53	66.8	7.53	6.8	-.22	93.4	-2.10	1.8	3.1
3	8	3	.32	+/- 1.56	7.85	6.7	7.85	66.7	.35	84.5	-.03	.0	3.1
4	8	4	-.64	+/- 1.49	8.13	66.8	8.13	6.8	-.47	97.4	-.17	.0	3.1
5	8	5	2.62	+/- 1.57	10.75	32.1	5.93	32.1	2.35	40.5	.27	.0	3.1
6	8	6	-2.80	+/- 1.56	6.25	32.1	11.07	32.1	-2.13	126.1	-.67	.2	3.3
7	8	7	-.52	+/- 1.66	11.33	32.0	6.51	32.0	1.94	57.5	-2.46	2.2	5.5
8	8	8	-1.92	+/- 1.60	6.85	32.1	11.67	32.1	-1.69	117.8	-.23	.0	5.5
9	8	9	4.31	+/- 1.60	11.97	32.1	7.15	32.1	1.45	66.4	2.86	3.2	8.7
10	8	10	-1.11	+/- 1.58	7.45	32.2	12.28	32.2	-1.20	109.3	.09	.0	8.7
11	9	1	2.57	+/- 1.61	12.10	6.5	12.10	66.5	1.03	73.4	1.54	.9	9.7
12	9	2	-2.21	+/- 1.62	12.41	66.7	12.41	6.7	-1.00	104.0	-1.21	.6	10.2
13	9	3	1.11	+/- 1.57	12.72	6.5	12.72	66.5	.93	75.1	.18	.0	10.2
14	9	4	.62	+/- 1.52	12.68	66.5	13.15	6.7	-.76	102.2	1.38	.8	11.1
15	9	5	-.93	+/- 1.50	13.32	6.5	13.32	66.5	.79	77.4	-1.22	.8	11.8
16	9	6	-1.90	+/- 1.93	13.27	66.5	13.74	6.7	-.57	99.1	-.83	.3	12.2
17	9	7	-2.10	+/- 1.99	16.20	31.4	11.39	32.3	-2.13	126.0	.03	.0	12.2
18	9	8	3.30	+/- 1.63	11.72	32.4	16.53	31.4	2.35	49.4	.95	.3	12.5
19	9	9	-2.34	+/- 1.61	16.82	31.9	12.01	31.9	-2.53	134.4	.19	.0	12.5
20	9	10	1.23	+/- 1.45	12.32	31.9	17.14	31.9	2.71	41.4	-1.48	1.0	13.5
21	9	11	-4.30	+/- 1.56	17.45	31.9	12.64	31.9	-2.87	142.7	-1.43	.8	14.4
22	9	12	4.78	+/- 1.62	12.92	31.9	17.74	31.9	3.00	33.8	1.78	1.2	15.6
23	10	7	1.75	+/- 1.56	11.39	32.8	6.58	31.0	1.89	58.5	-.14	.0	15.6
24	10	8	-2.81	+/- 1.58	6.91	32.8	11.72	31.0	-1.66	117.2	-1.15	.5	16.1
25	10	9	1.82	+/- 1.59	9.75	6.2	9.75	66.2	.92	75.3	.90	.3	16.4
26	10	10	-1.86	+/- 1.54	10.11	66.7	10.11	6.7	-1.01	106.2	-.85	.3	16.8
27	10	11	.68	+/- 1.51	10.53	6.3	10.29	66.2	1.05	73.1	-.37	.1	16.8
28	10	12	.91	+/- 1.98	10.89	66.7	10.77	6.7	-1.08	107.3	1.99	.9	17.7
29	11	1	.48	+/- 1.39	12.91	10.1	9.99	60.7	.64	79.9	-.16	.0	17.7
30	11	2	1.55	+/- 1.66	10.41	61.3	13.18	9.6	-.50	98.0	2.05	1.5	19.2
31	11	3	1.66	+/- 1.62	13.54	10.1	10.61	60.7	.29	85.4	1.37	.7	20.0
32	11	4	-2.44	+/- 1.57	11.01	61.3	13.78	9.6	-.17	92.7	-2.27	2.1	22.0
33	11	5	-.57	+/- 1.64	14.06	9.6	11.29	61.4	.01	89.8	-.58	.1	22.2
34	11	6	1.33	+/- 1.70	11.53	60.4	14.44	9.8	.26	85.9	1.07	.4	22.6
35	11	7	-4.24	+/- 1.54	16.23	46.9	11.84	18.7	-2.11	125.7	-2.13	1.9	24.5
36	11	8	2.83	+/- 1.57	12.13	19.2	16.55	46.5	2.25	51.4	.58	.1	24.6
37	11	9	-2.66	+/- 1.65	16.82	45.4	12.36	19.8	-2.38	131.2	-.28	.0	24.6
38	11	10	1.71	+/- 1.50	12.79	18.1	17.13	48.0	2.41	48.2	-.70	.2	24.9
39	11	11	-4.28	+/- 1.62	17.42	45.9	12.98	19.5	-2.55	135.0	-1.73	1.1	26.0
40	11	12	4.13	+/- 1.52	13.15	21.4	17.71	43.5	2.72	41.2	1.41	.9	26.9
41	12	1	-1.62	+/- 1.42	17.29	8.9	20.14	59.6	.31	85.1	-1.93	1.8	28.7
42	12	2	.98	+/- 1.57	20.48	59.6	17.62	8.9	-.12	91.9	1.10	.5	29.2
43	12	3	.55	+/- 1.57	17.92	8.9	20.78	59.6	-.06	90.9	.61	.2	29.3
44	12	4	.55	+/- 1.46	21.08	59.6	18.22	8.9	.24	86.2	.31	.0	29.4
45	12	5	2.83	+/- 1.58	18.57	8.9	21.38	59.6	-.43	94.8	3.26	4.2	33.6
46	12	6	-2.68	+/- 1.60	21.68	59.6	18.82	8.9	.61	80.2	-3.29	4.2	37.9
47	12	7	2.00	+/- 1.56	22.17	25.1	17.46	19.0	-3.05	147.8	1.05	.6	38.5
48	12	8	2.14	+/- 1.55	17.75	19.0	22.46	25.1	2.91	36.3	-.67	1	38.6
49	12	9	.07	+/- 1.52	22.79	25.1	18.08	19.0	-2.73	139.1	2.66	3.1	41.6

[1]The first nine columns are the data reproduced from Table IV.1.

[2]DIPOLE is $\vec{T}\cdot(\hat{n}_1 - \hat{n}_2)$, the fitted signal for the leg-measurements.

[3]THETA is the angle between $\vec{T}$ and $(\hat{n}_1 - \hat{n}_2)$, plotted on the horizontal axies of Figure V.1.

[4]DIFF is the difference between SIGNAL and DIPOLE, in milli-degrees Kelvin.

[5]DCHI and CHI-SQ are, respectively, the contribution to S (eq. V.3) and the cumulative value of S. (S is distributed as χ^2 of 73 DOF if the cosine hypothesis correctly models the data.)

Table V.2 (continued)

					$\hat{n}_1$		$\hat{n}_2$						
NUM	FLT	LEG	SIGNAL	SIGMA	R.A.	DEC	R.A.	DEC	DIPOLE	THETA	DIFF	OCHI	CHI-SQ
49	12	9	-.07 +/-	1.52	22.79	25.1	18.08	39.0	-2.73	139.1	2.66	3.1	41.5
50	12	10	2.11 +/-	1.56	18.37	39.0	23.08	25.1	2.55	45.1	-.44	.1	41.6
51	12	11	-5.09 +/-	1.49	23.39	25.1	18.68	39.0	-2.35	130.6	-2.74	3.4	45.0
52	12	12	2.64 +/-	1.52	18.97	39.0	23.68	25.0	2.19	53.6	.50	.1	45.1
53	13	1	2.65 +/-	1.50	6.83	31.5	2.04	31.5	3.34	22.4	-.69	.2	45.3
54	13	2	-3.61 +/-	1.62	2.30	31.4	7.16	31.4	-3.39	159.8	-.22	.0	45.3
55	13	3	1.79 +/-	1.62	7.46	31.5	2.68	31.5	3.41	19.2	-1.62	1.0	46.3
56	13	4	-3.63 +/-	1.57	2.99	31.4	7.78	31.4	-3.41	160.8	-.22	.0	46.3
57	13	5	5.67 +/-	1.52	8.08	31.4	3.30	31.4	3.39	20.2	2.28	2.3	48.6
58	13	6	-2.26 +/-	1.61	3.61	31.4	8.40	31.4	-3.34	157.8	1.08	.5	49.0
59	13	7	-1.50 +/-	1.50	7.34	9.7	4.38	59.7	1.33	68.4	-2.83	3.6	52.6
60	13	8	-2.31 +/-	1.52	4.70	59.5	7.69	9.4	-1.41	113.0	-.90	.4	53.0
61	13	9	2.05 +/-	1.61	7.96	9.7	5.00	59.7	1.49	65.6	.56	.1	53.1
62	13	10	-1.67 +/-	1.51	5.32	59.5	8.26	9.4	-1.54	115.3	-.13	.0	53.1
63	13	11	2.18 +/-	1.52	8.58	9.7	5.62	59.7	1.59	63.8	.59	.1	53.2
64	13	12	.18 +/-	1.57	5.93	59.5	8.88	9.4	-1.61	116.5	1.79	1.3	54.5
65	14	1	- 78 +/-	1.63	13.80	30.7	9.06	30.7	-.18	92.9	-.60	.1	54.7
66	14	2	-1.20 +/-	1.56	9.35	30.7	14.09	30.7	.43	83.1	-1.63	1.1	55.8
67	14	3	-.73 +/-	1.64	14.45	30.8	9.71	30.8	-.76	102.1	.03	.0	55.8
68	14	4	1.54 +/-	1.58	9.98	30.7	14.72	30.7	.99	74.1	.55	.1	55.9
69	14	5	.01 +/-	1.66	15.01	29.6	10.28	31.5	-1.23	109.8	1.24	.6	56.4
70	14	6	- 23 +/-	1.60	10.60	30.7	15.34	30.7	1.50	65.4	-1.73	1.2	57.6
71	14	7	-.03 +/-	1.74	13.34	5.4	13.34	65.4	.72	78.5	-.75	.2	57.8
72	14	8	3.73 +/-	1.56	13.76	65.6	13.76	5.6	-.73	101.7	4.46	8.2	66.0
73	14	9	-.19 +/-	1.66	13.95	5.4	13.95	65.4	.54	81.4	-.73	.2	66.2
74	14	10	1.43 +/-	1.57	13.96	65.6	13.96	5.6	-.55	98.7	1.98	1.6	67.8
75	14	11	2.37 +/-	1.72	14.51	5.4	14.51	65.4	.33	84.7	-2.70	2.5	70.3
76	14	12	1.74 +/-	1.59	14.53	65.6	14.53	5.6	-.34	95.1	-1.42	.9	71.1

Figure V.1 - Comparison of Data to Cosine Anisotropy, Flights 8-14

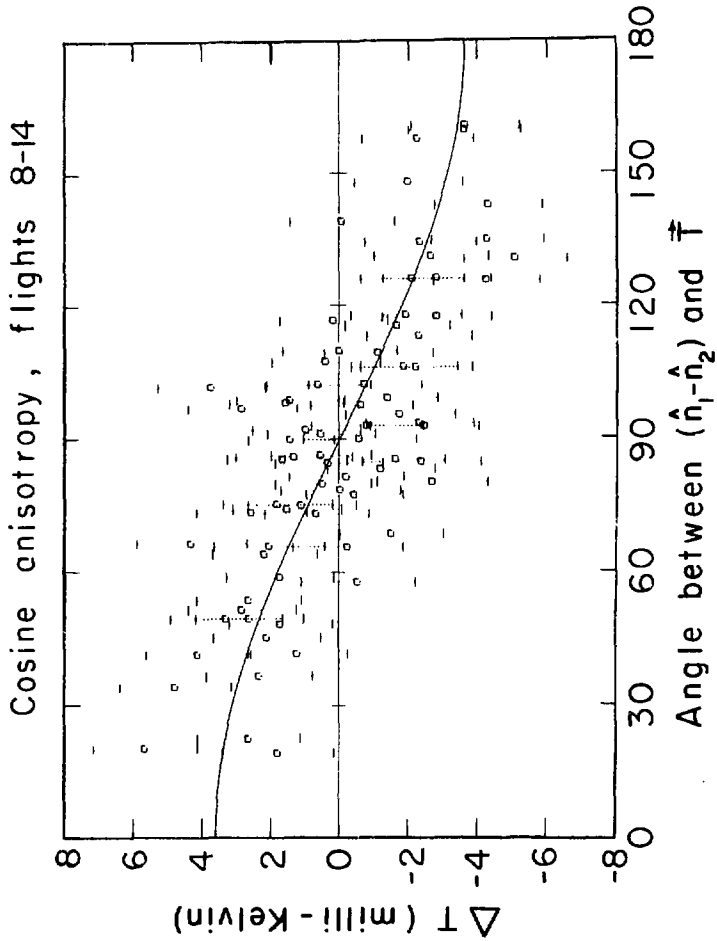

Cosine anisotropy at
emission at 43 GHz

Table V.3 - Fit to Cosine Anisotropy for Alternate Selections of Data[1]

Data Selection	*Amplitude* (m°K)	*R.A. (hours)*	*Dec.* (°)	*S/DOF*	*confidence level*
Flt. 8-14	3.61±0.43	11.23±0.37	19.0±6.0	*71.0/73*	*55%*
Flt. 4-11[2]	3.[illegible]±0.6	11.0±0.6	6±10	*91/77*	*13%*
Flt. 4-11	3.37±0.47	10.57±0.50	5.0±6.6	*72.9/67*	*29%*
Flt. 4-14	3.23±0.32	10.95±0.38	13.3±5.3	*121.5/103*	*10%*
Flt. 4,6,8, 10,12,14	2.51±0.68	11.25±0.72	13.8±10.5	*79.3/51*	*0.5%*
Flt. 5,7,9 11,13	3.61±0.54	10.97±0.72	14.8±7.4	*39.9/49*	*82%*
Flt. 8-14 uncorrected data[3]	*3.4*	*11.0*	*16*		
Flt. 8-14 roll correction[4]	*0.04*	*13.1*	*77.1*		
Flt. 8-14 galaxy correction[4]	*0.13*	*20.4*	*-21.5*		

[1]Errors quoted in this table are statistical only.

[2] *Smoot, Gorenstein & Muller, 1977*

[3]Fit to data with no corrections for aircraft roll, galactic backgrounds, and no subtraction of rotation offset.

[4]Results of cosine fit to corrections only. Inclusion of corrections changes cosine parameters by less than one-standard-deviation.

legs flown with north-south headings gave 2.41 ± 0.65 m°K for the anisotropy between east-west directions. The "east-ward" antenna direction, towards 11.5 hours R.A. and $+32°$ declination, gave the hotter signal. This right ascension was determined by the take-off time of 6 pm PST, just at sunset. The ninth flight checked the $\cos\theta$ hypothesis by investigating the anisotropy of a new part of the sky. We arranged the take-off to be at 10 pm PST so the east-ward antenna direction now pointed toward a region of the sky *away* from the (expected) hotter direction. The average of the six legs gave -2.76 ± 0.65 m°K, with the expected sign reversal.

The sign reversal verified the celestial origin of the anisotropy; it is unlikely that spurious signals inherent in the aircraft, or due to the earth's magnetic field or thermal microwave emission from the earth's surface would occur at this magnitude and exhibit this sign change. Moreover, the measurements taken in the east-west headings were small and consistent with the $\cos\theta$ effect from previous flights. Finally, the tenth flight was flown as a check of the results of the eighth flight. Take-off was at sunset, and the east-ward antenna gave the hotter signal, as predicted.

V.4 Comparison with Other Measurements

Table V.4 compares two other microwave measurements of cosine anisotropy with the results of this work. Corey and Henry employed balloon-borne platforms and collected their data with twin-antenna Dicke-type microwave radiometers. Both radiometers operated at frequencies where synchrotron emission from the Galaxy required substantial milli-degree Kelvin corrections to the data. Their values of cosine anisotropy agree with the result reported here in magnitude and in right ascension, but disagree in declination; Corey's measurement points 40° more to the south than our own, and Henry's points 50° to the south. Corey's data were collected at the higher frequency and is probably less contaminated by systematic errors from the galactic synchrotron corrections.

We quantitatively compare our measurements with Corey's, checking the consistency of the results. The difference vector between the measurements should be statistically consistent with a vector of zero length. Combining the error matrices of the measurements yields the error matrix for this difference vector. We compute a quantity S in analogy with eq. V.3 whose value is distributed as a χ^2 distribution for three DOF *if* the two measurements are consistent. This calculation is conveniently carried out in rectangular coordinates where the errors are Gaussianly distributed. The details are described in Section H.2. Subtracting the measurements yields a difference vector whose magnitude is 2.5m°K. The value of S for this vector is 8.5, for a confidence level of 3.5%. This indicates that the measurements agree, but perhaps either or both experiments underestimate their errors by about $\sqrt{8.5/3} = 1.7$.

Table V.4 - Comparison with Other Measurements of Cosine Anisotropy

Reference	Frequency (GHz)	Amplitude (m °K)	R.A. (hours)	Dec. (deg.)
Henry, 1971	10.2	3.2±0.8	10.5±4	−30±25
Corey, 1978	19.0	2.9±0.7	12.3±1.4	−21±21
This work	33.0	3.61±0.54	11.23±0.46	19±7.5

Table V.4a - Corey's result in rectangular celestial coordinates
(Corey, 1978)

Γ_x (m °K)	T_y (m °K)	T_z (m °K)
−2.70±0.85	−0.22±1.00	−1.02±0.92

Correlation Coefficients

$C_{(x,y)}$	$C_{(x,z)}$	$C_{(y,z)}$
0.39	−0.44	−0.55

V.5 Limits on Quadrupole Anisotropy

One of the motivations for investigating angular variations in the 3 °K background radiation is the search for higher order multipoles in $T(\hat{n})$. As discussed in Chapter I, the existence of multipole anisotropy higher than dipole would present a challenge to the Cosmological Principle. We have analyzed the data for evidence of a quadrupole anisotropy.

The quadrupole distribution, $Q(\hat{n})$, is formed from a linear combination of five basis functions, $q_i(\hat{n})$,

$$Q(\hat{n}) \equiv \sum_{i=1}^{5} A_i q_i(\hat{n}) \qquad \text{V.5}$$

Table V.5 defines the basis functions in terms of the second order, $l = 2$ spherical harmonics. The five parameters, A_i, are the rms amplitudes of quadrupole anisotropy expressed in millidegrees Kelvin. Adding $Q(\hat{n})$ to eq. V.1 models the sky temperature as the sum of dipole plus quadrupole anisotropy. Thus,

$$T(\hat{n}) = T_o + \vec{T}\cdot\hat{n} + Q(\hat{n}) \qquad \text{V.6}$$

Minimizing the following expression for S yields the three dipole and five quadrupole parameters:

$$S = \sum_{i=1}^{M} \frac{[\Delta T_{3\,°K} - \vec{T}\cdot(\hat{n}_1' - \hat{n}_2') - (Q(\hat{n}_1') - Q(\hat{n}_2'))]}{\sigma_i^2} \qquad \text{V.7}$$

Table V.5 - Basis Functions for Quadrupole Anisotropy

θ is the polar angle measured from north celestial pole.
ϕ is the azimuthal angle, measured from 0 hours R.A.

Function	*Spherical Harmonic*	*Angular dependence*
$q_1(\theta,\phi)$	$\sqrt{4\pi}\ Y_{20}$	$\sqrt{5}(\frac{3}{2}\cos^2\theta - \frac{1}{2})$
$q_2(\theta,\phi)$	$\sqrt{4\pi}\frac{Y_{21} + Y_{2-1}}{\sqrt{2}}$	$-\sqrt{15}\sin\theta\cos\theta\cos\phi$
$q_3(\theta,\phi)$	$\sqrt{4\pi}\frac{Y_{21} - Y_{2-1}}{i\sqrt{2}}$	$-\sqrt{15}\sin\theta\cos\theta\sin\phi$
$q_4(\theta,\phi)$	$\sqrt{4\pi}\frac{Y_{22} + Y_{2-2}}{\sqrt{2}}$	$\frac{\sqrt{15}}{2}\sin^2\theta\cos 2\phi$
$q_5(\theta,\phi)$	$\sqrt{4\pi}\frac{Y_{22} - Y_{2-2}}{i\sqrt{2}}$	$\frac{\sqrt{15}}{2}\sin^2\theta\sin 2\phi$

Table V.6 presents the fitted results for this eight parameter hypothesis for data from flights 8-14. It is worthwhile comparing the cosine (dipole) parameters in Table V.1 with the dipole parameters listed in Table V.6. For the dipole fit alone, T_2 dominates the anisotropy signal with a value of $-3\ 34 \pm 0.44$ m °K. In the combined fit of dipole with quadrupole, the T_2 parameter retains its significance in the presence of the competing quadrupole hypothesis, with a value of -2.32 ± 0.66 m °K. This is evidence that the major component of global anisotropy is correctly interpreted as a dipole signal, and cannot be due to a quadrupole signal from a partially surveyed sky.

The A_i parameters do not indicate the presence of quadrupole anisotropy:

(1) The values of the parameters A_i listed in Table V.6 are consistent with zero. (The large correlated errors in A_1 and T_2 will be explained presently as due to the restriction of sky coverage to one hemisphere.)

Table V.6 - Fit to Combined Hypothesis: Dipole ($\cos\theta$) and Quadrupole ($\cos^2\theta$)

Corrected data flights 8-14

χ^2/Degree of freedom is 62.6/68, Confidence level is

Dipole parameters

T_x (m°K)	T_y (m°K)	T_z (m°K)
-2.32 ± 0.66	0.36 ± 0.68	62.8 ± 29.1

Quadrupole parameters

A_1 (m°K)	A_2 (m°K)	A_3 (m°K)	A_4 (m°K)	A_5 (m°K)
-18.1 ± 8.5	-0.55 ± 0.33	0.0 ± 0.23	0.05 ± 0.13	-0.05 ± 0.22

Correlation coefficients

T_x	T_y	T_z	A_1	A_2	A_3	A_4	A_5	
1.0	*0.12*	*-0.04*	*0.03*	*-0.80*	*-0.24*	*0.38*	*0.12*	T_x
	1.0	*-0.29*	*0.29*	*-0.34*	*-0.68*	*-0.03*	*0.76*	T_y
		1.0	*-1.00*	*0.01*	*0.31*	*-0.30*	*-0.09*	T_z
			1.0	*0.00*	*-0.31*	*0.30*	*0.08*	A_1
				1.0	*0.30*	*-0.23*	*-0.42*	A_2
					1.0	*-0.24*	*-0.39*	A_3
						1.0	*-0.14*	A_4
							1.0	A_5

(2) The value of S for the 8 parameter fit is 62.6 compared to $S = 71.0$ for the fit to the three parameter cosine hypothesis alone. This demonstrates, without reference to a particular parametrization, that the inclusion of the quadrupole hypothesis is not required by the data. The change in S between these fits is distributed as χ^2 for five DOF *if* the quadrupole amplitudes have zero mean *(Martin, 1971, pg. 146)*. Since the confidence level for S of 8.4 with five DOF is 15%, we conclude that the data is consistent with zero mean quadrupole amplitude.

(3) The dipole parameters listed in Table V.6 are consistent with those in Table V.1. This was directly checked by evaluating the difference vector of cosine anisotropy between the data fitted to the cosine hypothesis alone and for the data fitted to the combined hypothesis of cosine and quadrupole. The rms errors on the vector difference was then computed by repeatedly "jittering" the input leg-measurements and re-evaluating the difference vector each time. The resulting difference and errors, in milli-degree Kelvin, are:

$$\vec{T}_{\text{cosine only}} - \vec{T}_{\text{combined}} = \qquad \text{V.8}$$
$$(-1.03 \pm 0.54)\,\hat{x} + (0.31 \pm 0.61)\,\hat{y} + (-60.2 \pm 30.3)\,\hat{z}$$

It is natural then to ask what limit the data places on quadrupole anisotropy in the cosmic background radiation. The lack of sky coverage in the southern hemisphere complicates this calculation [illegible] data flights were flown from 37° north latitude where the most southernly declination [illegible] the antennas pointed was about +7°, Figure III.3. Sky coverage restricted to the northern hemisphere cannot distinguish between a $\cos\theta$ angular distribution (z component of dipole) and a $\cos^2\theta$ distribution (z^2 component of quadrupole). This is because the sum of these functions cancels (within the errors) in the northern hemisphere, while adds with opposite sign in the southern hemisphere. Thus the amplitude of the z component of the dipole fit, T_z, and the z^2 component of the quadrupole fit, A_1, have large correlated errors*. A fit that included simulated sky coverage in the southern hemisphere showed that only one flight from an airfield situated below the earth's equator is enough to break this correlation, yielding milli-degree Kelvin significance for all eight parameters.

Despite the correlation between A_1 and T_z, the data does place a significant limit on the remaining 4 amplitudes of the basis functions $q_i(\hat{n})$. In general we can express this limit as the rms amplitude of a quadrupole distribution, defined as

$$Q \equiv \left[\frac{1}{4\pi}\int\int Q^2(\hat{n})\,d\Omega\right]^{1/2} = \left[\sum_{i=1}^{5} A_i^2\right]^{1/2} \qquad \text{V.10}$$

Restricting eq. V.10 to the four amplitudes determined with good sensitivity, we define Q' as

*The data in Table V.6 does measure the *sum* of the amplitudes of T_z and A_1 with small errors. To find the sum of a $\cos\theta$ and $\cos^2\theta$ anisotropy, we first renormalize A_1 according to the definition of q_1 given in Table V.5. The sum of the components is then given by

$$T_z + \sqrt{5}\,\frac{3}{2}\,A_1 = (62.8 \pm 29.1) + \sqrt{5}\,\frac{3}{2}\,(-18.1 \pm 8.5) = 2.1 \pm 0.6\,\text{mK} \qquad \text{V.9}$$

The nearly complete anti-correlation between the T_z and A_1 parameters accounts for the small errors on their sum.

$$Q' \equiv \left[\sum_{i=2}^{5} A_i^2\right]^{1/2} \qquad \text{V.11}$$

The data from Table V.5 gives

$$Q'_{data} = 0.56\,\text{m}^\circ\text{K} \qquad \text{V.12}$$

A monte-carlo simulation generates the distribution of Q' by first adding independent error signals to each leg-measurement, simulating the effect of receiver noise. Repeating this procedure generates several thousand sets of "jittered" leg-measurements, and the best fit solution for A_i and $\vec{T}$ from each set yields values of Q'. The distribution of these values shows that 90% of the time Q' is less than 1.1 m°K. Thus at the 90% confidence level we expect that future measurements of these four quadrupole amplitudes will yield a net rms amplitude of less than 1.1 m°K.

The lack of quadrupole anisotropy puts a limit on global deviations from isotropy. As mentioned in Section I.5, rotation of the distant matter in the Universe relative to the local inertial frame would yield a quadrupole distribution. For a present mass density of $2\times10^{-29}\,\text{gm/cm}^3$, the limit of quadrupole anisotropy at one part in 3000 yields a limit of $10^{-17}\,\text{rad/yr}$ *(Hawking, 1969)*. In another context Burke has speculated that the Universe may be permeated by gravitational radiation with wavelengths encompassing galaxies. If the Milky Way is embedded in a megaparsec wavelength gravitational wave, then that would give rise to a distortion of the microwave background with a quadrupole component *(Burke, 1975)*. According to Burkes's formula, the limit on quadrupole anisotropy means that the energy density of long wavelength gravitational radiation is insufficient to close the Universe *(Smoot, Gorenstein & Muller, 1977)*.

V.6 Limit on Sky-roughness on a 7° Angular Scale

The following analysis places a 0.5 m°K upper limit on the amplitude of uncorrelated fluctuations (sky-roughness) in the 3°K background on an angular scale of the antenna beam width, about 7°. Including a term for sky-roughness in eq. V.1 gives

$$T(\hat{n}) = T_o + \vec{T}\cdot\hat{n} + T_s(\hat{n}) \qquad \text{V.13}$$

where $T_s(\hat{n})$ is the term describing sky-roughness. We take $T_s(\hat{n})$ to have the following statistical properties (the indicated averages are understood to be taken over areas in the sky separated by more than the 7° antenna beam width):

$$\langle T_s(\hat{n})\rangle \equiv 0$$

$$\langle T_s^2(\hat{n})\rangle \equiv \sigma_s^2 \qquad \text{V.14}$$

$$< T_s(\hat{n}_i)\, T_s(\hat{n}_j) > \equiv 0 \quad \text{if } \hat{n}_i \cdot \hat{n}_j >> \cos^{-1}(7°)$$

Note that σ_s is the rms fluctuation of the *absolute* sky temperature. This means that the *difference* temperature between two directions in the sky, which is what the radiometer measures, will fluctuate by $\sqrt{2}\,\sigma_s$.

If there is reason to expect, *a priori*, a sky-roughness σ_s^2 on a 7° angular-scale, then we should quadrature the errors on the points in Figure V.1 with $2\sigma_s^2$ before we compute S, the cumulative squared deviation from the fit. This will obviously reduce S:

$$S_{rough} = S\,\frac{\sigma^2}{\sigma^2 + 2\sigma_s^2} \qquad \text{V.15}$$

where

S is 71.0 from the cosine fit.

σ^2 is $(1.6\,\text{m}°\text{K})^2$, the mean value of σ_i^2 from the leg-measurements in flights 8-14.

$2\sigma_s^2 = <[T_s(\hat{n}_i) - T_s(\hat{n}_j)]^2>$ from eq. V.14.

Now assuming that the estimate of receiver noise is correct, we put a limit on σ_s by increasing its value in eq. V.15 until the confidence level approaches 100%. Table V.7 lists the values of σ_s for corresponding values of the confidence level. The tabulation shows that increasing σ_s by more than 0.5 m°K increases the confidence level past 90%. Thus, if the sky-roughness is 0.5 m°K or more, we would measure $S = 71.0$ or greater 90% of the time (rather than 55% for $\sigma_s = 0$). Thus we rule out a prediction of sky-roughness greater than one part in 6000 of 3 °K on a 7° angular-scale with 90% confidence.

Table V.7 - Limits on Sky-roughness on a 7° Angular Scale

σ_s (m°K)	$\frac{\sigma_s}{\sigma}$	S_{rough}	Confidence level
0	0	71	55%
0.50	0.31	59	90%
0.60	0.37	55	95%
0.77	0.48	48	99%

The lack of sky-roughness re-emphasizes the problem of accounting for the high degree

of isotropy in the microwave background radiation. In section I.5 it was pointed out that in the standard picture it seems impossible for physical processes acting prior to the decoupling to isotropise the radiation on distances that now appear a few degrees apart in the sky. The amplitude and angular structure of the as yet undiscovered sky-roughness may be crucial in understanding the physical isotropising mechanisms, and will likely fix the initial conditions determining galaxy formation subsequent to the epoch of decoupling.

V.7 The Motion of the Sun and Nearby Groups of Galaxies Relative to the 3°K Background

After setting limits on higher order multipole anisotropy we return to the cosine anisotropy and interpret it as due to the motion of the sun relative to the sources — "last scatterers" might be the more appropriate term — of the 3 °K radiation. It may seem that discussing the peculiar motion of the earth takes us away from cosmology proper, but this is not the case. The cosine anisotropy identifies the local co-moving coordinate frame, and is the prime link in computing the peculiar motions of the Milky Way, the local group, and perhaps even larger "super clusters" spanning cosmological distances.

We begin by interpreting the cosine anisotropy as due to the motion of the sun. The following expression, from eq. I.1, gives the magnitude of a velocity relative to an isotropic thermal background radiation given the radiation temperature and the magnitude of cosine anisotropy:

$$|\vec{V}| = \frac{|\vec{T}| \cdot c}{T_o} \quad ; \quad |\vec{T}| << T_o \qquad \text{V.16}$$

where

$|\vec{V}|$ is the magnitude of velocity relative to the thermal background.

$|\vec{T}|$ is the amplitude of cosine anisotropy.

c is the velocity of light.

T_o is the temperature of the thermal background in the frame of isotropy.

Thus from the data in Table V.1, we arrive at

$$|\vec{V}| = \frac{3.61 \pm 0.54 \times 10^{-3}\,°K}{3\,°K} \left(\frac{3\,°K}{T_o}\right) 3 \times 10^5 km/sec \qquad \text{V.17}$$

$$= 361 \pm 54 \left(\frac{3\,°K}{T_o}\right) \text{km/sec}$$

Table V.8 summarizes the parameters of cosine anisotropy interpreted as due to the motion of the sun relative to the sources of the 3 °K background radiation.

Table V.8

The Motion of the Sun with Respect to the 3°K Radiation

Flights 8-14, cosine anisotropy

Celestial Coordinates

$\lvert\vec{V}\rvert$ (km/sec)	right ascension (hours)	declination (degrees)
361 ± 54	11.23 ± 0.46	19.0 ± 7.5

Correlation Coefficients

$C_{(vel.,\ dec.)}$	$C_{(vel.,\ R.A.)}$	$C_{(dec.,\ R.A.)}$
+0.57	−0.07	+0.06

From analysis of motions of globular clusters and nearby stars the inferred value for the circular velocity of the sun about the center of the Milky Way Galaxy is about 250 ± 40 km/sec toward $l^{II} = 90°$, and $b^{II} = 0°$ *(Schmidt, 1965)*. The motion of the Milky Way relative to the centroid of the "local group" of galaxies is also known, and is about 50 km/sec, small by comparison to the sun's motion about the Milky Way. The local group (LG) is a collection of about 20 galaxies generally taken to be within a radius of about 1 Mpc from the Milky Way. The net motion of the sun relative to the centroid of the LG is reasonably well established to be 300 km/sec in the direction $l = 90°$, $b = 0°$ *(de Vaucouleurs & Peters 1968, de Vaucouleurs 1972; Yahil, Tammann & Sandage, 1977)*. Unless otherwise specified, (l, b) are understood as the new galactic coordinates (l^{II}, b^{II}).

Although the speed of the sun relative to the local group is comparable to that of the sun relative to the 3°K background, inspection of Table V.9 shows that the directions differ, the angle of separation being about 110°. Thus the cosine anisotropy of the 3°K radiation is not accounted for by the motion of the sun about the Milky Way, or relative to the LG. The resulting difference velocity, the motion of the LG relative to the 3°K background, is large, over 500 km/sec, Table V.10.

Table V.9 - Motions of the Sun Relative to Groups of Galaxies

Speed (km/sec)	Celestial coordinates R.A.(hrs.)	dec.(°)	Galactic coordinates l^{II}°	b^{II}°
Motion of Sun relative to Local Group				
300±50	21.2	+48°	90°	0°
Motion of Sun relative to Galaxies[1]; 600 < cz < 1800 km/sec				
350±50	11.5	+32°	200°	72°
Motion of Sun relative to Galaxies[2]; 3500 < cz < 6500 km/sec				
600±125	2.13±1.33	53°	135°	−8°

[1] *de Vaucouleurs, 1977.*

[2] *Rubin et. al., 1976b.*

What are the motions of larger groupings of galaxies relative to the 3°K radiation? De Vaucouleurs *(de Vaucouleurs, 1977, and references therein)* and Rubin *(Rubin et. al., 1976a,b)* have each analysed the red shifts and brightnesses of galaxies external to the LG for evidence of anisotropy in the velocity field. They both choose galaxies of selected morphological types, restricted to a specified range of red shifts. Table V.9 also lists the results of their analyses of the local motion relative to each shell of galaxies and the range of red shifts that their samples span.

Interpreting these results as true measures of motion, we subtract the velocity of the sun with respect to the galactic groupings from the velocity of the sun with respect to the 3°K radiation. Table V.10 presents these vector differences, listing the velocity of the sun and the velocities of the galactic groupings relative to the 3°K background. Both the LG and the two galactic shell samples have motions relative to the 3°K background of comparable magnitude and all are significantly different from zero. This is surprising, because one might expect that the larger the

group of galaxies sampled the smaller their velocity relative to the 3 °K background should be. The more distant shell analysed by Rubin *et. al.* encompasses a volume containing some 50 million galaxies. But the analyses of de Vaucouleurs and Rubin *et. al.* are disputed. Schechter *(Schechter, 1977)* has criticized the statistical analysis of the Rubin result, claiming that they have underestimated their errors. And there has been a continuing dispute concerning the existence of anisotropy in the local galactic velocity field out to red shifts, cz, of about 6000 km/sec *(e.g. Sandage & Tammann, 1975; de Vaucouleurs, 1976).*

Table V.10 - Solar and Galactic Velocities Relative to the 3°K Radiation

Speed	Celestial coordinates		Galactic coordinates	
(km/sec)	R.A.(hrs.)	dec.(°)	l^{II}°	b^{II}°
Motion of sun relative to 3 °K background radiation				
362±54	11.2±0.5	19±8°	229±19°	66.6±7°
Motion of Local Group Relative to 3 °K Radiation				
534±75	10.47	−11°	257°	+38°
Motion of Galaxies[1], 600 < cz < 1800 Relative to 3 °K Radiation				
381±75	9.3	−49°	270°	0°
Motion of Galaxies[2], 3500 < cz < 6500, Relative to 3 °K Radiation				
745±140	12.7±1.33	−29°	300°	30°

[1] Combine velocity from cosine anisotropy with measurement of *de Vaucouleurs, 1977.*

[2] Combine velocity from cosine anisotropy with measurement of *Rubin et. al., 1976b.*

It is worth pointing out that these large velocities of galactic groupings cannot be reasonably accounted for as a residual motion from the time of galaxy formation at about $z = 1500$. In an expanding Universe that is isotropic and homogeneous the momentum of a test particle

decreases in time relative to the co-moving coordinate system. Drifting past co-moving observers, the test particle asymptotically approaches the coordinate point whose recessional velocity equals its own peculiar velocity *(Peebles, 1971, pg. 169)*. A present speed of 500 km/sec would require relativistic velocity at the epoch of decoupling, $z = 1500$.

De Vaucouleurs has claimed that the LG is a member of a larger super-cluster which makes its presence known by a distortion of the local Hubble flow *(de Vaucouleurs, 1958, 1972; de Vaucouleurs & Peters, 1968)*. The supercluster is centered on the Virgo Cluster (12 hrs. 28' R.A., 12° 40' dec.) of some thousand galaxies. The cluster's mean recessional velocity is about 1050 km/sec *(de Vaucouleurs & de Vaucouleurs, 1973; Sandage & Tammann, 1976)*, and it is at a distance of about 20 Megaparsecs. From Table V.10 the velocity of the LG relative to the 3°K background points within 38° of the direction towards the Virgo cluster, yielding a velocity component of 421 km/sec. According to de Vaucouleurs, the rate of the local Hubble expansion in the direction of the Virgo cluster is reduced some 250 km/sec *(de Vaucouleurs & Peters, 1968)*. But Visvanathan and Sandage have analysed the relationship between the color and absolute magnitude for type E and S0 galaxies in nine nearby clusters, including Virgo, that have recessional velocities of up to 10,000 km/sec. In the Hubble diagram generated by their analysis they find that the Virgo cluster departs from the mean solution by less than ± 25 km/sec *(Visvanathan & Sandage, 1977; also see Sandage & Tammann, 1975; de Vaucouleurs, 1976)*.

V.8 Conclusion

The principal result of this work is the detection of cosine anisotropy in the 3°K cosmic background radiation. The magnitude of the anisotropy is 3.61 ± 0.54 m°K, one part in 800 of 3°K, in a direction not accounted for by the velocity of the sun about the Galaxy or relative to the local group. The inferred motion of the sun relative to the 3°K radiation is 361 ± 54km/sec, towards 11.23 ± 0.46hours R.A., 19.0 ± 7.5° declination.

The limits the data places on most components of quadrupole anisotropy are about 1 part in 3000 of 3°K, or less than one part in 3 of the amplitude of cosine anisotropy. The limits the data places on "sky-roughness" on a 7° angular scale is about one part in 6000 of 3°K, less than one part in 6 of the cosine amplitude. The cosine anisotropy identifies the local co-moving frame with respect to which the dynamics of the neighboring galaxies should be best understood. However, the "discovery" of the local frame of rest seems to exacerbate the already existing conflicts in the determination of the local velocity field of galaxies. The lack of additional anisotropy re-emphasizes the theoretical problem of accounting for the extreme isotropy of the radiation.

Two important extensions of this work are being planned. Observations in the southern hemisphere are a crucial check of the global nature of cosine anisotropy, and would complete

the measurement of the quadrupole parameters. These flights will take place pending final approval from the National Aeronautics and Space Administration (NASA).

Secondly, a next generation experiment is being designed as part of a proposed satellite, the Cosmic Background Explorer (**COBE**). Preliminary design studies are being undertaken by a collaboration including the astrophysics group at the Lawrence Berkeley Laboratory, which is responsible for the work reported here. The plan is for a year long survey of the entire celestial sphere at four microwave frequencies. With increased sensitivity afforded by the long exposure and improvements in receiver design, it will be possible to search for higher moments of anisotropy with a sensitivity of about one part in 50 of the 3.6 m °K cosine amplitude.

The discovery of the 3 °K cosmic background radiation continues inspiring vigorous experimental investigation. We are privileged to live and work in an era when our fundamental origins have become open to scientific inquiry.

Detection of Anisotropy in the Cosmic Blackbody Radiation

G. F. Smoot, M. V. Gorenstein, and R. A. Muller

Lawrence Berkeley Laboratory and Space Sciences Laboratory, University of California, Berkeley, California 94720

(Received 6 July 1977)

We have detected anisotropy in the cosmic blackbody radiation with a 33-GHz (0.9 cm) twin-antenna Dicke radiometer flown to an altitude of 20 km aboard a U-2 aircraft. In data distributed over two-thirds of the northern hemisphere, we observe an anisotropy which is well fitted by a first-order spherical harmonic with an amplitude of $(3.5 \pm 0.6) \times 10^{-3}$ °K, and direction 11.0 ± 0.6 h right ascension (R.A.) and $6° \pm 10°$ declination (dec). This observation is readily interpreted as due to motion of the earth relative to the radiation with a velocity of 390 ± 60 km/sec.

The observed isotropy of the 3°K cosmic blackbody radiation to about one part in 10^3 is the strongest evidence in support of the cosmological principle, the basic assumption of cosmology that the universe is isotropic and homogeneous on a large scale. Anisotropy at the 10^{-3}–10^{-4} level is expected to exist from the Doppler shift due to the motion of the earth with respect to the ancient matter which emitted the radiation.[1] Anisotropies would also exist if there were nonsymmetric expansion of the universe or large-scale irregularities in the distribution of matter or energy. Until recently, interference from galactic emissions had prevented anisotropy in the cosmic blackbody radiation from being unambiguously observed.[2] Preliminary reports of a positive effect have been made now by Corey and Wilkenson[3] and by this group.[4] We present here the results of a survey spanning approximately two-thirds of the northern hemisphere, taken at 0.9 cm, a wavelength at which the galactic background is small.

The experiment was conducted in a series of eight flights aboard the NASA-Ames Earth Survey (U-2) Aircraft. Anisotropy in the cosmic radiation was detected at 33 GHz with a twin-antenna Dicke radiometer which measured the difference in sky temperature between two regions 60° apart and on opposite sides of the zenith. The best receiver, used on the final four flights, has a sensitivity limited by thermal noise with an rms fluctuation of $0.044°K/Hz^{1/2}$. The receivers used on the earlier flights had rms fluctuations about twice as large. The apparatus is shown schematically in Fig. 1; details of its design and construction will be given elsewhere.[5]

Effort was made in the design of the apparatus to reduce all expected systematic errors well below the millikelvin level. To achieve the desired sensitivity, the apparatus was radio-frequency and magnetically shielded, and carefully thermally stabilized.[6] The antennas were specially designed (dual-mode corrugated cones) with a beam pattern 7° wide full width at half-maximum (FWHM). The measured antenna gain in the direction of the earth was below 10^{-7}; anisotropic emission from the earth and aircraft contributed less than 0.2 m°K. A second twin-antenna radiometer operating at 54 GHz was used to monitor and eliminate anisotropic atmospheric background. This second system was sensitive to the strong-oxygen-emission region centered at 60 GHz and was calibrated at altitude by banking the airplane at angles of 5° to 25°. The monitor showed that the autopilot maintained level flight during data-taking periods to better than 0.2° of bank; the resulting spurious signal at 33 GHz

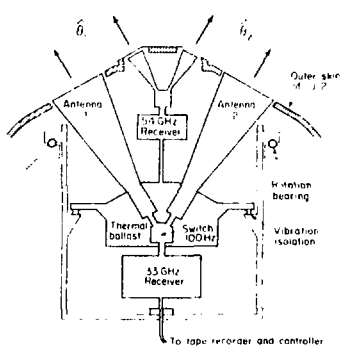

FIG. 1. Schematic view of the apparatus mounted in the U-2 aircraft. The anisotropy reported in this Letter was detected with the 33-GHz radiometer; the 54-GHz radiometer monitored the oxygen anisotropy above the aircraft.

due to aircraft tilt is less than 0.2 m°K.

Spurious anisotropies were detected and eliminated through a hierarchy of reversals. Rapid switching (100 Hz) between the two antennas reduced the effects of gain fluctuations ($1/f$ noise). Spurious anisotropy generated by imbalance in the two arms of the radiometer (≈ 60 m°K) was canceled by interchange of the two antennas through a rotation of the apparatus by 180° about the vertical every 64 sec. Spurious anisotropy associated with the rotation state of the antennas (≈ 2 m°K) was eliminated by reversing the flight path of the airplane every 20 min.

The data reported here were taken on eight flights between December 1976 and May 1977. Each flight yielded about 3.5 h of data taken at altitude; Fig. 2 shows the total sky coverage. A typical flight plan consisted of six pairs of "legs" flown in opposite directions along the ground. In addition to the data legs, when possible the flights included a "moon leg" in which one antenna pointed directly at the moon for a few minutes; this allowed us to determine our absolute calibration at altitude to about 5%.

Before the data were analyzed for astrophysical content, the signals recorded during aircraft banks, equipment rotation, moon-looking legs, and other "contaminated" data were eliminated. The "contaminated" data consisted of a total of 6 min when the roll monitor indicated a bank angle of more than 1° or when the rms fluctuations in the 33-GHz signal were abnormally high. The remaining 21 h of observations were fitted by a

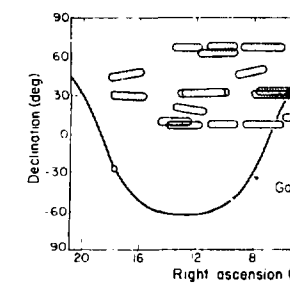

FIG. 2. Sky coverage for the eight flights is indicated by the shaded regions. Each oval region consists of several "legs" from the same flight. The width of each region was determined from the antenna pattern (7° FWHM), and the length was set by the motion of the U-2 and the rotation of the earth.

least-squares method to a sum of spherical harmonics. Only the first spherical harmonic is necessary to obtain a good fit ($\chi^2 = 91$ for 80 data points). Thus the temperature in the direction $\hat{\theta}$ is given by

$$T(\hat{\theta}) = T_0 + T_1 \cos(\hat{\theta}, \hat{n}). \quad (1)$$

Here T_0 is the average blackbody temperature (not measured in this experiment), T_1 and $\hat{n}$ are the parameters of the fit, and $(\hat{\theta}, \hat{n})$ is the angle made by the unit vectors $\hat{\theta}$ and $\hat{n}$. The best fit is obtained for $T_1 = 3.2 \pm 0.6$ m°K and $\hat{n} = [10.8 \pm 0.5$ h right ascension (R.A.), $5 \pm 10°$ declination (dec)]. In galactic coordinates $\hat{n} = (54° \pm 10°$ lat., $245° \pm 15°$ long.).

Inclusion of second-order spherical harmonics in the fit changes the values of T_1 and $\hat{n}$ by much less than 1 standard deviation. An additional fit was made in which background contributions from the galaxy, the atmosphere, the motion of the earth around the sun, the antenna side lobes, and residuals in the apparatus were calculated and subtracted for each leg prior to the least-squares minimization. These corrections individually and cumulatively were less than 0.5 m°K per leg and were small compared to the signal. We will discuss these corrections in more detail in a subsequent paper. The resulting best-fit values were $T_1 = 3.5 \pm 0.6$ m°K and $\hat{n} = (11.0 \pm 0.5$ h R.A., $6° \pm 10°$ dec).

The data, with and without corrections, are plotted in Fig. 3, along with the best-fit curve to the uncorrected data. The residuals are small; to a 70% confidence level they are $\lesssim 10^{-3}$ K. Thus, *except for a component that varies as* $\cos(\hat{\theta}, \hat{n})$, the cosmic blackbody radiation is isotropic to 1 part in 3000.

The cosine anisotropy is most readily interpreted as being due to the motion of the earth relative to the rest frame of the cosmic blackbody radiation—what Peebles calls the "new aether drift." Using 2.7°K for T_0 and the fit to the corrected data, we calculate that the earth is moving at a velocity of $v = (T_1/T_0)c = 390 \pm 60$ km/sec in the direction $\hat{n}$ towards the constellation Leo. This result differs from the preliminary result reported by Corey and Wilkinson by less than twice their reported errors.[6] In addition it differs substantially from the values of the peculiar velocity for the motion of the sun measured with respect to nearby galaxies by Rubin *et al.*[7] and by Visvanathan and Sandage.[8] If we subtract from our measured velocity the component due to the rotation of the Milky Way galaxy,[9] ≈ 300 km/sec, we calculate

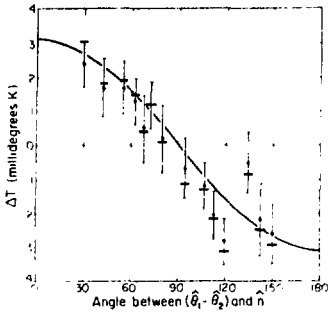

FIG. 3. Comparison of the data with the fit to Eq. (1). The temperature difference $\Delta T = T(\hat{\theta}_1) - T(\hat{\theta}_2)$ is plotted versus the angel between the vectors $(\hat{\theta}_1 - \hat{\theta}_2)$ and $\hat{n}$ 10.8 h R.A., 5° dec, the direction of maximum temperature. Data from legs at nearly equal angles were combined; each datum point plotted represents ~ 2 h of data. The large dots represent the uncorrected data; the horizontal bars show the data with expected systematic effects subtracted out. The errors shown are statistical only.

the net motion of the Milky Way with respect to the canonical reference frame of cosmology to be ~ 600 km/sec in the direction (10.4 h R.A., −18° dec). These various velocities are summarized in Table I. The large peculiar velocity of the Milky Way galaxy is unexpected, and presents a challenge to cosmological theory.

The limits on the second- and higher-order spherical harmonics place new constraints on several phenomena of cosmological importance. Collins and Hawking have shown[13] that vorticity, equivalent to a net rotation of the universe, can contribute a second-order spherical harmonic due to the transverse Doppler shift. The limit which one can place on this rotation depends strongly on the model of the universe that is assumed. Using a semiclassical model, and assuming the blackbody radiation has not scattered since it was emitted at a redshift z, the rotation of the universe contributes a second-order harmonic of amplitude[14]:

$$T_2 = \frac{T_0 \omega_0^2 (1+z)^4}{8H_0^6 (1+2q_0 z)}, \qquad (2)$$

where ω is the present value for the angular velocity of the universe. If we take $H_0^{-1} = 2 \times 10^{10}$ yr for the present value of Hubble's constant, $q_0 = 0.03$ for the deceleration parameter, $T_0 = 2.7$ K for the present temperature of the radiation, $z = 1500$, and $T_2 < 10^{-3}$°K, we calculate that the rotation of the universe is presently less than 10^{-9} sec of arc per century.

Our limit on the second-order spherical harmonic also puts a constraint on the existence of large-wavelength gravitation radiation. Using the calculation of Burke,[15] we conclude that the mass

TABLE I. Peculiar velocities (km/sec).

Reference	V (km/sec)	R.A. (h)	dec	Galactic (long.) l	Galactic (lat.) b
Motion of sun relative to cosmic blackbody radiation					
3	270 ± 70	13 ± 2	−25° ± 20°	306°	38°
This work	390 ± 60	11 ± 0.6	6° ± 10°	248°	56°
10	≲ 350				
Motion of sun relative to nearby galaxies					
11	299 ± 45	7.3	51°	167° ± 13°	25° ± 6°
7	600 ± 125	2 ± 1	53° ± 11°	135°	−8°
8	300 ± 25	21.2	48°	90°	0°
9	308	23.1	51°	105° ± 4°	−7° ± 5°
12	346 ± 76	18	45°	72°	28°
Motion of sun in orbit around Milky Way galaxy (rotation of galaxy)					
8	300 ± 50	21.2	48°	90°	0°
Motion of Milky Way galaxy relative to cosmic blackbody (this work and rotation of galaxy)					
	603	10.4	−18°	261°	33°

density of such radiation in the universe is $\lesssim \rho_c$, where ρ_c is the critical mass density necessary to close the universe.

In summary, we have observed anisotropy that varies as $\cos(\hat{\theta}, \hat{n})$. Excluding this component, the cosmic blackbody radiation is isotropic to 1 part in 3000. The cosine component is most readily interpreted as due to the motion of the earth with respect to the radiation with a velocity of 390 ± 60 km/sec (the "new aether drift"), but we cannot eliminate the possibility that some of the anisotropy is due to an intrinsic variation of the cosmic blackbody radiation itself.

This work was supported by the U. S. Energy Research and Development Administration and the National Aeronautics and Space Administration. We gratefully acknowledge contributions to the design of the experiment by L. W. Alvarez, T. S. Mast, H. B. Dougherty, J. H. Gibson, J. S. Aymong, and R. G. Smits, and participation in the experiments by J. A. Tyson and S. Pollaine. The experiment was made possible by the support and encouragement of H. Mark, A. Sessler, R. Birge, R. Cameron, and N. Boggess. Important contributions and suggestions were made by A. Buffington and C. D. Orth, and by the members of the Earth Survey Aircraft facility at NASA-Ames, including M. Knutson, J. Barnes, C. Webster, R. Williams, R. Erickson, and S. Norman. This experiment was inspired by J. Peebles's book, *Physical Cosmology* (Ref. 1).

[1]P. J. E. Peebles, *Physical Cosmology* (Princeton Univ. Press, Princeton, N. J., 1971); S. Weinberg, *Gravitation and Cosmology: Principles and Applications of the General Theory of Relativity* (Wiley, New York, 1972).

[2]Both E. K. Conklin [Nature (London) 222, 971 (1969)] and P. Henry [Nature (London) 231, 516 (1971)] claimed to observe a first-order harmonic. However, in both experiments backgrounds were much larger than the observed effect, and the resulting fits were very poor [see A. Webster, Mon. Not. Roy. Astron. Soc. 166, 355 (1974)]. In both experiments the 1-standard-deviation errors in the direction of the earth's velocity cover a large part of the sky. (Conklin quotes probable errors, not standard deviations.)

[3]B. E. Corey and D. T. Wilkinson, Bull. Astron. Astrophys. Soc. 8, 351 (1976).

[4]G. F. Smoot, in Proceedings of the Spring Meeting of the American Physical Society, Washington, D. C. 1977 (unpublished); M. V. Gorenstein, G. F. Smoot, and R. A. Muller, Bull. Astron. Astrophys. Soc. 9, 431 (1977).

[5]M. V. Gorenstein, R. A. Muller, G. F. Smoot, and J. A. Tyson, to be published.

[6]The reported errors in the preliminary results of Corey and Wilkinson (Ref. 3) at 19 GHz were statistical only. New results (300 ± 70 km/sec, 12 ± 2 h, $-10° \pm 20°$) from their group (D. Wilkinson, private communication) are in closer agreement with our results.

[7]V. G. Rubin, W. K. Ford, N. Thonnard, M. S. Roberts, and J. A. Gordon, Astron. J. 81, 687 (1976).

[8]N. Visvanathan and A. Sandage, to be published.

[9]A. Yahil, G. A. Tammann, and A. Sandage, to be published.

[10]D. Muehlner and R. Weiss, *Infrared and Submillimeter Astronomy*, Astrophysics and Space Sciences Library (Reidel, Hingham, Mass., 1976), Vol. 63.

[11]G. deVaucouleurs and W. L. Peters, Nature (London) 220, 868 (1968).

[12]P. L. Schecter, to be published.

[13]C. B. Collins and S. W. Hawking, Mon. Not. Roy. Astron. Soc. 162, 207–220 (1973).

[14]S. Pollaine and G. F. Smoot, Lawrence Berkley Laboratory, Astrophysical Note No. 343, 1977 (unpublished).

[15]W. L. Burke, Astrophys. J. 196, 329–334 (1975).

Radiometer system to map the cosmic background radiation

Marc V. Gorenstein, Richard A. Muller, George F. Smoot, and J. Anthony Tyson[a)]

University of California, Lawrence Berkeley Laboratory and Space Sciences Laboratory, Berkeley, California 94720

(Received 14 November 1977)

We have developed a 33-GHz airborne radiometer system to map large angular scale variations in the temperature of the 3 K cosmic background radiation. A ferrite circulator switches a room-temperature mixer between two antennas pointing 60° apart in the sky. In 40 min of observing, the radiometer can measure the anisotropy of the microwave background with an accuracy of ±1 mK rms, or about 1 part in 3000 of 3 K. The apparatus is flown in a U-2 jet to 20 km altitude where 33-GHz thermal microwave emission from the atmosphere is at a low level. A second radiometer, tuned to 54 GHz near oxygen emission lines, monitors spurious signals from residual atmospheric radiation. The antennas, which have an extremely low side-lobe response of less than -65 dB past 60°, reject anisotropic radiation from the earth's surface. Periodic interchange of the antenna positions and reversal of the aircraft's flight direction cancel equipment-based imbalances. The system has been operated successfully in U-2 aircraft flown from NASA-Ames at Moffett Field, CA.

INTRODUCTION

We have developed and tested an airborne radiometer to detect and map anisotropy of the 3-K cosmic blackbody radiation on a large angular scale. This radiometer represents a state of the art improvement of the basic twin-antenna Dicke radiometer used by several groups[1-3] to set previous limits on the anisotropy.

Anisotropy in the background radiation of a few millikelvins (mK) should result from the motion of the solar system with respect to the 3-K cosmic blackbody radiation. In addition, the motion of the earth around the sun produces an annually varying anisotropy of 0.3 mK. Anisotropies would also be expected from asymmetric expansion of the universe, large scale irregularities in the distribution of matter or energy, or various other dynamical effects important in the evolution of the universe.

Our radiometric system is designed to detect anisotropic radiation in the cosmic background with a sensitivity of a few tenths of a millikelvin. The design incorporates several new features that reveal or cancel systematic effects. In this section we shall briefly describe the system operation. In the balance of the paper we expand on this description, detail the design criteria and document the system's performance.

Two antennas that point 30° from the zenith and oppositely in azimuth collect the 33-GHz radiation (see Fig. 1–3). Thus the sky provides both the source and the reference for differential detection of anisotropy. The 33-GHz frequency is in a "window" where the sum of atmospheric and galactic microwave backgrounds is minimal. The antennas are dual-mode corrugated horns that reject side-lobe illumination from the direction of the earth by more than −65 dB and thereby reduce signals due to anisotropic terrestrial radiation below the 0.2 mK level.

A switching ferrite circulator, alternating between the antennas at 100 Hz, directs the radiation to a room-temperature mixer. Rapid switching between antennas reduces $1/f$ noise from the receiver. Two 1000-MHz bandwidth i.f. gain stages amplify the signal, and a lock-in amplifier analyzes the detected output for a component synchronous with the switching. Thus the radiometer detects *only* the difference in sky temperature, not its absolute intensity. The 33-GHz receiver rms sensitivity is 44 mK/Hz$^{1/2}$.

The equipment is carried on board a U-2 jet to 20 km altitude where atmospheric microwave emission is greatly reduced. Pointing the antennas at the same zenith angle cancels most of the remaining thermal emission from the residual atmosphere. Slight departures from level flight are the primary cause of the remaining imbalance in atmospheric radiation received by the antennas. A second radiometer, functionally identical to the primary 33-GHz radiometer measures these im-

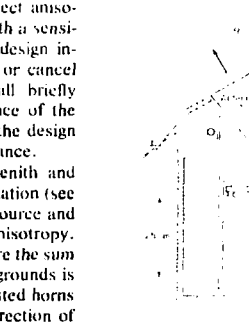

FIG. 1. Schematic layout of the radiometer apparatus in the U-2 equipment bay. The main electronics and mechanical components of the system are illustrated. The antennas are shown in the data taking position, with the direction of flight perpendicular to the plane of the drawing. Interchange of the antennas is accomplished by a periodic (once per 64 s) rotation of the equipment 180° about the vertical center-line.

 0034-6748/78/4904-0440$00.60

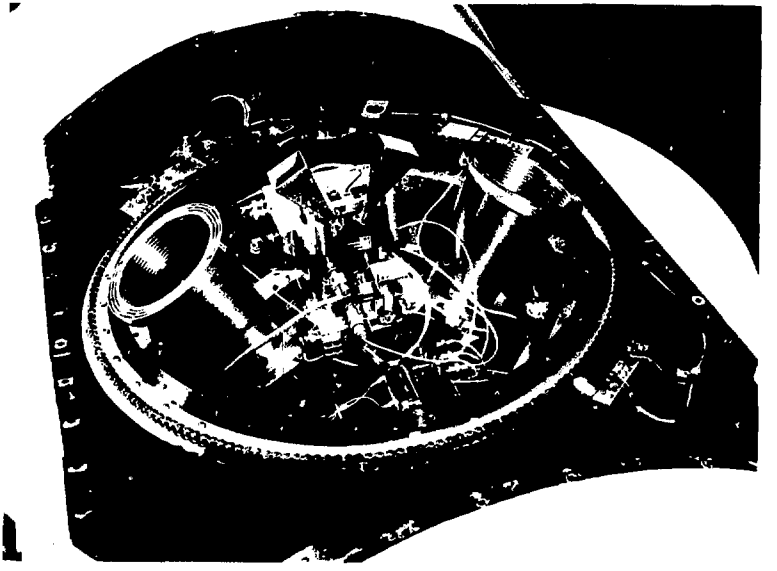

FIG. 2. The 33- and 54-GHz radiometers in the modified upper hatch of a U-2 jet. The rf shields and protective air cover have been removed to expose the horn antennas of the radiometer systems, the monitoring and demodulating electronics packages, and the outer bearing clamp and chain drive of the rotation system.

balances. This "roll monitor" is tuned to 54 GHz, in a region near strong oxygen emission lines.

Two switching techniques cancel and detect equipment-based imbalances. Periodic interchange of the antennas cancels insertion loss differences between the radiometer arms. The system is mounted in a bearing that rotates the radiometers 180° every 64 s. Periodic reversal of the aircraft flight path (about once per 20 min)

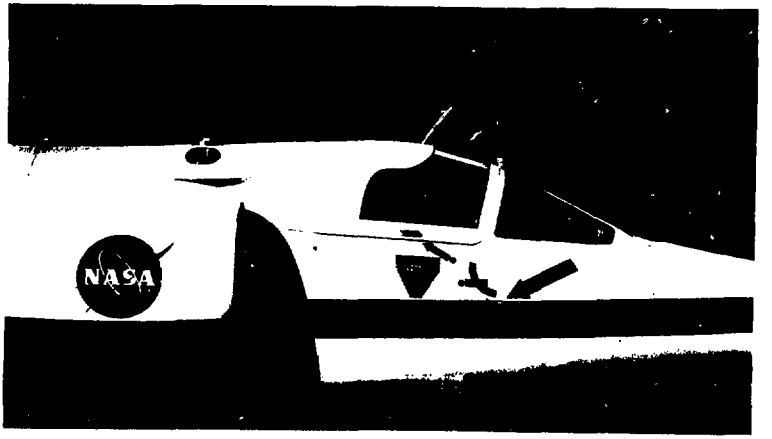

FIG. 3. The forward section of U-2 jet with a 33-GHz antenna mouth and a 54-GHz Teflon window visible. The modified upper hatch, situated just aft of the pilot's canopy, is easily removed from the U-2 equipment bay with the equipment installed, for checkout and testing. The top surfaces of the airscoops are 72° from the 33-GHz antenna beam axis.

detects asymmetries in the equipment correlated with rotation state.

The system incorporates thermal controls that regulate and monitor the temperatures of crucial components. All anisotropy, roll, and housekeeping data are recorded in flight on a magnetic tape cassette for later processing. The data collection is fully automated. Except for turning the equipment on, and initiating the rotation sequence at altitude, the pilot's primary responsibility is to orient the airplane according to the flight plan.

I. CHOICE OF FREQUENCY AND OBSERVING PLATFORM

In choosing a receiver frequency one must consider astrophysical backgrounds, emission from the atmosphere, and receiver sensitivity. Synchrotron radiation from the Milky-Way Galaxy places a fundamental limit on the sensitivity of any experiment which measures the anisotropy of the cosmic background radiation. At about 1 GHz the intensities of galactic synchrotron emission and the cosmic background are comparable. Fortunately, compared to the cosmic background, galactic synchrotron radiation falls off rapidly with frequency.

Fig. 4 shows antenna temperature[6] of typical galactic synchrotron emission is plotted as a function of frequency in Fig. 4. This plot shows that by 20 GHz the magnitude of *the extrapolated galactic background falls below 1 mK*. The thermal spectra of ionized hydrogen (H II) regions and dust clouds, which are mainly localized near the galactic plane, are also shown.

Also plotted in Fig. 4 is our estimate of state-of-the-art room-temperature receiver sensitivity as a function of frequency for 1 h of integration. The need to detect anisotropies on limited time scales constrains the choice of receiver frequency to frequencies where the expected anisotropy is on the order of a millikelvin or more.

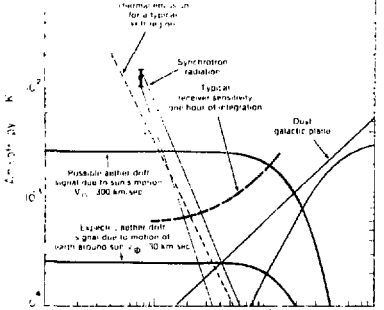

FIG. 4. Estimates of galactic radiation backgrounds as a function of frequency compared to a possible "Aether Drift" signal. The large scale anisotropy of galactic microwave radiation is comparable to the absolute intensity of the sources. The dust and HII regions are concentrated in the galactic plane and tend to be greatest near the galactic center. An estimate of receiver sensitivity for 1 h of integration is included.

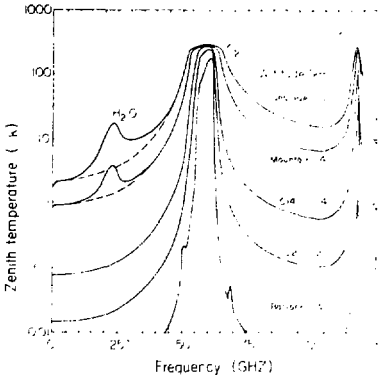

FIG. 5. An estimate of the zenith temperature due to atmospheric emission as a function of frequency and altitude, computed from the formulae of Meeks and Lilley.[7] We used these calculations in combination with other considerations described in the text to choose the 33 GHz observation frequency. Atmospheric emission at 54 GHz gives sufficient signal strength to monitor rolls at the 12 altitude, but is sufficiently unsaturated on the ground to permit verification of the predicted emission.

Thermal microwave emission from the earth's atmosphere is an important background. Figure 5 is a plot of the expected zenith temperature due to atmospheric emission as a function of frequency and altitude. The oxygen spectrum is calculated using a standard model of the earth's atmosphere together with formulae that describe the microwave spectrum of O_2 as a function of temperature and pressure.[7] This plot shows that there are preferred windows—below 20 GHz, around 35 GHz, and around 90 Ghz—in which atmospheric effects are greatly reduced relative to the peaks. The choice of the 33-GHz receiver frequency was based on the above considerations. This is a frequency where the effects of galactic background and atmospheric emission are minimized, and where receiver performance and signal strength are adequate.

A high-altitude platform is required for this measurement because fluctuations of precipitable water vapor do not allow a sensitive experiment to be done on the ground. Even at mountain-top altitude fluctuations of 2 mK are common.[8] The experiment must be conducted at altitudes above 14 km, where all significant water vapor has been frozen out.[9] Pointing the antennas at nearly the same zenith angle can cancel the residual thermal radiation from the oxygen above this altitude.

There are several vehicles which could be used for altitudes of 14 km and above: satellites, balloons,

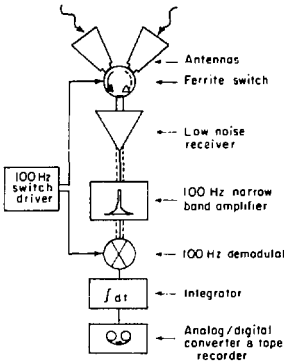

FIG. 6. Components of the 33- and 54-GHz radiometers. The individual components making up the receiver section are shown in Fig. 8.

and aircraft. Although a satellite experiment is potentially the most sensitive, having no atmospheric background and long integration times, it is also the most expensive. Such an experiment (the Cosmic Background Explorer) is now being planned, but it will not be flown for several years. The results from an airplane experiment will aid in the design and planning of the satellite experiment. Other anisotropy experiments sensitive to the millikelvin range are currently being flown,[4-10] and use balloons to reach the necessary altitudes. The U-2 is a particularly good vehicle for this experiment because of its high-altitude (20 km), excellent roll stability, and quiet electrical and mechanical environment. The U-2 has the advantage over balloons of being piloted and less at the mercy of weather. Recovery of the instrument after a flight is straighforward.

II. RADIOMETER

Figure 6 shows a schematic drawing of the 33- and 54-GHz radiometers. Rapid switching between a source and a reference load is a standard technique used to reduce the effect of receiver gain fluctuations ($1/f$ noise) in a microwave radiometer. We use a dual antenna configuration where the sky is both the source and the reference. Thus difficulties in monitoring the temperature of a reference load within a few tenths of a millikelvin are eliminated. Radiation from the atmosphere is canceled by pointing the antennas at the same zenith angle. The primary components of the radiometers are the antennas, the ferrite ("Dicke") switch, the receiver, and the downstream electronics. A discussion of each of these components for the 33-GHz radiometer follows.

A. Antennas

The anisotropy in the blackbody radiation is minute compared to anisotropies in the radiation from the earth and aircraft. Thus a first requirement of the antenna system is that its side-lobe response reduce the differential emission from the earth and aircraft below the design sensitivity, about 0.2 mK. Thus the integrated 300-K signal from the earth must be reduced by a factor of about 10^{-6} compared to the main beam. Secondly, this performance must be achieved with a compact design. Mechanical and aerodynamic considerations make installation of antennas with large apertures or ground shields impractical in the U-2. Thirdly a beam width of more than 1° is needed. A small beamwidth would make the measurement susceptible to spurious signals from pointlike astrophysical sources of radiation. Finally to eliminate potential systematic errors, the insertion loss of the antennas must be small, or comparable to losses of other components upstream of the receiver.

These criteria were met by corrugated horn antennas based on the work of Simmons and Kay.[11] A matched pair of antennas with a beam width of 7° FWHM were built by TRG Division of Alpha Industries for this experiment. Each antenna is an aluminum cone with concentric grooves machined down the full length of the inside surface. The grooves force the electric field at the edges to zero, effectively apodizing the aperture. This effect is enhanced by the excitation of two modes in the antenna throat phased to cancel at the mouth of the antenna. At the throat end of the antenna a transition is made from circular to rectangular waveguide.

A sensitive measurement of the antenna beam patterns was made at the JPL–NASA test range of the Jet Propulsion Laboratory in Pasadena, CA. Figure 7 shows the results of the experimental measurement along with the theoretical predictions of antenna patterns.[12] These re-

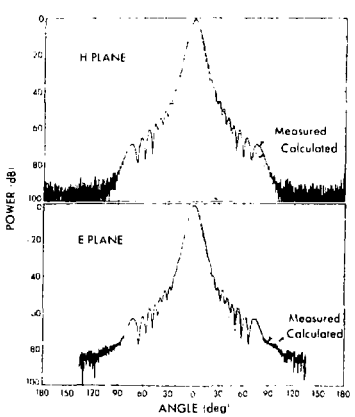

FIG. 7. The E and H plane one-way power pattern of the 33-GHz corrugated horn antennas used in this experiment, as measured at the JPL test range. Low side-lobes are necessary to reduce anisotropic radiation from the earth and aircraft. The integrated power received from the earth is reduced by over 10^{-5} compared to the main beam

sults imply that the earth should contribute a total antenna temperature of no more than 2 mK, and the airplane no more than 2.1 mK into either antenna during level flight. Radiation from terrestrial surface features with different emissivity illuminating the side-lobes should result in differential reception between the two antennas of no more than 0.2 mK.

The aircraft made 20° banks over the California coast to check the calculations. During the banks, terrestrial radiation illuminated the side-lobes of the lowered antenna to within 40° of the central beam axis. Systematic differences of ~ 4 mK out of the 22-mK bank signal were observed as the lowered antenna swept over terrain of varying emissivity. This limit is in agreement with the predicted value calculated from convolving the antenna beam pattern with the varying thermal emission from the earth at 33 GHz.

B. Ferrite switch

A latching ferrite circulator switches the input of the receiver between the two antennas at 100 Hz. The switch was manufactured by Electromagnetic Sciences Corporation of Atlanta, GA. The input ports are canted at 30° so the antennas connect directly to the switch without any intervening waveguide. Small adjustable attenuation stubs in each port reduce the insertion loss imbalances between switch states to less than 50 mK.

The switching is accomplished by reversing the magnetic field of a ferrite embedded in the circulator. If an interaction between the earth's magnetic field and the switch has a significant orientation dependence, then a signal synchronous with the antenna rotation may result; thus the earth's field is a potential background. To avoid this background we had the manufacturer shield the switch with μ-metal and we enclosed the switch in additional magnetic shielding. We tested the shielding by immersing the entire hatch in a periodically reversing 10 G field. Based on these tests, we conclude that an interaction of the earth's field with the switch results in a spurious signal of less than 0.1 mK.

C. Receiver

A primary limitation in the measurement of differential signals of a few tenths of a millikelvin is the noise added to the signal by the receiver. The sensitivity of a radiometric system is defined as the root-mean-square (rms) noise fluctuation in the power output of the receiver (referenced to the input port) and is given by the formula[13]

$$\Delta T_{\rm rms} = K \frac{(T_R + T_A)}{\sqrt{B\tau}},$$

T_R is the receiver noise temperature in kelvins, T_A is the antenna temperature for this measurement, B is the i.f. bandwidth, τ is the integration time, and K is a constant depending on radiometer design (1 for a total power radiometer, 2.2 for this configuration).

FIG. 8. The components [illegible] 33-GHz this standard superheterodyne [illegible] a local oscillator klystron, isolator, the signal [illegible] up 63 for further amplification. The [illegible] wide bandwidth operation at room temperature.

Our design goal was a system that would have [illegible] sensitivity of less than 1 mK in 1 h of integration time and would operate at room temperature. It had to be rugged enough to perform satisfactorily in an aircraft environment.[2] These goals were met by a receiver based on a balanced mixer built by Spacek Komp in Santa Barbara, CA. The combination of a balanced mixer and i.f. preamplifier yielded an rms sensitivity of 35 mK in 1 s of integration or 0.8 mK in 1 h. The detector has a 26 dB rf to i.f. power gain with an i.f. bandwidth B of 1000 MHz, and a double sideband noise temperature of 500 K. Figure 8 illustrates the components of this receiver. Including 0.7 dB insertion loss from the upstream switch, isolator, and antennas, the system noise performance $\Delta T_{\rm rms}$ at altitude is 44 mK for 1 s of integration time. (T_R = 630 K) in agreement with measurements made in the laboratory.

D. Downstream electronics

The 33- and 54-GHz radiometers use similar demodulation, integration, and recording electronics. A narrow-band amplifier tuned to 100 Hz filters the detected output of the radiometer. A lock-in amplifier demodulates the sine wave component in phase with the 100-Hz switching between the antennas. The resulting difference signal is integrated for 2 s in an ideal integrator, then sampled, digitized, and recorded on magnetic tape for processing after the flight.

As a diagnostic of equipment performance the phase of the square wave that demodulates the 100-Hz component is switched by 180° every 12 s. The difference of the signals between the phase states provides a monitor of the radiometer imbalance which is observed to be about 50 mK for the 33-GHz radiometer. The average of the two signals is used to verify that the dc level of the system after demodulation is constant.

III. MONITOR FOR ATMOSPHERIC ANISOTROPY

Atmospheric microwave emission at 33 GHz can yield a spurious signal if the U-2 aircraft tilts at a bank. A second twin antenna radiometer, of the standard Dicke design, operating at 54 GHz monitors this potential source of background. Its antenna beam widths are matched to those of the 33-GHz antennas. Figures 1 and 2 show the position of the radiometer in the airplane hatch. The 54-GHz radiometer has a double-sideband noise temperature of 1000 K, and 500-MHz i.f. band-

FIG. 9. The measured atmospheric signal at 33 and 54 GHz as a function of aircraft bank angle. Data taken during banks of the aircraft show the magnitude of the atmospheric signals to be in reasonable agreement with predictions based on the work of Meeks and Lilley.[7] Both sets of data can be empirically fit to a secant θ law with zenith temperatures of 3.8 ± 2 mK at 33 GHz and 1.1 ± 0.2 K at 54 GHz. The 33-GHz data are expected to include a contribution to the 1 Ω signal from differential earthshine in the back antenna lobes as indicated.

width, yielding an rms sensitivity of 100 mK for 1 s of integration time. The choice of 54 GHz satisfies the requirements that the oxygen signal due to aircraft rolls be strong and easily monitored at the 20-km altitude, yet not be saturated on the ground, facilitating check out.

In several flights the U-2 performed a series of banks from 5° to 25° during which the 33- and 54-GHz radiometers measured the differential atmospheric emission. The results of these runs are shown in Fig. 9 along with the predictions based on our calculations of atmospheric zenith temperature (Fig. 5). Due to the small optical depth, atmospheric emission at this altitude varies approximately as the secant of the zenith angle. A 0.25° bank results in a differential signal of 0.2 ± 0.03 mK at 33 GHz and 95 ± 5 mK at 54 GHz, a ratio of 1 to 420. Thus in 1 s of integration the 54-GHz radiometer can measure the atmospheric contribution to the 33-GHz signal to ± 0.2 mK rms.

In level flight the 54-GHz roll monitor indicates that the U-2 autopilot, a Lear 201 automatic flight control system, maintains the aircraft at constant average bank angles of less than 0.25° for periods up to an hour. For departures from level flight of a few degrees or less, the average roll monitor signal is proportional to the average atmospheric signal at 33 GHz. Since a 0.25° roll yields a signal of only 0.2 mK at 33 GHz, the subsequent corrections to the anisotropy data during post-flight analysis are small. As with the 33-GHz signal, the 54-GHz signal is integrated and recorded every 2 s. On this time scale the rms fluctuations about the mean bank in level flight are less than 1° in roll angle. The output of the roll monitor is displayed to the pilot, but the average bank is so small that there has been no need to make corrections to the attitude of the aircraft in flight.

IV. U-2 AIRCRAFT AND ENVIRONMENT

The NASA–Ames Earth Survey Aircraft (U-2) is a single-seat aircraft designed as a high-altitude (20 km), long-range (2500 km), reconnaissance jet by Clarence "Kelly" Johnson of Lockheed Aircraft Company of California. In appearance the U-2 is like a glider with a single powerful jet engine. Our apparatus fits in a modified upper hatch replacing the standard access hatch above the equipment bay. It is located just aft of the cockpit and foward of the wings, Fig. 3. The two radiometers and most of the accompanying electronics are sealed off from below by a pressure can which maintains the equipment bay atmosphere at 0.28 kg cm^{-2}.

Twenty-eight volts dc supplied by the aircraft powers the equipment. The voltage is filtered against rf interference and regulated at 24 V. All data are recorded on board; no telemetry is used. The pilot flies the aircraft on a predetermined path. Normally there is no communication to the ground during data taking.

The equipment is operated in a carefully regulated thermal environment. Due to the finite emissivity of the horn antennas, a 0.05 °C physical temperature difference between the 33-GHz antennas would produce a 1 mK signal. However there is considerable variation in the loss per unit length along the horn. In flared smooth-wall horn antennas each transverse section radiates power approximately in inverse proportion to its diameter. But in the dual-mode corrugated design, the greatly reduced fields at the surface of the antenna mouth result in correspondingly lower loss per unit length. In the 33-GHz antennas the power per unit length contributed by the mouths is only $\frac{1}{3000}$ that of the throats.

A 20-kg aluminum block thermally shorts the throats together, and an aluminum bar shorts the midpoints of the antennas together. The temperature of the block, containing the antenna throats and the ferrite switch, is regulated at 26°C by embedded resistive heaters. The antenna mouths cool in the air-stream where they reach −35°C during the flight.

Silicon diodes used as temperature sensors monitor the absolute and differential temperatures of the antenna mouths and midpoints. Measurements made during the flight show the differential temperatures to be less than 0.05°C. Additional heaters maintain the 54-GHz ferrite switch at 35°C and regulate the digitizing and sequencing electronics at 25°C. Total heat dissipation through the antennas is about 70 W from the electronics and 50 W from the heaters. The equipment cools for 20 min after the rotation sequence is initiated at altitude, allowing the system to reach thermal stability. The aluminum block gradually cools an additional 1.6°C during the remainder of the flight.

Teflon windows protect the mouths of the 54-GHz antennas. The windows are 1.9 mm thick, or ½ wave-

length at 54 GHz, thereby minimizing reflections of an incoming signal. The emissivity of the windows is less than 1%. A physical temperature difference between the windows of a few kelvins results in a thermal signal of a few hundredths of a kelvin. This is negligible compared to the 85-mK signal generated at 54 GHz by the minimal roll to be detected, 0.2°. In contrast, at 33 GHz, windows with sufficient mechanical strength to withstand aerodynamic stress cannot be used. Differences in physical temperature of a few kelvins would produce spurious signals large compared to a few tenths of a millikelvin to be detected with this radiometer.

The entire assemblage is mounted on three vibration dampers that reduce potential microphonics due to aircraft vibration. The electronic components are packaged in modules that are shielded against radio-frequency interference and a double-shielded container encloses the entire assembly except for the actual antenna mouths.

A. Rotation system

As with previous anisotropy experiments, it is essential that the position of the antennas be periodically interchanged to cancel anisotropy inherent in the instrument. The main portion of the equipment is suspended on a 56-cm-diam bearing mounted in the U-2 hatch. A motor drives the bearing through a worm gear, a clutch, and a stainless steel chain. This system rotates the instrument 180° every 64 s to the alternate observing position.

A rotation takes 5 to 6 s during which the instrument is accelerated through a 90° turn and then decelerated until it coasts to rest against a positioning stop. The motor is shut off with a sensing microswitch. The design of the system insures proper alignment of the antennas in the observing positions to within 0.1°. A ten-turn potentiometer and four microswitches measure the rotation angle to within 0.5°. Their outputs are recorded, and the analog rotation angle signal is displayed on the pilot's instrument panel.

During ascent and descent the equipment is rotated 90° away from the observing positions to protect the 33-GHz antennas from the external environment. In this "stored" position, the 33-GHz antennas are positioned inside the hatch, and plugs, lined by brushes, seal the open ports.

B. Aircraft reversals

A spurious anisotropy signal would appear if the output depended on rotation state or if the apparatus were not located symmetrically in the U-2 aircraft. We detect and cancel any such signal by taking data in pairs of "legs" flown in opposite directions with respect to the ground and sky. During each leg the pilot flies the aircraft straight and level for 20 min. Six pairs of legs are flown in a typical flight. The final three pairs are usually flown in directions perpendicular to the first three.

TABLE I. Data recorded. The 28 analog and 4 digital words sampled in an 8-s data cycle. The 33- and 54-GHz integrated signals are sampled and recorded once every 2 s during each cycle. The other signals, primarily monitors of equipment performance and environmental conditions, are sampled less frequently.

Analog	Number of times sampled in 8 s
1. 33-GHz radiometer signal	4
2. 33-GHz noise monitor	2
3. Atmospheric (54-GHz) monitor signal	4
4. Atmospheric noise monitor	2
5. Heater circuit current	2
6. Antenna orientation	2
7. Absolute temperature, antenna mouth	1
8. Differential temperature between antenna mouths	1
9. Absolute temperature at middle of antenna	1
10. Differential temperature across middle of antennas	1
11. Temperature of 35-GHz ferrite switch	1
12. Five temperatures of 33- and 54-GHz radiometers	5
13. Accelerometer output	1
14. Power supply voltage	1
Digital	
Universal time	2
Antenna position, status bits	3
	32 words

V. DATA RECORDING AND ANALYSIS SYSTEM

The experiment is run in an automated mode. Controlling electronics, activated by the pilot at take-off, provide the necessary timing and sequencing signals to the equipment. A Datel LPS-16 data logger, a light weight low-power incremental tape recorder, digitizes and records four words of data per second on a magnetic tape cassette. Table I lists the quantities measured and recorded in an 8-s data cycle.

During post-flight analysis we use computer programs to display, edit, and average the measurements. The bulk of the editing consists of deleting data taken during banks and antenna rotations. The scatter of the edited data is generally consistent with a gaussian distribution, as expected for signals from a noise-limited radiometer. On two occasions during data-taking flights transients occurred that were inconsistent with statistical fluctuations about the mean. These points were removed, resulting in a loss of 20 s of data. Data taken during course corrections made by the pilot are deleted if the 54-GHz roll monitor indicates a bank of more than 1°. The cuts due to rolls and transients amount to less than 6 min out of 32 h of data taken over nine flights.

The remaining data are grouped by "legs" and averaged. The anisotropy is found in each leg by subtracting the averages of data taken in one antenna orientation from the average of data taken in the other orientation. Corrections are applied to these averages for astrophysical, local, and equipment-based backgrounds. Table II lists these corrections, and tabulates the 90 percentile limits on the magnitudes of the corrections that are ap-

TABLE II. Residual systematic effects. The 90 percentile limits on the magnitude of the corrections applied to data averaged over a leg. Most systematic corrections applied to the data are small compared to the integrated sensitivity of a flight, about 0.5 mK.

Effect	90% of the corrections in each category result in change of less than (mK)
Galactic backgrounds	
Synchrotron radiation	0.32
Ionized hydrogen (H II regions)	0.01
Radio sources	0.06
Dust	0.01
Atmospheric anisotropy (Banks)	0.15
Antenna side lobes	0.20
Antenna temperature difference	0.27
Motion of Earth around Sun	0.23
Jupiter	0.01
Combined	0.56

plied to each leg. The 90 percentile limits for the combined corrections applied to each leg is 0.56 mK.

VI. RESULTS OF ENGINEERING AND DATA FLIGHTS

Three engineering flights were used to study the thermal environment of the equipment in the U-2 by monitoring the external temperatures and the heat flow through the antennas. During these flights the effect on the equipment of radio transmissions from the plane and engine restart were checked and found not to cause significant interference.

The statistical and systematic properties of the 33-GHz signals in nine subsequent data flights were studied by a variety of methods. The data were auto-correlated, and signal averaged at the rotation period. In the initial three data flights correlations were seen with time periods of 40 to 120 s, and amplitudes that varied from 10 to 45 mK. After these flights were made a number of changes and improvements including the following: A parametric amplifier[13] was replaced with the SpaceKom mixer, and regulation of the temperatures of the aluminum block and the controlling electronics was improved. In the final six data flights no correlations were observed, nor anomalous effects in the signal-averaged plots, down to sensitivities limited by statistics. Figure 10 shows a segment of data taken with the 33- and 54-GHz radiometers from the fifth data flight.

A spurious signal of about 2 mK, of yet unexplained origin, is associated with the rotation state of the system. Reversing the heading of the aircraft measures this effect, and shows it is constant during a flight. This offset is subtracted from the data for later analysis. It may be inherent in the system, or due to an asymmetry in the way the equipment is mounted in the plane. This problem is being investigated.

Microwave absorbers maintained at room temperature and at liquid nitrogen temperature are used in the laboratory as the primary calibrators of the 33- and 54-GHz radiometers. The equipment was also calibrated during pre- and post-flight checkout with a secondary calibrator. In several flights the moon provided a check of the calibration. The U-2 flew the equipment over a predetermined location at the proper time and heading so that one of the antennas pointed at the moon to within 0.5°. The observed signals of (675 ± 25) mK imply a surface temperature of (228 ± 12) K consistent with measurements made on the ground by us and others[15] at similar wavelengths.

During the flights the anticipated thermal, terrestrial, and atmospheric backgrounds were at the expected level. Data were accumulated for directions distributed over the northern hemisphere. Anisotropy in the cosmic background radiation has been detected in these data with an overall sensitivity of ±0.6 mK. Details are published elsewhere.[16]

ACKNOWLEDGMENTS

This work was supported by the Department of Energy and the National Aeronautics and Space Administration. We gratefully acknowledge contributions to the design of the experiment by L. W. Alvarez, T. S. Mast, H. B. Dougherty, J. H. Gibson, J. S. Aymong, R. Lane, W. Ferguson, and R. G. Smits, and participation in the experiment by S. Pollaine and P. Lubin. One of us (JAT) is grateful to the University of California Physics Department at Berkeley, the Space Sciences Laboratory, and the Lawrence Berkeley

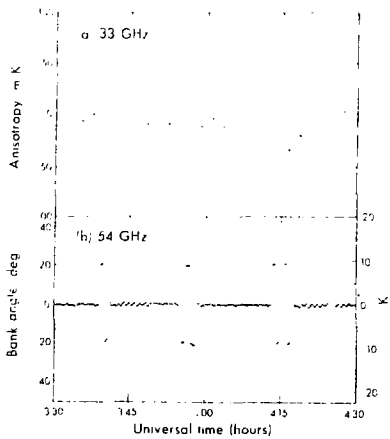

FIG. 10. The 33- and 54-GHz data from the fifth data flight. (a)—Each point is the measured anisotropy at 33 GHz averaged for 56 s during successive antenna orientations. The data are combined from both phase states of the 100-Hz demodulating wave form. The error bars are the computed rms fluctuations of the 2 s data divided by the square root of the number of measurements. (b)—The corresponding 54-GHz data, where no averaging has been done, show the scatter for 2 s of integration, and the roll signal during 20° banks of aircraft. There is more oscillation about the mean in legs flown north (e.g., 3:41 to 3:55) than in alternate legs flown south. This effect is produced by an interaction between the aircraft's magnetic heading sensor and the autopilot. Averaging the data shows that only the amplitude, not the mean, of the roll oscillation is affected.

Laboratory for their hospitality during a sabbatical year. The experiment was made possible by the support and encouragement of Dr. H. Mark, Dr. A. Sessler, Dr. R. Birge, Dr. R. Cameron, Dr. N. Boggess, and Dr. N. Roman. Important contributions and suggestions were made by A. Buffington, C. D. Orth, A. Webster, W. J. Welch, D. D. Thorton, and B. Leskovar, and by the members of the Earth Survey Aircraft facility at NASA-Ames including M. Knutson, J. Barnes, C. Webster, R. Williams, R. Erickson, and S. Norman.

This work was supported by NASA Grant 2125 and ERDA Contract #W-7405-ENG-48.

* Visiting scientist from Bell Laboratories, Murray Hill, NJ 07974.

[1] R. B. Partridge and D. T. Wilkinson, Phys. Rev. Lett. **18**, 557 (1967).
[2] E. K. Conklin, Nature **222**, 971 (1969).
[3] P. S. Henry, Nature **231**, 516 (1971).
[4] B. J. Corey and D. T. Wilkinson, Bull. Am. Astron. Soc. **8**, 351 (1976).
[5] P. J. E. Peebles, *Physical Cosmology* (Princeton U. P., Princeton NJ, 1971), pp. 142.
[6] Throughout this paper we shall refer to microwave intensities in the units of *antenna temperature*. The antenna temperature of a source is the temperature of a blackbody radiator filling the antenna beam, observed at a frequency ν in the Rayleigh-Jeans region that matches the power of the source. Kelvins can be converted to W m^{-2} Hz^{-1} by multiplication by the coefficient which appears in the Rayleigh-Jeans blackbody formula $(2\nu^2/c^2)kT$. Here k is Boltzmann's constant, ν is the frequency, and c is the speed of light. At 33 GHz the coefficient is $2k\nu^2/c^2 = 3.3 \times 10^{-26}$ W m^{-2} Hz^{-1} K^{-1}.
[7] M. L. Meeks and A. E. Lilley, J. Geophys. Res. **68**, 1683 (1963).
[8] D. E. Burch, J. Opt. Soc. Am. **58**, 1383 (1968).
[9] P. Kuhn, M. Lojko, and L. Peterson, Nature **223**, 267 (1969).
[10] D. Meuhlner and R. Weiss, *Infrared and Submillimeter Astronomy* (Astrophysics and Space Sciences Library, Reidel, 1970), Vol. 16, A. J. Sommers and A. E. Kay, IEEE Conf. Publ. **21**, 213 (1966).
[11] P. D. Potter, "A New Computer Program for the Design and Analysis of High Performance Conical Feedhorns," Deep Space Network Technical Report #32-1526, Vol. XIII, pp. 92–107, Jet Propulsion Laboratory, Pasadena CA, February 15, 1973).
[12] See for example, J. D. Kraus, *Radio Astronomy* (McGraw Hill, New York, 1966), p. 251.
[13] Originally, a low noise room temperature receiver based on a 9 GHz degenerate parametric amplifier was used in the engineering and initial data flights in 1976. The receiver built by ERG Division of Alpha Industries had a noise temperature in the lab of 700 K, with a IF bandwidth of 300 MHz having a system sensitivity in 1 s of integration of 38 mK. However gain stability was difficult to achieve in flight because its thermal gain coefficient was −0.4 dB °C^{-1}. In 1977 the SpaceKom mixer became available and we used it because of its greater gain stability, its simplicity, and its equivalent sensitivity.
[14] C. H. Mayer, *Surfaces and Interfaces of Physical and Solid State*, edited by A. Dalliuss (Academic, New York, 1970), pp. 180.
[15] T. Hagfors, Radio Sci. **5**, 189 (1970).
[16] G. F. Smoot, M. V. Gorenstein, and R. A. Muller, Phys. Rev. Lett. **39**, 898 (1977).

Appendix C - The Ferrite Switch and Radiometer-arm-offset

C.1 Introduction

In an ideal radiometer, balanced signals applied to each of the two antenna inputs should yield a null output. In practice, asymmetries between the two antennas and between the two circulation states of the ferrite switch result in a spurious output called the radiometer-arm-offset. The primary source of this offset is insertion loss imbalance in the ferrite switch. Interchange of the radiometer arms was, of course, expressly incorporated into the equipment design to cancel such imbalance. However, in the second order, the offset must be stable within 0.2 m °K during the period of one rotation cycle. The ferrite switch's offset varies with temperature by about 17 m °K/ °K requiring thermal regulation to within a few tenths of a degree Kelvin. The offset must also be of small enough magnitude that small variations in receiver gain throughout a rotation cycle will yield acceptably small variation in signal strength. Variations in receiver gain of about 0.3 db/hour require that the radiometer-arm-offset be less than about 100 m °K, in order that signal drift be less than 0.2 m °K in the 128 second antenna cycle.

This Appendix summarizes our experience with the ferrite switch. Section C.2 describes the switch and the cold-load adjustment technique that nulls, or balances, its insertion loss. Section C.3 describes the phase switching technique that measures the radiometer-arm-offset in flight. The ground based test that demonstrates the negligible interaction of the switch with the earth's magnetic field, is described in Section C.4.

C.2 The Ferrite Switch Offset

The ferrite switch reduces the effect of gain fluctuations ($1/f$ noise) in the receiver, by switching the receiver between the two antennas at 100 Hz. The switch is a symmetric three port circulator. Upon application of a current pulse, of the appropriate sign, it latches into a clockwise, or counterclockwise circulation state. The switch was manufactured by Electromagnetic Sciences Corporation of Atlanta, Georgia to our specifications. Its input ports are canted $\pm 30°$ so the antennas connect directly to the switch without any intervening waveguide. A pair of adjustable insertion loss stubs project from the broad wall of each input port. These stubs are functionally identical to standard microwave attenuators, though they can modify the insertion loss with a resolution of 10 m °K out of 290 °K, or about 10^{-4} db.

The insertion loss of the ferrite switch is about 0.35 db, or 8%. With the waveguide of the switch at 290 °K, the thermal signal injected into the receiver due to this insertion loss is then 24 °K. With no adjustment, there is a 4% difference in the insertion loss between the two circulation state, yielding a contribution to the radiometer-arm-offset of about 1 °K. We adjust the offset in the laboratory by replacing the antennas with a pair of identical terminations cooled in a bath of liquid nitrogen to 77 °K, adequately simulating the signal from the cold sky. The terminations are thermally isolated from the switch with one inch lengths of thin-walled stainless steel waveguide. The loads are periodically interchanged, canceling their intrinsic imbalance of about 50 m °K. The insertion loss of the "cooler" input port is increased by inserting the adjustable stub until an adequate balance is achieved. In flight the radiometer-arm-offset was usually below about 50 m °K, Figure III.1.

The difficulties with this procedure center on maintaining a stable signal difference between the two cold loads. The loads are an informal collection of stainless steel waveguide, mylar windows that keep out condensation, and masking tape that keeps the liquid nitrogen from filling the immersed termination. However, the masking tape seal is unreliable. With some care and patience the system does yield reproducible measurements, and the adjustment of the insertion loss can be made to about ± 10 m °K.

In flights 8-11 the offset was below 50 m °K but increased to about 142m °K in flight 12, requiring additional adjustment to the switch. In the pre-flight tests for flight 13 and 14 the offset as measured and adjusted with the cold load technique was different from the offset as measured in the pre-flight configuration by some 100m °K.

C.3 Phase Switching

Imbalance in insertion loss between the 33-GHz radiometer arms results in a non-zero 100-Hz amplitude detected by the lock-in amplifier. In principle, it is possible to know the DC level sufficiently well that the offset can be determined from the recorded output alone. But, in practice, reversing the sign of the 100-Hz demodulation waveform in the lock-in amplifier determines the radiometer-arm-offset more accurately. Since this is equivalent to changing the demodulation phase by 180°, we call this feature the 180° phase-switch. Thus in the 0° phase state,

$$\Delta T^{0}_{record} = \Delta T_{offset} + T_{DC-level} \qquad C.1$$

where

ΔT^{0}_{record} is the digitized signal recorded in the 0° phase state.

ΔT_{offset} is the radiometer-arm-offset, appearing as a 100-Hz amplitude, detected by the lock-in amplifier.

$T_{DC-level}$ is the arbitrary voltage level that the recording system adds to the signal.

We assume that the signals injected into the 33-GHz horn antennas are equal and independent of the rotation orientation of the antennas. Changing the demodulation phase by 180° gives

$$\Delta T^{180}_{record} = -\Delta T_{offset} + T_{DC\ level} \qquad C.2$$

whence

$$\Delta T_{offset} = (\Delta T^{0}_{record} - \Delta T^{180}_{record})/2. \qquad C.3$$

The phase-switch is implemented in the demodulation electronics of the 33-GHz and 54-GHz lock-in amplifiers. The switch is either set manually to one phase state, or is operated in the automatic mode, switching phase state after every 6th recording of a 33-GHz data word. The data-recording system tags each 2-second integration with a status bit according to the phase state. Signal averaging the data recorded in-flight at the 24 second phase period verifies proper operation of the switch. The algebra that extracts anisotropy measurements and ΔT_{offset} is described in Section IV.2.

C.4 Limits on Switch Interaction with the Earth's Magnetic Field

The alternation of the circulation state is accomplished by reversing the magnetic field of a ferrite embedded in the circulator. If an interaction between the earth's magnetic field and the switch has a significant orientation dependence then a signal synchronous with antenna rotation may result: thus the earth's field is a potential background. To avoid this background we had the manufacturer shield the switch with mu-metal and we enclosed the switch in additional magnetic shielding. We test the shielding by immersing the entire hatch in a periodically reversing magnetic field. The tests are carried out with the hatch in its usual flight configuration. Measurements show no effect at the level of ± 0.9mK in fields up to 10.8 gauss. This puts a limit of 0.06 mK at the two sigma level on the size of a magnetically induced background. The magnetic field is produced by two coils, about 80 cm in diameter with field lines directed across the narrow dimension of the hatch. The antenna's are positioned so the field is either oriented perpendicular or parallel to the plane containing the two antennas.

Appendix D - Flight Profile and Preparation

This section describes the procedures that have evolved in executing a data flight. Pre-flight preparations begin with a ground test conducted outdoors that measures the radiometer-arm-offset. Two aluminum reflectors re-direct both antenna beams so they point towards the zenith insuring that both inputs to the radiometer see balanced low level signals. Periodic reversal of the 100-Hz demodulation phase, and interchange of the reflectors about the antennas, measures the offset of the radiometer arms to a few milli-degrees Kelvin.

If the offset is above 100m°K, additional tuning of the ferrite switch is needed. This is a laborious procedure. The equipment must be disassembled so that the adjustment screws on the switch are exposed, and so the horn antennas can be replaced with liquid nitrogen cold loads. When the ground test shows that the offset is reduced sufficiently and all signals recorded on a test cassette appear normal, the equipment is ready to be taken to Ames Research Center at Moffett Field, California.

The flight crew is generally available only for sunset launches, although flights at later times in the night would sometimes be more convenient for us. The flight time is limited by the fuel load of the U-2 to about 5 hours. There are generally more flight opportunities in the fall and winter months. During the summer the U-2's are needed for agricultural photography and forest fire monitoring, limiting their availability for astrophysical research.

The pre-launch check-out commences about 3 hours before take-off and lasts 45 minutes. The main purpose of the check-out is the verification of proper operation of the equipment in the aircraft. A series of calibration runs, recorded on the installed flight cassette, documents the radiometer performance. This period is the last experimenter access to the equipment until after the flight.

The take-off of the U-2 is spectacular and often brings out a crowd of friends and well-wishers to watch. Always on schedule, the single engine pushes the aircraft along the runway into the air after a short 100 meter roll. The pilot quickly takes advantage of the U-2's 26 meter wing-span as he rotates the aircraft to its 40° climb angle. Watching the U-2 race towards 20-km altitude we understand why Moffett field air controllers are careful to clear air traffic from its steep ascent path.

Figure III.2 shows, as an example, the geographical flight plan for flight 9. A flight plan optimizes the following considerations, ordered roughly from most important to least important:

(1) Flight time and date are chosen to maximize new sky coverage.

(2) Legs are flown by the pilot in pairs of opposing headings.

(3) Headings are chosen that avoid the galactic plane and the moon during data taking

(4) Flight dates and flight plans are chosen that allow a calibration leg that points one antenna at the moon.

Pointing one antenna at the moon during a flight provides a check on equipment performance and gives and in-flight calibration of the radiometers good to about ± 5%. A moon run, usually 20 minutes in duration, has a considerable impact on the flight plan. Not only must the pilot orient the aircraft properly at the correct time, but, for the rest of the flight, the data legs must be flown so the antenna beams point away from the moon by more than 20° reducing the moon signal to less than 0.1 m°K in the sidelobes of the horn antennas. Moon calibrations were performed at least once with each receiver configuration.

The pilot's main responsibility is orienting the aircraft according to the flight plan and maintaining level flight during data legs. Table D.1 lists the pilot's responsibilities during a data flight. The operation of the radiometer system normally makes minimal demands on the pilot. However during the engineering flights, the pilots made significant unplanned contributions to the data taking. In the second flight the rotation system jammed during most rotations as it attempted to interchange the radiometer arms. The pilot, realizing the problem, toggled the antenna **Operate/Store** switch working the rotation bearing loose each time the monitoring meter indicated trouble. On the third flight, the rotation system failed at altitude, leaving the antennas stuck in the CCW position. Although the aircraft was out of radio range at that time, the pilot, aware of the problem, left the power on the equipment throughout the remainder of the flight. Thus the initiative of the pilots was responsible for acquisition of much of the valuable engineering data.

The post-flight instrument check-out commences after the ground crew releases the plane to the experimenters some 15 minutes after landing. The completion of equipment checks and the pilot's debriefing requires an additional 45 minutes. The radiometer and hatch are then lifted from the U-2, and we drive the equipment back to the Lawrence Berkeley Laboratory. Post-flight data analysis commences with the transfer of the data from the flight cassette to a standard computer tape in the early morning after the flight.

Table D.1 - Pilot's Flight Operations Profile

Time (hours)	*Pilot operation*	*Flight operation*
-0.10	POWER ON DATA RECORD	Preflight warm-up. Start tape recorder. Data acquisition.
0.00	Take-off	
0.16	ANTENNA OPERATE all switches up	Initiate antenna roation sequence at 15.2 km altitude.
0.30	Reach 19.8 km altitude	Equipment approaches thermal stability at altitude.
0.60	Level Flight.	Start data taking legs.
"	"	"
"	"	"
"	"	"
"	"	"
"	"	"
4.25	ANTENNA STORE	End data taking legs. Store antennas. Begin descent.
4.40	DATA STANDBY POWER OFF All switches down	Shut down for landing.
4.50	Land Aircraft.	

Appendix E - Radiometer Gain and Calibration

E.1 Introduction

The cramped quarters in the equipment bay of the U-2 make inclusion of an accurate in-flight calibrator difficult. However because of the stability of the mixer-based receiver we are able to calibrate the system within an error of ± 3% on the ground and demonstrate the relative gain stability to ±1% with in-flight monitors.

The voltage after the detector diode and the rms fluctuations of the recorded 33-GHz signals measures the product of system noise temperature times receiver gain; these quantities are monitored throughout each flight. These two techniques, described in section E.2, demonstrate

that the product of receiver noise times system gain is stable to better than ± 1%. Aircraft banks performed periodically throughout each flight inject unequal signals into the antennas providing a standard signal source external to the radiometer and show that the system gains is stable to within the 10% measurement error.

Converting the empirical units recorded on the flight cassette to units of antenna temperature is the subject of Section E.2. Ground based measurements using targets of Eccosorb, a commercially made microwave "blackbody", provides the values of the conversion constant C used in eq. IV.5. The accuracy of these measurements seems limited by slight variations in technique employed throughout the series of calibrations from flight 8 to flight 14.

The 33-GHz radiometer measured the antenna temperature of the moon in flights 4,6,8, and 14. The main systematic uncertainty is determining the actual brightness temperature of the lunar surface. According to published measurements this error is small enough that we could use the lunar calibration by itself in the data analysis. However, this calibration would then rely on other measurements that are outside of our direct experience.

E.2 Stability of the 33-GHz Radiometer Gain and Noise Temperature

Three in-flight indicators monitor the stability of the system noise temperature and the system gain of the 33-GHz radiometer. Firstly, a noise-monitor circuit measures and records the voltage level at the output of the detector diode. At altitude, the total noise temperature of the system, nominally 650 °K, is dominated by the noise generated in the mixer. Contributions to the noise temperature external to the radiometer system are minimal: the cosmic background adds a few degrees Kelvin, and the atmospheric signal adds only 34 m °K. Thus the noise monitor measures a signal proportional to the product of the noise power of the radiometer and the system gain up-stream of the detector diode. In flights 8-14 the noise-monitor signal dropped 2% during the initial cooldown leg, then drifted downward an additional 2% during the remainder of the flight. The rms fluctuations between the mean noise monitor signals for flights 8-14 was ± 0.3%.

A second monitor of relative system gain is the magnitude of the rms fluctuations of the 33-GHz data words recorded every 2 seconds. The rms fluctuations are proportional to the system noise temperature. The **Average** Programs compute the rms fluctuations of some 5000 edited 33-GHz data words recorded in a typical flight. Data from each flight flown with the SpaceKom mixer yields a measurement of rms fluctuations that varies between flights by ± 0.75%. Receiver noise alone accounts for this variation: With 5000 words recorded in a flight we expect the rms fluctuations to be measured with an error of $\pm \frac{\sqrt{5000}}{2} = \pm 0.0071$, or 0.71%.

Lastly, aircraft banks inject a 24m °K signal into the 33-GHz radiometer and provide a final indicator of system gain. In a typical flight the U-2 changes headings between data legs by banking at a nominal roll angle of 21 °. During a bank each antenna receives unbalanced contributions of atmospheric thermal radiation yielding the 24m °K signal. The atmospheric thermal radiation then provides a test signal which we use to compare system gain between flights. There are three sources of error in the measurement of this bank signal yielding a net uncertainty of ± 2.4m °K, or ± 10% of the total signal. Within these errors, the bank data from flights 8-14 are consistent with the hypothesis of constant system gain.

The sources of the error are the following:

(1) The 33-GHz receiver noise, 46 m °K/$\sqrt{\text{Hz}}$, contributes a ± 1 m °K error due to the limited integration time during the twelve 3 minute banks in each flight.

(2) During a 21 ° bank the sidelobes of the lowered 33-GHz antenna receive a 3 m °K signal from terrestrial microwave emission. The signal varies by ± 1 m °K depending on the terrain swept over by the lowered antenna.

(3) Correction of 8 m °K variations in the 33-GHz signal due to deviation from 21 ° bank angle, using the 54-GHz roll monitor signal, introduces a ± 2 m °K error. During the banks the earth-directed sidelobes of the 54-GHz horn antennas receive atmospheric emission whose intensity varies depending on the surface weather.

Although we would prefer independent measurements of both receiver gain and system sensitivity to ±2% or better, we feel that the various limits described here, taken together, justify using a single calibration constant for the data in flights 8-14. As is described in the following section, the error in this conversion constant is limited by the uncertainty of the absolute receiver calibration to about ± 3%.

E.3 Absolute Radiometer Calibration

Blackbody targets of Eccosorb AN 72 placed over the mouths of the horn antennas are used to calibrate the 33-GHz radiometer in the laboratory. Eccosorb AN 72 is a commercial microwave absorber made of urethane foam impregnated with graphite. The radiometer is calibrated by covering one horn mouth with a room-temperature target at 300 °K and the other with a target soaked in liquid nitrogen (LN) at 77 °K . This fills both antenna beam patterns with uniform temperature blackbodies and establishes a nominal 223 °K signal difference between the arms of the radiometer. The recorded digitized signal difference yields the desired calibration. Several repetitions of the procedure, with the loads interchanged over the antenna mouths, check the consistency of the measurements.

The AN 72 is porous; a target withdrawn from a bath of LN maintains a stable temperature within a degree Kelvin for more than 30 seconds while the LN boils off. The measured difference in signal strength between a target immersed in LN and one withdrawn from a bath is less than a degree Kelvin. The withdrawn target, although prone to drip liquid nitrogen over

the equipment, is more convenient to use in practice. In flight, the full scale output of the lock-in amplifier corresponds to an amplitude of $\pm 20\mu$Volts at the 33-GHz detector diode. The Datel recorder digitizes the integrated output of the lock-in amplifier with 12 bit resolution. Thus the digitized voltage resolution is 9.8 nV/least count, referenced to the 33-GHz detector diode.

The LN calibration procedure was performed before the flights 4,6, and 7 in the initial series of data flights, and before flights 8, 13 and 14 in the final series of data flights, and several times since flight 14. The empirical rms variation between these calibrations is $\pm$ 2.1%. The contribution of receiver noise to this error is negligible. The uncertainty in physical temperature difference between the two loads for any one measurement is about $\pm$ 0.5%. The probable origin of the 2% fluctuation is a combination of receiver temperature variation between the calibrations, and variations in the exact way the cold target is held over the antenna mouths. If the cold target is held exactly perpendicular to the antenna beam axis then dielectric reflection from the LN decreases the signal difference between the calibrators. After flight 14 we measured this reflection to be about 1% and found that tilting the surface of the cold Eccosorb about 10° from the beam axis reduces the reflection below 0.1%.

There are two additional systematic corrections. The first is correction for the saturation of the detector diode during the LN calibration procedure. Two different operating points of the diode are used for the room-temperature versus LN calibration. Ideally the detector diode is a square law device whose voltage output is proportional to the IF input power. However, we try to get the maximum signal out without badly saturating the diode, an HP 8472 B negative. Putting various attenuators before the detector diode measures the diode response and shows that the target signal of 290 °K slightly saturates the detector diode, reducing the system gain by 5% compared to the case when both antennas see cold signals.

The second systematic correction, discovered after flight 14, is the variation in the lock-in amplifier gain between the setting used for the low-level signals in flight, and the coarser setting used for calibrations. Nominally there is a factor of 250 gain change between the two settings, but it was discovered that the gain in fact changes by an additional 2% requiring a corresponding adjustment to the calibration constant. In the previous publication *(Smoot, Gorenstein & Muller, 1977)* diode saturation and the reflectivity of the Eccosorb were not corrected for, and the small deviation in nominal gain between lock-in amplifiers setting was not known. The inclusion of these additional corrections changes the net calibration by less than 5%.

E.4 Moon Calibration

The moon calibrations, performed in-flight, cross-check the ground based measurements. Each receiver configuration has been calibrated at least once by pointing an antenna at the moon during a flight. The calibration constant determined from moon runs in flights 8 and 14 is within 5.4% of the ground based results, consistent with the 6% uncertainty of the moon calibrations.

The moon fills a small fraction of the solid angle subtended by the antenna beam, thus the antenna temperature of the moon T_{ant}, is given by

$$T_{ant} = T_{lunar\ disk} \frac{\Omega_{moon}}{\Omega_{antenna}} \qquad \text{E.1}$$

where

$T_{lunar\ disk}$ is the mean antenna temperature of the lunar disk, used to calibrate the radiometer.

Ω_{moon} is the solid angle subtended by the moon. The mean solid angle is 0.211 square degrees, and varies by ± 15% during the lunar orbit. The apparent diameter of the moon is tabulated in the American Ephemeris and Nautical Alamanc with an error that is negligible for our purposes.

Ω_{ant} is the antenna beam width which spans a solid angle of 69.3 ± 0.7 square degrees.

The temperature of the lunar disk is the main uncertainty in this calibration procedure. The radiation temperature at the center of the lunar disk has been measured *(Hagfors, 1970; Mayer, 1970; Linsky, 1973)* to be

$$(215 \pm 4)\,°K + (34 \pm 3)\cos(\phi - 41 \pm 3°)\,°K \qquad \text{E.2}$$

where

ϕ is the phase of the moon after the new moon.

But our measurement includes the whole lunar disk. This has the advantage that the variations in antenna temperature due to the lunar phase are reduced, but adds additional uncertainty as now we must include an estimate of variations of temperature and emissivity over the lunar disk. According to Hagfors, the emissivity of the center of the lunar disk is 0.97 due to dielectric reflection. And greater reflection near the edges reduces the net thermal signal by an additional 6% compared to the center. The result is

$$T_{lunar\ disk} = (202 \pm 7.5)\,°K + (27^{+5}_{-2.5})\cos(\phi - 41 \pm 3°) \qquad \text{E.3}$$

A final correction to the lunar antenna temperature is due to navigational errors that misdirect the antenna slightly during a moon run. The pilots check the altitude of the moon during

the run, and the resulting corrections have amounted to a few percent at most, with less than a percent increase in error in the final calibration constant.

Appendix F - Astrophysical and Atmospheric Corrections to the Leg-measurements

F.1 Galactic Synchrotron Radiation

The primary astrophysical background in this experiment is microwave emission from relativistic electrons spiraling in the weak magnetic field of our Galaxy. This "synchrotron" radiation is highly anisotropic: the radiation is most intense towards the galactic center and is about a factor of 10 lower towards the anti-center and the galactic poles. Moreover the radiation is intense: at 1 GHz its flux is comparable to the 3 °K background whose angular properties we wish to study. Fortunately the intensity of synchrotron radiation decreases above 1 GHz while the intensity of the 3 °K radiation increases. At sufficiently high frequencies the synchrotron background is a relatively minor correction to the microwave background anisotropy for most directions in the celestial sphere.

Measurements show that the spectral intensity of synchrotron radiation obeys a power law given by

$$\frac{dI_{synchrotron}}{d\nu} \propto \nu^{-n} \qquad \text{F.1}$$

where the spectral index, n, clusters around 0.8 *(Kellerman, 1964)*. The spectral intensity of the 3 °K radiation increases as the square of the frequency in the Rayleigh-Jeans region, below 100 GHz:

$$\frac{dI_{blackbody}}{d\nu} \propto T\nu^2 \qquad \text{F.2}$$

Thus the intensity of synchrotron radiation relative to the blackbody radiation, *i.e.* the antenna temperature of the synchrotron radiation, falls with increasing frequency according to the formula,

$$T_{synchrotron} \propto \nu^{-2} \frac{dI_{synchrotron}}{d\nu} \propto \nu^{-2-n} \qquad \text{F.3}$$

The frequency at which the antenna temperature of galactic synchrotron radiation is below 0.2 m °K is then estimated by

$$(1\ \text{GHz}) \times \left[\frac{2\times10^{-4}\,°\text{K}}{3\,°\text{K}}\right]^{-1/2.8} = 31\ \text{GHz} \qquad \text{F.4}$$

Figure 4 in Appendix B illustrates this frequency dependence of the antenna temperature of galactic synchrotron emission.

The corrections to the 33-GHz data are based on a map of galactic synchrotron emission at 400 MHz, compiled by R.E. Taylor *(Taylor, 1973)*. We use this map, scaled to antenna temperature at 33 GHz, to generate corrections to the data. A single scale factor carries out this extrapolation:

$$T_{33\,GHz} = T_{0.4\,GHz}\left[\left(\frac{33\,GHz}{8\,GHz}\right)^{-2.9}\left(\frac{8\,GHz}{4\,GHz}\right)^{-2.8}\right] \qquad \text{F.5}$$

These two values of spectral indices account for the apparent steepening of synchrotron emission above 8 GHz *(Hirabayashi, 1974; Webster, 1974; Penzias & Wilson, 1966; Conklin, 1969)*. This data, folded with the antenna beam pattern, corrects the measurements for each leg. Figure F.1 is a three dimensional projection of the sum of the contributions of diffuse galactic synchrotron emission with point like emission from HII sources along the galactic plane.

F.2 HII Regions

The second major source of radio interference from the galaxy is thermal emission from clouds of hydrogen gas that are ionized and heated by ultra-violet radiation from nearby stars. The Orion nebula is one classic example. For wavelengths shorter than 30 cm, the HII regions are optically thin and the power spectrum is nearly flat *(Kraus, 1966, pg. 311)*

$$\frac{dI_{HII}}{d\nu} \propto \nu^0 \qquad \text{F.6}$$

Thus the antenna temperature drops with increasing frequency,

$$T_{HII} \propto \nu^{-2} \qquad \text{F.7}$$

The sources thus have approximately the same power spectrum as synchrotron radiation, and in fact have similar intensity. Figure 4 in Appendix B shows the antenna temperature spectrum of a typical HII region. Unlike synchrotron emission, which is diffuse throughout the celestial sphere, most HII regions are localized within 2° of the galactic plane, and appear as the point-like structures in Figure F.1. We obtained a list of sources from a compilation by Lang and Kraus *(Lang, 1974, pg. 121-127; Kraus, 1966, pg. 246-248)*. The sky coverage avoids most of these sources and the contamination of the data by HII emission is slight: two leg-measurements in the data from flights 8-14 required corrections between 0.1 and 0.2 m °K, with errors of ±15%. All other corrections were less than 0.05 m °K.

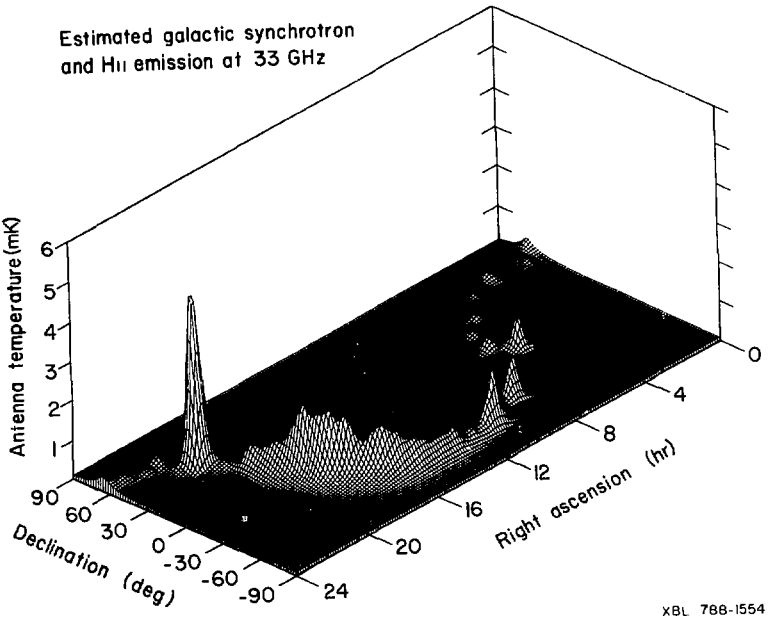

Figure F.1 - Galactic Synchrotron and HII Emission Extrapolated to 33 GHz

F.3 Corrections for Aircraft Roll

The aircraft roll generates an almost negligible background for the anisotropy measurement. The U-2 roll-attitude is quite stable; deviations from the mean roll for a leg were typically less than 0.3°, requiring corrections to the leg-measurements of no more than 0.4m°K. A series of aircraft banks from 5° to 20°, performed over several flights, determined the ratio of atmospheric imbalance signal to bank angle,

$$\frac{\Delta T_{33\text{-}GHz}}{\text{roll}} = 1.22 \pm 0.12\,\text{m°K/°roll} \qquad \text{F.8}$$

$$\frac{\Delta T_{54\text{-}GHz}}{\text{roll}} = 220 \pm 10\text{m°K/°roll} \qquad \text{F.9}$$

Since the rms receiver sensitivity at 54 GHz is $100\,\text{m°K}/\sqrt{\text{Hz}}$, an integration for two seconds measures a roll to an accuracy of ± 0.32° in angle. This in turn corresponds to a measurement of atmospheric imbalance at 33 GHz with an error of ± 0.4m°K.

The 3% error in eq. F.8 is statistical only; the precision of the measurement is limited by the 33-GHz receiver noise for the short time of the aircraft banks. The 5% error in eq. F.9 is considerably larger than the fluctuations due to radiometer noise alone. The error is likely due to deviations from the mean roll during an aircraft bank, and variations in the atmospheric temperature.

The correction to the 33-GHz signal for roll is straight-forward. The mean roll signal, ΔT^{roll}_{54GHz}, is computed for each leg in a manner which is exactly analogous to the computation of the mean 33-GHz anisotropy signal. The mean roll signal over the flight is computed in analogy with the rotation offset of the 33-GHz signal*. The correction to the 33-GHz signal is then in proportion to the deviation of the 54-GHz signal from its mean value.

F.4 The Motion of the Earth about the Sun

The motion of the earth about the sun produces an anisotropy of 0.3 ± 0.03 m°K magnitude; the 10% uncertainty is in the measured temperature of the 3°K background radiation. The 0.3 m°K signal is not a correction in the usual sense, but it must be removed from the data to compute the anisotropy in a barycentric coordinate system. The value subtracted from each leg-measurement is proportional to the component of the earth's motion along the difference vector of the antenna directions,

* The rotation offset at 54 GHz is no more than 50 m°K in each flight, equivalent to a 0.25° roll. Assuming such a signal is due to a roll, then it would contribute 0.3 m°K to the rotation offset at 33 GHz, which cannot account for the observed 2 m°K rotation offset.

$$\Delta T^{leg}_{33GHz} = 3\,^{\circ}\mathrm{K} \cdot \frac{\vec{v}_{earth}}{30\times10^{5}\mathrm{km/sec}} \cdot (\hat{n}_1 - \hat{n}_2) \qquad \text{F.10}$$

where

$\hat{n}_1$, $\hat{n}_2$ are the direction vectors of antenna 1 and 2 for the leg-measurement

$\vec{v}_{earth}$ is the velocity of the earth about the sun for the epoch of the leg-measurement.

$|\vec{v}_{earth}|$ is 30 km/sec

The uncertainty of this correction is negligible compared to the statistical uncertainty of the leg-measurement.

With data of sufficient sensitivity we could detect the earth's orbital motion about the sun. This would be an important cross-check of the experiment, but unfortunately, the noise in our data does not allow a significant measurement. Nevertheless it is worth going through the exercise. We do a four parameter fit to the data from flights 8-14, uncorrected for the earth's motion. Three parameters are the usual cosine anisotropy, and the fourth is the *magnitude* of the expected signal; i.e. we use the known motion of the earth about the sun to determine the relative amplitude and sign of the effect in each leg-measurement, and we fit only for the overall magnitude - the speed of the annual motion. The result of the fit is $-0.2 \pm 0.4\,\mathrm{m}^{\circ}\mathrm{K}$, the minus sign meaning the fit gives a speed opposite the expected direction.

Appendix G - The Rotation Offset

The rotation offset is an oscillation in the 33-GHz signal that changes in synchrony with the antenna rotation. Plots of the 33-GHz data words, signal-averaged at the rotation period, show that the change in signal level between the two antenna orientations is consistent with a square wave shape. There is no evidence for a slope or spurious fluctuation during the 64 second period between antenna interchanges. Dividing the flight data into segments gives consistent values of the offset. Flying data legs in opposing headings along the ground detects and cancels the rotation offset. Thus the mean difference between sequential pairs of leg-measurements is the celestial anisotropy, while the mean sum is the rotation offset. The offset is measured in a flight with an uncertainty of $\pm$ 0.5 m°K. Its value for each flight is shown in Figure IV.3. In the final seven flights the value has been the smallest and most stable. Comparable values have occured in flights flown in both U-2 aircraft based at Moffett Field. The rotation offset is a concern because its origin is uncertain.

The data in Figure IV.3 suggest that a major component of the effect is internal to the apparatus simply because the rotation offset changes so much between the early flights as the equipment was being modified. However, care was taken to minimize or eliminate electrical interaction between the rotation system and the 33-GHz radiometer. The rotation electronics is isolated from the 33-GHz radiometer by employing different grounds and power feeds, and resistors isolate the monitoring limit-switches from the data recording system. A mechanical relay shuts off the power to the rotation system during periods of data taking. After flight 12, a five hour ground test, in which care was taken to insure equal signals in each antenna, attempted to measure the offset. It gave an inconclusive result of 1.1 $\pm$ 0.5 m K.

Two other possible origins for the rotation offset that have been investigated are asymmetric radiation into the antenna sidelobes from the aircraft wings and asymmetric cooling of the antennas by the airstream. This latter effect would arise if an antenna is cooled by the airstream differently depending on whether it is on the pilot's left or right. Integration of the antenna sidelobe pattern over the airplane wings gives a signal for each antenna of about 0.5 m°K. And since the equipment is mounted symmetrically in the equipment bay of the U-2, this signal should cancel to below this level. Asymmetric cooling of the antennas by the airstream is a possible origin of the offset because the cold airstream, rapidly flowing along the aircraft, maintains a large, 1 °K/cm, gradient along the horn bodies. Presumably minor asymmetries in either rotation angle of the antennas, or in the surface geometry of the aircraft and hatch, could result in differential cooling, causing a few degrees temperature difference between the antennas.

By estimating the insertion loss for the mid-section of a horn antenna we can calculate the physical temperature change on the inner surface that yields a 2 m°K offset. The insertion loss

per unit length is about 0.02%/cm at the mid-point, or about 0.2% for a 10 cm length. A 2 m °K variation then results from a 2 m °K/0.002 = 1 °K variation in the temperature of the aluminum surface.

A pair of temperature sensors, one at each mid-point, measured the temperature difference in flight. The sensors were placed along a flange 4 cm from the horn surface to avoid drilling into the horn body. Therefore it is difficult extrapolating from this data the temperature variations within the 1 micron skin depth at the horn surface. However, the sensor signals did have one striking property in common: in all flights the signal showed clear triangular or quasi-sinusoidal oscillations synchronized with the rotation period. This is evidence that the mid-point temperatures are in fact driven up and down by the wind as the antennas rotate. Moreover the amplitude and shape of the signal was stable throughout a flight. However, the amplitude of the effect is small, between 40 and 100 m °K between the different flights, and the flight where the amplitude was highest, 100 m °K in flight 12, the rotation offset was the smallest, about 0.3 m °K.

Although the behavior of the temperature sensor signals does not correlate well with the behavior of the rotation offset, we can use the magnitude of the rotation offset to place a limit on the size of spurious anisotropy that results from variations in the physical temperature of the antennas. The amplitude of the mid-point temperature sensor oscillation is stable within 10% from leg to leg within a single flight. Residual difference in the spurious signal between leg-measurements should be at most 10% of 2 m °K or 0.2 m °K. In addition, the amplitude of oscillation changes smoothly between legs so differences cancel even below 0.2 m °K. Finally, the residual differences between pairs of legs are uncorrelated with antenna directions in the sky, and the net change in the parameters of cosine anisotropy is negligible compared to the statistical errors.

Thus the origin of the rotation offset is not known. However, since it appears constant and stable throughout a flight, we believe that it cancels to a low level as the aircraft heading is periodically reversed.

Appendix H - Fitting Procedures

H.1 Linear Least-squares-fit to cosθ Hypothesis

The leg-measurements are fit to the following hypothesis that describes a $\cos\theta$ (dipole) modulation of the 3°K background radiation:

$$T(\hat{n}) = T_o + \vec{T}\cdot\hat{n} \qquad \text{H.1}$$

where

$T(\hat{n})$ is the radiation temperature in the direction $\hat{n}$.

T_o is the mean temperature of the background, not measured in this experiment.

$\vec{T}$ is the vector describing the direction and amplitude of $\cos\theta$ anisotropy.

The 33-GHz radiometer measures the difference temperature between two antenna directions $\hat{n}_k^1$ and $\hat{n}_k^2$ for the k^{th} datum. Define

$$\vec{d}_k = \hat{n}_k^1 - \hat{n}_k^2 . \qquad \text{H.2}$$

Then from eq. H.1 and H.2,

$$\vec{T}\cdot\vec{d}_k = T(\hat{n}_k^1) - T(\hat{n}_k^2) . \qquad \text{H.3}$$

We wish to find the value of $\vec{T}$ that best fits the data. We generally use rectangular celestial coordinates, defined in Table IV.2. In this coordinate system we express $\vec{T}\cdot\vec{d}_k$ as

$$\vec{T}\cdot\vec{d}_k = T^1 d_k^1 + T^2 d_k^2 + T^3 d_k^3 . \qquad \text{H.4}$$

Given a set of anisotropy measurements ΔT_k, each with variance σ_k^2, then the best estimate of $\vec{T}$ is the one that minimizes the following expression for S.

$$S(\vec{T}) = \sum_{k=1}^{M} \frac{[\Delta T_k - \vec{T}\cdot\vec{d}_k]^2}{\sigma_k^2} \qquad \text{H.5}$$

where

M is the number of measurements.

Let $\vec{T}$ now be understood as that vector which uniquely minimizes S. Minimizing S maximizes the *a posteriori* probability that given $\vec{T}$ we arrive at the set of measurements ΔT_k. The details and justification of least-squares-fitting for data corrupted by Gaussian noise are covered in many texts *(see for example Martin, 1971; Solmitz, 1964)*.

Setting the partial derivatives of $S(\vec{T})$ in eq. H.5 to zero with respect to T^1, T^2, and T^3 gives three equations for the minimum of $S(\vec{T})$. After some algebra these become,

$$[\mathbf{H}]\ \vec{T} = \vec{T}_m \qquad \text{H.6}$$

where

$$[\mathbf{H}]_{ij} = \sum_{k=1}^{M} \frac{d_k^i\, d_k^j}{\sigma_k^2} \qquad \text{H.7}$$

and

$$[\vec{T}_m]_i = \sum_{k=1}^{M} \frac{d_k^i \Delta T_k}{\sigma_k^2}\,. \qquad \text{H.8}$$

The indicies i, and j, take on the component indices x, y, and z.

Inverting the matrix $[\mathbf{H}]$ finds the solution we seek,

$$\vec{T} = [\mathbf{H}]^{-1}\ \vec{T}_m\,. \qquad \text{H.9}$$

Note that $[\mathbf{H}]$, and $[\mathbf{H}]^{-1}$, contain only the variances σ_k^2 and the difference of the antenna directions $\vec{d}_k$; all reference to the measured anisotropy is compressed in the 3-vector $\vec{T}_m$. This fact will have some significance later.

We now wish to find the error in each component of $\vec{T}$ and the correlated error between components of $\vec{T}$. Uncertainties in components of $\vec{T}$ result from uncorrelated fluctuations present in the input data. Let δT_k be an independent fluctuation about ΔT_k that induces a corresponding variation, $\delta \vec{T}$ in the solution vector, $\vec{T}$. Then the variation in $\vec{T}$ is given by

$$\delta \vec{T} = [\mathbf{H}]^{-1}\ \delta \vec{T}_m \qquad \text{H.10}$$

where

$$[\delta \vec{T}_m]_i = \sum_{k=1}^{M} \frac{d_k^i\ \delta T_k}{\sigma_k^2} \qquad \text{H.11}$$

from eq. H.8 and H.9. The correlated error between components of $\vec{T}$ is expressed by

$$\begin{aligned} <\delta \vec{T}\ \delta \vec{T}^{\dagger}> &= <([\mathbf{H}]^{-1}\delta \vec{T}_m)\ ([\mathbf{H}]^{-1}\delta \vec{T}_m)^{\dagger}> \qquad \text{H.12} \\ &= [\mathbf{H}]^{-1} <\delta \vec{T}_m \delta \vec{T}_m{}^{\dagger}> [\mathbf{H}]^{-1\dagger} \end{aligned}$$

where the brackets indicate an ensemble average. It is straightforward to show from eq. H.7, 11, and 12 that

$$<\delta \vec{T}_m\, \delta \vec{T}_m{}^{\dagger}> = [\mathbf{H}]^{\dagger} \qquad \text{H.13}$$

whence

$$<\delta\vec{T}\,\delta\vec{T}^{\dagger}> = [\mathbf{H}]^{-1}. \qquad \text{H.14}$$

Thus the errors on the components of $\vec{T}$ are weighted averages of the errors σ_k, and are independent of the measurements $\delta\vec{T}_k$. This is in contrast to the expression of the dipole anisotropy in polar coordinates in which $\vec{T}\cdot\vec{d}_k$ would be a non-linear expression in polar parameters, and the errors would depend on the best fit values of $\vec{T}$.

The diagonal elements of $[\mathbf{H}]^{-1}$ give the rms errors on the components of $\vec{T}$:

$$\delta\vec{T}_{rms} = \sqrt{[\mathbf{H}]_{ii}^{-1}}. \qquad \text{H.15}$$

It is convenient to express the off-diagonal terms that are the correlated errors in unitless form:

$$C_{ij} = \frac{<\delta\vec{T}^{i}\delta\vec{T}^{j}>}{\sqrt{(\delta\vec{T}^{i})^2\,(\delta\vec{T}^{j})^2}} = \frac{[\mathbf{H}]_{ij}^{-1}}{\sqrt{[\mathbf{H}]_{ii}^{-1}\,[\mathbf{H}]_{jj}^{-1}}} \qquad i \neq j. \qquad \text{H.16}$$

The main results of this Appendix are the solutions for $\vec{T}$, eq. H.9, the expression for S, eq. H.5, and the expressions for the errors on the components of $\vec{T}$, eq. H.15 and H.16.

The polar parameters of cosine anisotropy are computed from the rectangular components. We numerically compute the errors on the polar parameters by jittering the input data with Gaussian distributed noise and then calculate the rms fluctuations, and cross-correlations in analogy with eq. H.15 and H.16.

H.2 Comparison Between Two Independent Measurements of Cosine Anisotropy

This section describes the algebraic details of a test that checks the consistency of two independent measurements of a vector quantity. The results are applied to the data in Section V.4. The idea is that the difference vector between the two measurements should be consistent with a null vector, and we test this by constructing a variable that has a χ^2 distribution if the null hypothesis is correct.

We work in a rectangular coordinate system (usually rectangular celestial coordinates) so the errors on the parameters are Gaussian. Assume two measurements $\vec{v}$ and $\vec{t}$ with error matrices [V] and [T] as defined in eq. H.14. (The reader won't be confused by the change in convention from the last section where it was convenient to express the error matrix as an inverse of another matrix.) The difference vector we are interested in is the

$$\vec{d} = \vec{t} - \vec{v}. \qquad \text{H.17}$$

Computing the errors on the components of $\vec{d}$ generates an error matrix [D]. From the definition of the correlated errors we find:

$$[\mathbf{D}] \equiv <\delta d_i\,\delta d_j> = <\delta(t_i - v_i)\,\delta(t_j - v_j)> \qquad \text{H.18}$$

$$= \langle \delta t_i \delta t_j \rangle + \langle \delta v_i \delta v_j \rangle - \langle \delta t_i \delta v_i \rangle - \langle \delta v_i \delta t_j \rangle .$$

But the latter two terms have zero mean, because the errors of components from different vectors are, by hypothesis, uncorrelated. Thus the error matrix for the difference vector is just the sum of the error matrices for each measurement:

$$[\mathbf{D}] = [\mathbf{V}] + [\mathbf{T}] . \qquad \text{H.19}$$

We now define a variable S in terms of $[\mathbf{D}]$ and $\vec{d}$ and show that it is distributed as χ^2 if the vector $\vec{d}$ is of zero length:

$$\langle d_i \rangle = 0 \qquad i = x,y,z . \qquad \text{H.20}$$

Let S be defined as the following scalar quantity:

$$S \equiv \vec{d}^{\dagger} [\mathbf{D}] \vec{d} . \qquad \text{H.21}$$

Since $[\mathbf{D}]$ is a real symmetric matrix, there is a rotation that will re-orient the coordinate system, diagonalizing $[\mathbf{D}]$. In this rotated coordinate system the errors in the components of $\vec{d}$ are uncorrelated. We then expand S explicitly in terms of the components in the diagonalized coordinates, whence

$$S = \frac{d_i'^2}{\sigma_i^2} + \frac{d_j'^2}{\sigma_j^2} + \frac{d_k'^2}{\sigma_k^2} . \qquad \text{H.22}$$

The primes refer to the components of $\vec{d}$ in the diagonalized coordinates system. If the mean values of the components of $\vec{d}$ are zero, then this is just the definition of a quantity with a χ^2 of three degrees of freedom.

Acknowledgements

It is the privilege of a student to receive gifts. It has been my particular good fortune to have had the experience of working with Richard Muller and George Smoot on this project. Without Rich's initiative this project would not have come to be: he focused the group's energy on the problem of the microwave anisotropy. His imaginitive and original approach to research has been a major influence on my outlook. George Smoot's determined effort set the style for the execution of this work; he showed me how to focus on the major goals of the experiment and how to get the job done. The accomplishments presented in the pages of this thesis followed directly from Rich and George's ideas and efforts.

Andrew Buffington helped design the controlling and timing electronics. Terry Mast worked up the atmospheric model from which the 54 GHz frequency was chosen. I especially appreciate Andy and Terry for the personal interest they took in my education throughout the stages of this experiment. I have special thanks for J. Anthony Tyson who, during a sabbatical year at Berkeley, contributed his experimental skill in helping solve the problems in the initial flights, and moreover provided for me an example of a gifted experimentalist.

John Gibson designed and built the numerous electronics packages crucial for the project's success. It is evidence of his skill that they all performed flawlessly throughout the flights. Hal Dougherty turned out precision machined metal quickly and with great skill. Hal and John are unique in the effort and dedication they bring to the group's projects. Jon Aymong developed the efficient software that analysed the flight data. Robbie Smits designed the rotation system, and Richard Lane built the controlling and timing electronics. Chris Witebsky assembled the data on the galactic emission and provided the excellent computer drawings, Figures V.2 and F.1. Lynda Drexler contributed her skills as a fast and accurate typist, and John Yamada provided needed support services.

I have been fortunate to be surrounded with a marvelous group of contemporaries, Jonathan Schonfeld, Gary Channan, Phil Lubin, Steve Pollaine, Scott Friedman and Joe Feller. I look forward to a continued association with them all.

Luis Alvarez of the Lawrence Berkeley Laboratory provided wise and expert advice on all phases of the project. Hans Mark, former director of NASA-Ames, provided crucial support and our introduction to the U-2 aircraft. The pilots of the Earth Survey Aircraft facility at NASA-Ames, Chunky Webster, Jim Barnes, Ron Williams, and Bob Erikson, were, needless to say, indispensable. Their skills contributed immeasurably to the success of the experiment. The Lockheed Aircrart Company modified the special upper hatch for the U-2 that turned the aircraft into a flying observatory. W. J. Welch and Doug Thornton of the Space Sciences Laboratory of the University of California at Berkeley, and Branko Leskovar of the Lawrence Berkeley Laboratory contributed helpful advice and ideas. This experiment was made possible through

the active support of Andrew Sessler, the Director of the Lawrence Berkeley Laboratory, Robert Birge, the head of the Physics, Computer Science and Mathematics Division at LBL, and Nancy Boggess of the National Aeronautics and Space Administration. This project was supported by NASA grant #2125 and ERDA contract #W-7405-ENG-048. Finally, I would like to thank the Physics Department of the University of California at Berkeley, the Space Sciences Laboratory, and the Lawrence Berkeley Laboratory for their support and hospitalty during my tenure.

References

Alpher, R.A., Bethe, H. & Gamow, G., *Phys. Rev.* **73**, 803 (1948)

Alpher, R.A. & Herman, R.C., *Rev. Mod. Phys.* **22**, 153 (1950)

Batakis, N. & Cohen, J.M., *Phys. Rev.* **D12**, 1544 (1975)

Barrow, J.D., *Nature* **267**, 117 (1977)

Barrow, J.D, *Nature* **272**, 211 (1978)

Barrow, J.D. & Matzner, R.A., *Mon. Not. R. astr. Soc.* **181**, 719 (1977)

Boughn, S.P., Fram, D.M. & Partridge, R.B., *Ap. J.* **165**, 439 (1971)

Burke, W.L., *Ap. J.* **196**, 329 (1975)

Collins, C.B. & Hawking, S.W., *Mon. Not. R. astr. Soc.* **162**, 307 (1973a)

Collins, C.B. & Hawking, S.W., *Ap. J.* **180**, 317 (1973b)

Conklin, E.K., *Nature* **222**, 971 (1969)

Corey, B.E., *Ph. D. Thesis* Princeton University, 1978

Corey, B.E. & Wilkinson, D.T., *Bull. Am. Astro. Soc.* **8**, 351 (1976)

de Vaucouleurs, G., *Nature* **182**, 1478 (1958)

de Vaucouleurs, G., *IAU Symposium No. 44, ed. D.S. Evans* (Reidel, New York, 1972, pg. 353)

de Vaucouleurs, G., *Ap. J.* **205**, 13 (1976)

de Vaucouleurs, G., *IAU Sumposium No. 79 (Tallinn, Estonia, September 1977, to be published)*

de Vaucouleurs, G. & de Vaucouleurs, A., *A. A.* **28,** 109 (1973)

de Vaucouleurs, G. & Peters, W.L., *Nature* **220,** 868 (1968)

de Vaucouleurs, G., Peters, W.L. & Corwin, J., H.G., *Ap. J.* **211,** 319 (1977)

Dicke, R.H., Peebles, P.J.E., Roll, P.G. & Wilkinson, D.T., *Ap. J.* **142,** 414 (1965)

Godël, K., *Rev. Mod. Phys.* **21,** 447 (1949)

Godël, K., *in Proceedings of the International Congress of Mathematicians 1950, edited by L.M. Graves, E. Hille, P.A. Smith, and O. Zariski* (Am. Math. Soc., Providence, R.I., 1952) Vol I, pg. 175

Gorenstein, M.V., Smoot, G.F. & Muller, R.A., *Bull. Am. Astro. Soc.* **9,** 431 (1977)

Gorenstein, M.V., Muller, R.A., Smoot, G.F. & Tyson, J.A., *Rev. Sci. Instrum.* **49,** 440 (1978)

Hagfors, T., *Radio Sci.* **5,** 189 (1970)

Hawking, S., *The Observatory* **89,** 38, (1969a)

Hawking, S., *Mon. Not. R. astr. Soc.* **142,** 129 (1969b)

Hawking, S.W. & Ellis, G.F.R., *The Large Scale Structure of Space-Time* (Cambridge University Press, Cambridge, Eng., 1973)

Hawking, S.W. & Penrose, R., *Proc. R. Soc. London A* **314,** 529 (1969)

Henry, P.S., *Nature* **231,** 516 (1971)

Hirabayashi, H., *Publ. Astron. Soc. Japan* **26,** 63 (1974)

Kellermann, *Ap. J.* **140,** 969 (1964)

Kraus, J.D., *Radio Astronomy* (McGraw-Hill, New York, 1966)

Lang, K.R., *Astrophysical Formulae* (Springer-Verlag, New York, 1974)

Linsky, J.L., *Ap. J. Supplement Series No. 216* **25**, 163 (1973)

Martin, B.R., *Statistics for Physicists*, (Academic Press, 1971)

Mayer, C.H., *Surfaces and Interiors of Planets and Satellites*, edited by A. Dollfus, pp. 180 (Academic, New York, 1970)

Meeks, M.L. & Lilley, A.E., *J. of Geophys. Res.* **68**, 1683 (1963)

Misner, C. W., *Ap. J.* **151**, 431 (1968)

Misner, C.W., *Phys. Rev. Lett.* **22**, 1071 (1969)

Misner, C.W., Thorne, K.S., Wheeler, J.A., *Gravitation* (Freeman, San Fransisco, 1973)

Muehlner D. & Weiss, R., *Infrared and Submillimeter Astronomy* **63**, (Astrophysics and Space Sciences Library, Reidel, 1976)

Muller, R.A., *Scientific American*, (May, 1978, pg. 64)

North, J.D., *The Measure of the Universe* (Oxford University Press, Oxford, 1965)

Partridge, R.B., *Am. Sci.* **57**, 37 (1969)

Partridge, R.B. & Wilkinson, D.T., *Phys. Rev. Lett.* **18**, 557 (1967)

Peebles P.J.E., *Ap. J.* **146**, 524 (1966)

Peebles, P.J.E., *Physical Cosmology* (Princeton U. P., Princeton, N. J., 1971)

Peebles, P.J.E., *Ap. J.* **205**, 318 (1976)

Peebles, P.J.E. & Wilkinson, D.T., *Scientific American,* (June 1967)

Peebles, P.J.E. & Wilkinson, D.T., *Phys. Rev.* **174,** 2168 (1968)

Penzias, A. A. & Wilson, R. W., *Ap. J.* **142,** 419 (1965)

Penzias, A. A. & Wilson R. W., *Ap. J.* **146,** 666 (1966)

Rees, M. J., *Phys. Rev. Lett.* **28,** 1669 (1972)

Rubin, V.C., Ford Jr., W.K., Thonnard, N., Roberts, M.S., Graham, J. A., *Astro. J.,* **81,** 687 (1976a)

Rubin, V.C., Thonnard, N., Ford Jr., W.K., Roberts, M.S., *Astro. J.* **81,** 719 (1976b)

Sandage, A., *Q. Jl. R. astr. Soc.* **13,** 282 (1972)

Sandage, A. & Tammann, G.A., *Ap. J.* **196,** 313 (1975)

Sandage, A. & Tammann, G.A., *Ap. J.* **210,** 7 (1976)

Schechter, P.L., *Astron. J.* **82,** 569 (1977)

Schmidt, M., *in Stars and Stellar Systems, Vol. IX Galactic Structure,* (University of Chicago Press, 1965, pg. 513)

Schwartz, D.A., *Ap. J.* **162,** 439 (1970)

Simmons, A.J. & Kay, A.F., *IEEE Conf. Publ.* **21,** 213 (1968)

Smoot, G.F., *Proceedings of the Spring Meeting of the American Physical Society, Washington D.C., 1977a* (unpublished)

Smoot, G.F., *Proc. of the International School of Gen. Rel. Effects in Phys. and Astrophys.: Experiments and Theory* (Max-Planck-Institut Für Physik und Astrophysik, Munich, 1977b) pp. 285

Smoot, G.F., Gorenstein, M.V. & Muller, R.A., *Phys. Rev. Lett.* **39**, 898 (1977)

Solmitz, F.T., *Ann. Rev. Nuc. Sci.* **14**, 375 (1964)

Stewart, J.M. & Sciama, D.W., *Nature* **216**, 748 (1967)

Taylor, R.E., *Proc. IEEE* **61**, 469, (1973)

Thaddeus, P., *Ann. Rev. Astron. Astrophys.* **10**, 305 (1972)

Tolman, R.C., *Relativity, Thermodynamics and Cosmology* (Oxford, 1934)

Verschuur, G.L. & Kellerman, K.I., *Galactic and Extragalactic Radio Astronomy* (Springer-Verlag, New York, 1974)

Visvanathan, N. & Sandage, A., *Ap. J.* **216**, 214 (1977)

Wagoner, R.V., Fowler, W.A. & Hoyle, F., *Ap. J.* **148**, 3 (1967)

Webster, A.S., *Mon. Not. R. astr. Soc.* **166**, 355 (1974)

Weinberg, S., *Gravitation and Cosmology: Principles and Applications of the General Theory of Relativity* (John Wiley & Sons, New York, 1972)

Weinberg, S., *The First Three Minutes* (Basic, New York, 1977)

Wilkinson, D.T. & Partridge, R.B., *Nature* **215**, 719 (1967)

Wilson, R.W. & Penzias, A.A., *Science* **156**, 1100 (1967)

Woody, D.P., *Ph. D. Thesis* (University of California, Lawrence Berkeley Laboratory, LBL Report #4188, 1975)

Woody, D.P., Mather, J.C., Nishioka, N.S., & Richards, P.L., *Phys. Rev. Lett.* **34**, 1036 (1975)

Yahil, A., Tammann, G.A. & Sandage, A., *Ap. J.* **217**, 903 (1977)